I.R.Iran

ISSN:2423-5547
e-ISSN:2423-7469

Journal of Renewable Energy and Environment

Volume 7, Number 1, Winter 2020

Materials and Energy Research Center

Iranian Association of Chemical Engineers

CONTENTS

AIMS AND SCOPE

Journal of Renewable Energy and Environment publishes original papers, review articles, short communications and technical notes in the field of science and technology of renewable energies and environmental-related issues including:

- Generation
- Storage
- Conversion
- Distribution
- Management (economics, policies and planning)
- Environmental Sustainability

INSTRUCTIONS FOR AUTHORS

Submission of manuscript represents that it had neither been published nor submitted for publication elsewhere and is result of research carried out by author(s). Only the extended and upgraded articles presented in a conference and/or appeared in a symposium proceedings could be evaluated for publication.

Authors are required to include a list describing all the symbols and abbreviations in the paper. Use of the international system of measurement units is mandatory.

- On-line submission of manuscripts results in faster publication process and is recommended. Instructions are given in the JREE web sites: www.jree.ir
- References should be numbered in brackets and appear in sequence through the text. List of references should be given at the end of the paper. All journal articles listed in the References section must follow with article doi.
- Figure captions are to be indicated under the illustrations. They should sufficiently explain the figures.
- Illustrations should appear in their appropriate places in the text.
- Tables and diagrams should be submitted in a form suitable for reproduction.
- Photographs should be of high quality saved as jpg files.
- Tables' illustrations, figures and diagrams will be normally printed in single column width (8 cm). Exceptionally large ones may be printed across two columns (17 cm).

Journal of Renewable Energy and Environment

Research Article

Journal Homepage: www.jree.ir

Multi-Objective Optimization of the Humidification-Dehumidification Desalination System for Productivity and Size

Amir Reza Khedmati, Mohammad Behshad Shafii*

Department of Mechanical Engineering, Sharif University of Technology, Tehran, Iran.

PAPER INFO

Paper history:
Received 31 October 2019
Accepted in revised form 29 February 2020

Keywords:
Humidification-Dehumidification
Desalination
Gained Output Ratio
Multi-Objective
Optimization

ABSTRACT

The humidification-dehumidification system is one of the desalination technologies that can utilize non-fossil thermal sources and requires insignificant input energy. This system is usually suitable for rural areas and places far from the main sources of energy. The purpose of this study is to obtain the most suitable working conditions and dimensions of this system. In this research, thermodynamic modeling was first performed for a simple type of the system (water-heated); then, the effect of parameters on the system performance was investigated. Modeling was conducted through a numerical simulation; furthermore, the assumption of the saturation of exhaust air from the humidifier was also considered in the mentioned code. Afterward, a comparison was made between two different forms of the system, and the proper form was chosen for the rest of the research. Moreover, through heat transfer equations, the dimensions of the two main parts of the system, i.e., humidifier and dehumidifier, were calculated. Besides, multi-objective optimization was carried out for two objective functions, i.e., gained output ratio (GOR) and the system volume, to reduce the space occupied by the system and reach the desired efficiency simultaneously. The optimization was performed using a simulation program, and results were obtained for different weights in order to optimize each objective function. For instance, 379 liters of freshwater can be produced in a day with a total volume of 48 liters for the humidifier and the dehumidifier in the optimized system.

1. INTRODUCTION

The daily and rapid reduction of drinking water is one of the concerning problems worldwide. The entire water resources of the earth are about 1.4 billion cubic kilometers, of which 97.5 % is in the oceans and only 2.5 % is in the atmosphere, aquifers, and polar ice. Then, 0.014 % of all water reservoirs are directly accessible [2].

For this reason, the ability to implement water desalination systems is becoming more and more critical. Among such systems are the multi-effect distillation system, the multi-stage flash distillation system, and the reverse osmosis system as some common types. However, these systems use fossil fuels or high-exergy sources. For this reason, other types of desalination systems, which use renewable energies, will be further discussed by the scientific community in the future. In addition to the above, the high capital and operational expenses of these systems led us to launch systems such as the humidification-dehumidification desalination system for remote and low population areas.

The humidification-dehumidification desalination system is of various types: closed air-open water and closed water-open air [2]. Typically, these systems comprise three essential parts: humidifier, heater, and dehumidifier. First, seawater penetrates the low-temperature cooling coil. In this step, seawater is pre-heated with humid air, as shown in Figure 1, in order to increase the efficiency of the whole system. In the heater (e.g., a solar collector), the intake water absorbs the heat necessary for evaporation after pre-heating. In the humidifier, the hot water blows out from the spray after being heated in a heater (the heat source); brine drips out from the bottom of this compartment, and water droplets humidify the dry air. Eventually, in the dehumidifier, water vapor in the humidified air condenses through the reaction between heat and water entering from the sea and is removed from the bottom of the compartment. In Figure 1, one can see a sample of an HDH system.

Hou et al. [3] investigated the function of a solar humidification-dehumidification desalination system using the pinch method. At specified temperatures of spraying and cooling water, they found that there was an optimum mass flow rate ratio of water to dry air to maximize the thermal energy recovery ratio. It is also noted that, for minimum temperature differences at pinches (1 °C), HDH could reach 0.75 for the energy recovery ratio; however, the heat exchanger area would probably increase.

He et al. [4,5] studied the water-heated CAOW-HDH theoretically, where the waste exhaust gas from a furnace was the heat source. They analyzed the mentioned system in terms of cost and selected both humidifier and dehumidifier as packed-bed. The final results of GOR and productivity were found to be 1.44 and 84.60 kg/h, respectively. He et al. [6] investigated an air-heated CAOW-HDH from thermodynamic and economic perspectives, where the system is composed of a packed-bed humidifier, a plate-type dehumidifier, and a waste heat recovery exchanger. Zubair et al. [7] used ETC with heat pipes as a heat source for their water-heated CAOW-HDH system. For this system, thermo-economic considerations and optimization analyses were carried out in four different geographical areas.

Niroomand et al. [8] theoretically investigated an OAOW-HDH (open air-open water), where the dehumidifier is a direct contact type. They reported that the higher production of

*Corresponding Author's Email: behshad@sharif.edu (M.B. Shafii)

freshwater could be reached by raising the flow rate and temperature of hot water and lowering the two former parameters for cold water. Dehghani et al. [9] experimentally studied a water-heated OAOW-HDH with a packed-bed humidifier and a direct contact dehumidifier. A gas burner heater was chosen as the heat source. It should be noted that brine recirculation was studied to reduce adverse effects on the environment. They found that raising the salinity of the recirculated brine could increase the overall recovery ratio of the system. Moreover, a productivity rate of 49 kg/h for was achieved in the mentioned study.

Elminshawy et al. [10,5] used a solar still with reflectors as the humidifier, a shell, and a tube heat exchanger as the dehumidifier and electrical water heaters as the heat source for a novel water-heated OACW-HDH. The productivity of the freshwater increased by 366 % because of the immersed water heaters and an external reflector.

Gang et al. [11] applied a three-stage packed-bed system as a humidifier in order to reach a higher contact surface. They achieved a value of 182.47 kg/h for freshwater productivity.

Yıldırım and Solmuş [12] used a packed-bed humidifier with FPC heat sources of different configurations of the water/air-heated OACW-HDH system. They found the optimum values of the air mass flow rate and the inclination angle of FPCs. Rajaseenivasan and Srithar [13] investigated the OACW-HDH system with a special FPC, where both water and air were heated simultaneously [5]; then, air passed over the upper surface of the absorber plate and water crossed the riser tubes at the bottom of the absorber plate. The result showed 15.23 kg.day/m^2 productivity for freshwater. Deniz and Çınar [14] studied and tested a novel OACW-HDH solar system from exergy, economic, and environmental points of view. They found the amount of 1117.3 g/h for the maximum freshwater production rate and 0.0981 USD/L for the estimated cost of freshwater produced.

The present research focuses on minimizing the volume of a simple water-heated CAOW-HDH system while maximizing its efficiency. A thorough review of the literature revealed no such study with the objectives mentioned earlier on particular types of the humidifier (i.e., packed-bed) and dehumidifier (i.e., helical coil heat exchanger). The humidifier and dehumidifier used in this research have proper contact surface for the humidifying mechanism and the appropriate mixing mechanism for better heat transfer, respectively. Moreover, this research aims to find useful decision variables on the GOR and size of the system. New parameters such as coil diameter in the dehumidifier, velocity of air circulation in the dehumidifier, and some other parameters are the strengths of this study.

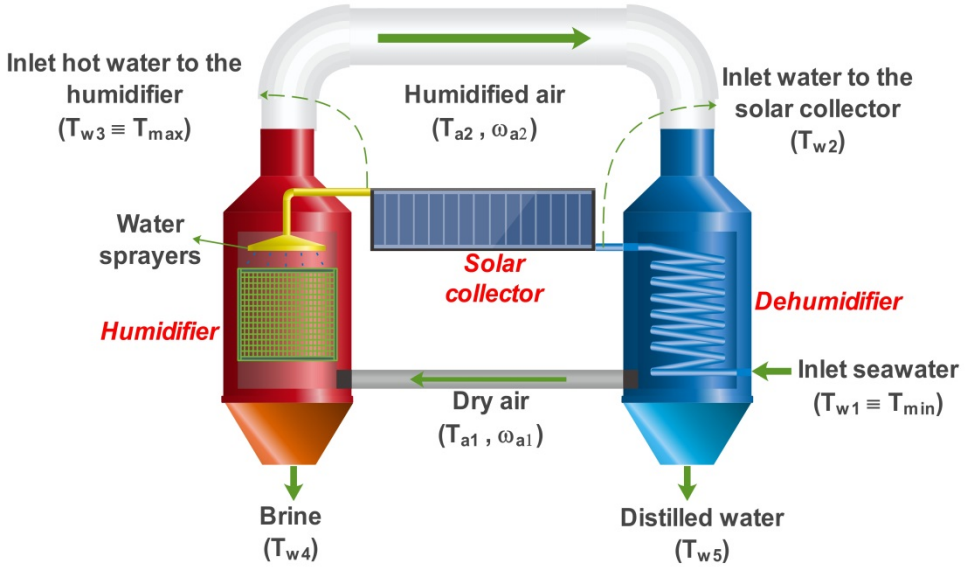

Figure 1. Schematic of a CAOW-HDH system.

2. MATERIALS AND METHOD

2.1. Thermodynamic modeling

In order to model the system in the simple form (closed air-open water), the mass-conservation, energy conservation, and second law of thermodynamics equations were written for all three parts of the system, i.e., humidifier, dehumidifier, and heater. In the simple model of the system, water is drawn from the sea and a steady stream of air circulates in the cycle. Equations for the humidifier are written below:

$$\dot{m}_{w1} - \dot{m}_{w4} = \dot{m}_{da} \times (\omega_{a2} - \omega_{a1}) \quad (1)$$

$$\dot{m}_{w1} \times h_{w3} - \dot{m}_{w4} \times h_{w4} = \dot{m}_{da} \times (h_{a2} - h_{a1}) \quad (2)$$

$$\dot{m}_{w4} \times s_{w3} - \dot{m}_{w1} \times s_{w3} + \dot{m}_{da} \times (s_{a2} - s_{a1}) = \dot{S}_{gen,h} \quad (3)$$

Similar to Equations 1-3, there are three equations for the dehumidifier, which are recognized by (4-6):

$$\dot{m}_{da} \times (\omega_{a2} - \omega_{a1}) = \dot{m}_{w5} \quad (4)$$

$$\dot{m}_{w1} \times h_{w3} - \dot{m}_{w4} \times h_{w4} = \dot{m}_{da} \times (h_{a2} - h_{a1}) \quad (5)$$

$$\dot{m}_{w4} \times s_{w3} - \dot{m}_{w1} \times s_{w3} + \dot{m}_{da} \times (s_{a2} - s_{a1}) = \dot{S}_{gen,h} \quad (6)$$

In addition, Equations 7 and 8 are written for the heater section:

$$\dot{m}_{w1} \times (h_{w3} - h_{w2}) = \dot{Q}_{in} \quad (7)$$

$$\dot{m}_{w1} \times (s_{w3} - s_{w2}) = \dot{S}_{gen,HS} \quad (8)$$

In this case, there are eight equations and ten unknowns, according to the data shown in Table 1 [1].

Table 1. Input data for the verification of the numerical simulation [1].

Variable (unit)	Value
T_{min} (°C)	30
T_{max} (°C)	80
e_h (-)	0.8
e_d (-)	0.7
φ_{a1}	1
φ_{a2}	1
S (ppm)	35000

It should be noted that T_5 is assumed to be the average of the inlet and outlet air temperatures of the humidifier (or dehumidifier) [1]. Further, T_1,T_3 are the minimum and maximum temperatures in the cycle, respectively. Therefore, two auxiliary equations, i.e., the effectiveness of the two heat exchangers, are used in the following to accommodate solving the equations simultaneously [15]. These equations were added to not only solve the thermodynamic modeling equations, but also prepare the simulation for heat transfer modeling in the upcoming section (i.e., Section 2.4).

$$e_1 = \frac{\dot{m}_{w1}\times h_{w3} - \dot{m}_{w4}\times h_{w4}}{\dot{m}_{w1}\times h_{w3} - \dot{m}_{w4}\times h_{w4,ideal}} \quad (9)$$

$$e_2 = \frac{\dot{m}_{w5}\times (h_{a2} - h_{a1})}{\dot{m}_{w5}\times (h_{a2.ideal} - h_{a1})} \quad (10)$$

$$e_h = \max(e_1, e_2) \quad (11)$$

$$e_3 = \frac{h_{w1} - h_{w2}}{h_{w1} - h_{w2,ideal}} \quad (12)$$

$$e_4 = \frac{h_{a1} - h_{a2}}{h_{a1.ideal} - h_{a2}} \quad (13)$$

$$e_d = \max(e_3, e_4) \quad (14)$$

where the first triple equations are for the humidifier and the rest for the dehumidifier. Note that the subscript ideal refers to the same condition (i.e., temperature) of the other inlet flow (e.g., inlet air) for the mentioned flow (e.g., inlet water) in the heat exchanger (i.e., the humidifier or dehumidifier).

The results of the verification of the simulation program are shown in Figure 2, in which GOR is the enthalpy ratio of evaporation of the produced freshwater to the input heat. Note that Figure 2 shows the same inputs used in Ref. [1]. This input data is shown in Table 1. A relative error of 2.38 % can be observed in the present work, which is acceptable. Moreover, the mass flow rate ratio was observed to have an optimum point for GOR due to the lower and upper bounds of the mass flow rate ratio; if the amount of water circulating in the system is much more than the air inside it, the air cannot carry much water. On the contrary, if the amount of air circulating in the cycle is much more than the water inside it, lower freshwater is made. It should be noted that the number of iterations, relative residuals, and the change in variables were fixed on 250, 1E-06, and 1E-09, respectively.

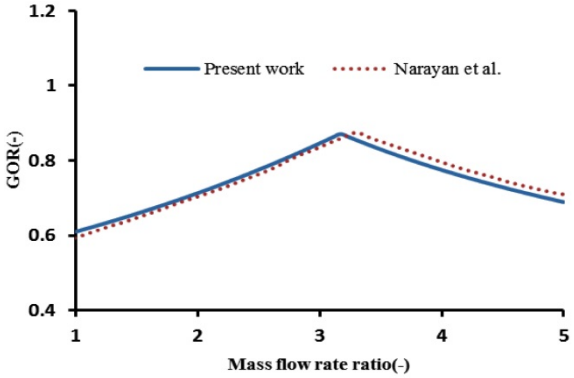

Figure 2. Verification of the simulation program.

Table 2. Input data for parametric study of a CAOW-HDH [1] (In each plot taken, one input data variable and the rest follow this table).

Variable (unit)	Value
T_{min} (°C)	35
T_{max} (°C)	80
e_h (-)	0.9
e_d (-)	0.9
φ_{a1}	1
φ_{a2}	1
S (ppm)	35000

2.2. Parametric study: Effect of input variables on GOR

Higher GOR is the reason for the higher efficiency of the overall system, yet with lower system irreversibility [1]. For this reason, the effect of input variables on GOR is evaluated. The input variables include the minimum temperature (i.e., the seawater inlet temperature), the maximum temperature (i.e., the temperature of the output water from the heater), and the effectiveness of the humidifier and the dehumidifier. To determine the effect of these inputs, in each step, one of them was selected to be a variable and the rest were kept constant. The base case data are shown in Table 2 [1]. In this case, the most effective variable is the effectiveness of the dehumidifier, which indicates the importance of this heat exchanger. For instance, the effects of three variables on GOR are discussed here (Figures 3, 4, and 5):

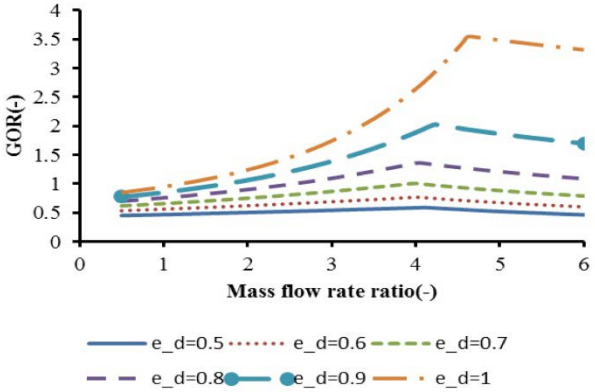

Figure 3. Effect of the dehumidifier on GOR.

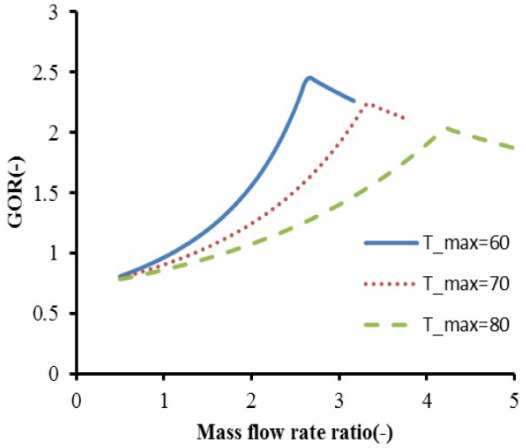

Figure 4. Effect of the maximum temperature on GOR.

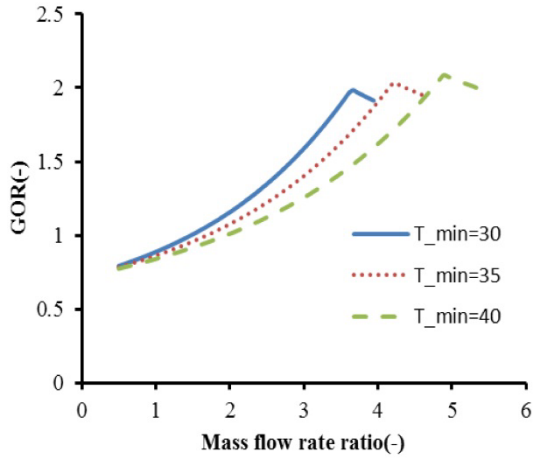

Figure 5. Effect of the minimum temperature on GOR.

As shown in Figure 3, the higher effectiveness of the dehumidifier resulted in higher GOR. Accordingly, changing the effectiveness from 0.9 to 1 (ideal) resulted in a considerable increase by 79 % for the maximum GOR (from 1.975 to 3.539). This phenomenon is evident because the function of the dehumidifier grew obviously. It should be noted that the mass flow rate ratio did not change regularly. Moreover, as demonstrated in Figure 4, the higher maximum temperature resulted in lower GOR. Accordingly, changing the maximum temperature from 70 to 80 ℃ resulted in a 16 % decrease in the maximum GOR (from 2.211 to 1.905). According to Figure 5, the higher minimum temperature resulted in higher GOR. On this basis, changing the minimum temperature from 30 to 35 ℃ resulted in a 4.2 % increase in the maximum GOR (from 1.929 to 2.011).

Furthermore, by comparing the effects of the minimum and maximum temperatures on GOR, it was observed that approaching the high and low temperatures of the cycle increased GOR and lowered its irreversibility, respectively. Furthermore, the effectiveness of the dehumidifier was higher than that of the humidifier.

2.3. Comparison of water-heated and air-heated types

In the air-heated type, the air is replaced by water only in the heater section. Note that if the air was heated before the humidifier, the heat given to the brine from the heated air would be dissipated (if there was no brine-recycling); thus, the air should be heated only after the humidifying process. Of course, the relative humidity of the outlet air from the heater was also added to the unknowns of the system; thus, this parameter was optimized for the air-heated type to find the maximum GOR. In this case, for the given data in Table 3 [1], the maximum GOR was found. It was observed that the maximum amount of GOR in the air-heated type was about 17 % more than that in the other type. Of course, due to the lack of temperature stability in the air-heated type system and its rigidity (e.g., for initial variant data in the system such as a change in the seawater temperature), this system is not highly functional (due to the lower heat capacity of air than water). For this reason, optimization was performed for the water-heated type in further sections in this research.

Table 3. Input data for a comparison of two types of HDH [1].

Variable (unit)	Value
T_{min} (°C)	35
T_{max} (°C)	80
e_h (-)	0.9
e_d (-)	0.9
φ_{a1}	1
φ_{a2}	1
S (ppm)	35000

2.4. Heat transfer modeling

The volume of the desalination system is calculated through heat transfer equations. In this case, the size of the heating section (heater) is not considered, and the other two (humidifier and dehumidifier) are evaluated. A helical coil heat exchanger was used to successfully reduce the volume of the system for the dehumidifier part. This heat exchanger is suitable for low fluxes, unlike shell and tube heat exchangers. Moreover, a packed-bed system is used for air humidification, which has a good contact surface for humidifying the air. As a result, the final system is compact and small in size.

2.4.1. Dehumidifier

2.4.1.1. Shell side equations

The equivalent diameter for this part is determined through Equation 15:

$$D_{eq}=\sqrt{\frac{4\dot{m}_s}{\pi\times\rho\times u_s}} \quad (15)$$

In addition, Reynolds and Prandtl's numbers are defined through Equations 16 and 17:

$$Re=\frac{\rho\times u_s\times D_{eq}}{\mu} \quad (16)$$

$$Pr=\frac{\mu\times C_p}{k} \quad (17)$$

Nusselt number and heat transfer coefficient in turbulent flows are evaluated by Equations 18 and 19 [16]:

$$Nu=0.023\times Re^{0.8}\times Pr^{0.4} \quad (18)$$

$$h=\frac{Nu\times k}{D_{eq}} \quad (19)$$

2.4.1.2. Coil side equations

Mass flow, which crosses the coil, is related to surface area and diameter of the coil by Equations 20 and 21:

$$u_c=\frac{\dot{m}_c}{\rho\times A_c} \quad (20)$$

$$A_c=(\pi/4)\times d_c^{\,2} \quad (21)$$

To determine Nusselt number and heat transfer coefficient, Equations 22 and 23 are used as follows:

$$Nu=0.023\times Re^{0.85}\times Pr^{0.4}\times(\frac{r}{R})^{0.1} \quad (22)$$

$$h=\frac{Nu\times k}{d_c} \quad (23)$$

2.4.1.3. Heat transfer analysis

The total heat transferred by the dehumidifier elements is determined through Equation 24:

$$\dot{Q}_d=U\times A\times(LMTD\times F_{helical}) \quad (24)$$

where LMTD is:

$$LMTD=\frac{(T_{s,in}-T_{c,out})-(T_{s,out}-T_{c,in})}{\ln((T_{s,in}-T_{c,out})/(T_{s,out}-T_{c,in}))} \quad (25)$$

In addition, the overall heat transfer coefficient is obtained through Equation 26:

$$\frac{1}{U}=\frac{A_e}{h_i\times A_i}+\frac{A_e\times\ln(\frac{d_e}{d_i})}{2\pi k\times L_c}+\frac{1}{h_e} \quad (26)$$

where A_e, d_e, and L_{coil} are the heat exchange area (external surface of the coil), the external diameter of the coil, and the coil length, respectively. Moreover, A_i and d_i are the internal surface and the internal diameter of the coil, respectively. Note that k is the thermal conductivity of the material used for the coil.

Remember that the effect of the centrifugal force generated by the curvature of the pipes should be taken into account. This effect is applied with a correction coefficient in the logarithmic mean temperature difference [17]:

$$F=1+3.6\times(1-\frac{r}{R})\times(\frac{r}{R})^{0.8} \quad (27)$$

Furthermore, because of the use of seawater in the coil side, one can apply Equations 28 and 24:

$$\dot{Q}_d=\dot{m}_w\times C_{p_w}\times(T_{out}-T_{in}) \quad (28)$$

Of note, the surface area for transferring heat can be calculated through Equation 29:

$$A=\pi\times d\times L_c \quad (29)$$

where L_c is the length of the coil and is related to helix radius of the coil (R) and the pitch of the coil (p) by Equation 30:

$$L_c=N\times\sqrt{(2\pi R)^2+p^2} \quad (30)$$

where the number of coils is related to the pitch by Equation 31:

$$L_s=p\times N \quad (31)$$

where L_s is the length of the shell.

The volume of the coil is determined by Equation 32:

$$V_c=(\pi/4)\times d_c^{\,2}\times L_c \quad (32)$$

The volume of the shell is obtained by Equations 33-35:

$$V_{av}=(\pi/4)\times D_{eq}\times d_e\times L_c \quad (33)$$

$$V_s=V_c+V_{av} \quad (34)$$

$$V_s=(\pi/4)\times D_s^{\,2}\times L_s \quad (35)$$

where Equation 33 is the volume available for the humidified air.

2.4.1.4. Pressure drop at shell side

To determine the pressure drop, Equations 36 and 37 are used:

$$f_s=0.184\times Re^{-0.2} \quad (36)$$

$$\Delta P=\frac{f_s\times\rho\times L_s\times u_s^{\,2}}{2D_e} \quad (37)$$

where Equation 36 is the friction factor.

2.4.1.5. Pressure drop at coil side

To obtain the pressure drop, Equations 38 and 39 are used:

$$f_c=0.046Re^{-0.2}\times\left[Re\times(\frac{r}{R})^2\right]^{0.05} \quad (38)$$

$$\Delta P=\frac{2f_c\times\rho\times L_c\times u_c^{\,2}}{d_c} \quad (39)$$

2.4.1.6. Verification of the dehumidifier model

The verification of this part was done with Ref. [16] for the preheater part of the heat exchanger mentioned in Ref. [16]. R134a refrigerant was used in the coil and the exhaust gas from the Diesel engine in the shell; Tables 4 and 5 show the initial data and results of this procedure, respectively. It could be seen that the errors are below 1 %.

Table 4. Input data for the verification of the dehumidifier model [16].

Working fluid	T inlet (K)	T outlet (K)	Pressure (kPa)
R134a	307.2	328.202	1500
Exhaust gas	487.465	403.507	200

Table 5. Verification of the dehumidifier model.

Parameter	Present model	Ref. [16]	Error (%)
Q_preheater (W)	3396	3409.52	-0.4
Shell length (m)	0.358	0.3582	-0.06

2.4.2. Humidifier

A packed-bed system has three main parts: spray zone (from spray nozzles to the surface of the packing), packing zone (consisting of the packing material), and rain zone (first part where water droplets contact with the air) [18]. It should be noted that 90 % of the heat and mass transfer occurs in the fill zone; therefore, this part is the most crucial part of this heat exchanger.

The following assumptions are reasonable to use for modeling the mentioned humidifier [18]:

- Uniform cross-sectional area for the humidifier.
- Constant pressure along with the humidifier.

It is common to use a dimensionless number called ‘’Merkel number’’ in this specific humidifier. This number is defined as follows [18]:

$$Me=\frac{h_d \times a \times V}{\dot{m}_w} \quad (40)$$

which relates the mass transfer coefficient to the effective surface area per unit volume, the volume of the humidifier, and mass flow rate of the inlet seawater. Because mass and energy balance equations for this humidifier are differential equations [18], an approximate equation for the height of the humidifier is used; thus, the optimization procedure in the upcoming sections has become possible. Moreover, the area of the humidifier is calculated through Equation (41):

$$A_h=\frac{\dot{m}_w}{flux} \quad (41)$$

where water flux is constant and assumed to be 2 $kg.m^2/s$ [18]. By combining Equation A.8 from Ref. [18] and an approximation in ε-NTU, the method for heat exchangers (Equation 11.29b from [19]), one can apply Equation 42 for the height of the humidifier.

$$H_h=\left[\frac{\ln\left(\frac{e_h-1}{e_h \times CR-1}\right)}{2.049(CR-1)\times MR^{0.221}}\right]^{\frac{1}{0.632}} \quad (42)$$

It is noted that CR is the $\min\left(\frac{MR\times C_{p_w}}{4},\frac{4}{MR\times C_{p_w}}\right)$.

The results of the approximate method are in agreement with those in [18]. For more information, check out the Appendix and [18]. Note that this equation is not almost accurate and is approximate.

2.5. Parametric study: The effect of input variables on the system dimensions

Data used in this parametric study for the system dimensions are shown in Table 6. Note that there are some technical constraints for the dimensions:

- d_e/D is chosen as 0.1 [16] as in almost all Figures; only in Figure 6, this quantity is chosen to be both 0.1 and 0.2.
- Pitch is usually set to $1.25d_e$ in heat exchangers [17].

Note that the conductivity of pure copper is used for the coil.

Table 6. Input data for the parametric study of CAOW-HDH dimensions.

Variable (unit)	Value
T_{min} (°C)	35
T_{max} (°C)	80
e_h (-)	0.9
e_d (-)	0.9
φ_{a1}	1
φ_{a2}	1
S (ppm)	35000
u_s (m/s)	5
P (kPa)	101.325
D (m)	0.2
$\dot{m}_w$ (kg/s)	0.1
T (m)	0.001
k_c (W/m.K)	386
p/d_e (-)	1.25

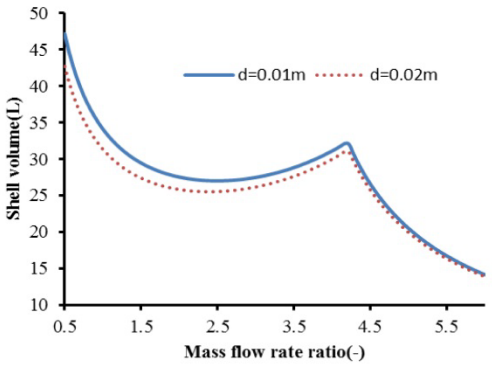

Figure 6. Effect of the inner coil diameter on the shell volume.

To determine the effect of these inputs, in each step, one of them is assumed to be a variable, and the rest are considered constant. It should be noted that only the important ones are discussed here. As shown in Figure 6, a lower inner coil diameter causes the higher volume of the dehumidifier shell. This is due to the lower overall heat transfer coefficient in this state (Equation 26). Accordingly, according to Figure 6, the volume increased from 31.02 L (d=0.02 m) to 32.13 L (d=0.01 m) at the highest GOR point in each case (a 3.5 % increase).

As shown in Figure 7, the lower maximum temperature resulted in the higher volume of the dehumidifier shell and also higher GOR, as shown in Figure 4. Moreover, these results created a two-objective optimization process (i.e., the system volume and GOR). On this basis, shell volume increased from 30.95 L (T_{max}=80 °C) to 36.57 L (T_{max}=70 °C) and 42.82 L (T_{max}=60 °C) at the highest GOR points,

which resulted in 14.6 % and 27.72 % increases in volume (relative to T_{max}=80 °C). The reason seems to be connected to the idea that lower irreversibility usually follows the area of heat transfer excess.

Moreover, for the height of the humidifier (the cross-section of the packed-bed system is constant), Figure 8 is plotted. As is shown, by increasing the effectiveness of the humidifier, the height and the volume of the system increase (as one has guessed); accordingly, changes are shown in Table 7, where there are massive changes by altering this input data. Given the effect of this parameter on GOR, one should optimize both functions simultaneously.

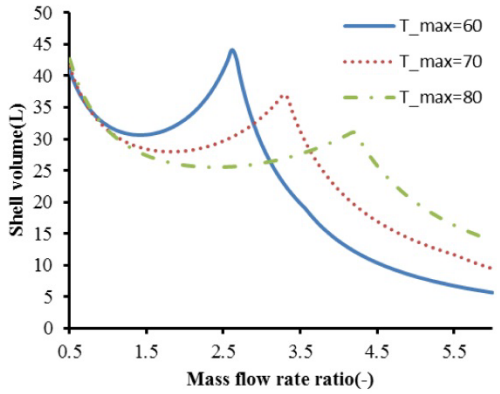

Figure 7. Effect of the maximum temperature on the shell volume (for d=0.02 m).

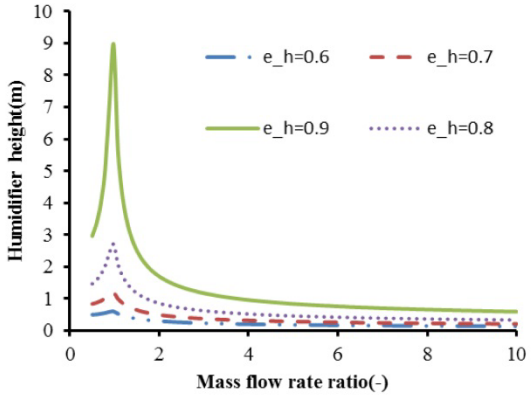

Figure 8. Effect of the humidifier on the humidifier height.

Table 7. Changes in the humidifier height with its effectiveness.

Effectiveness of humidifier	Height of humidifier (m)	Relative change (to the first case)
0.6	0.8691	-
0.7	1.009	16.1 %
0.8	2.7	210.7 %
0.9	8.96	930.9 %

In Figure 9, changing the air velocity is evaluated. As is shown, increasing this velocity caused an increase in the convection heat transfer and, consequently, a decrease in the volume of the shell. On this basis, shell volume increased from 31.02 L (u_{air}=5 m/s) to 60.66 L (u_{air}=3 m/s) and 264.2 L (u_{air}=1 m/s) at the highest GOR points; therefore, there are 95.5 % and 751.7 % relative changes to the u_{air}=5 m/s case, respectively, which are tremendous changes.

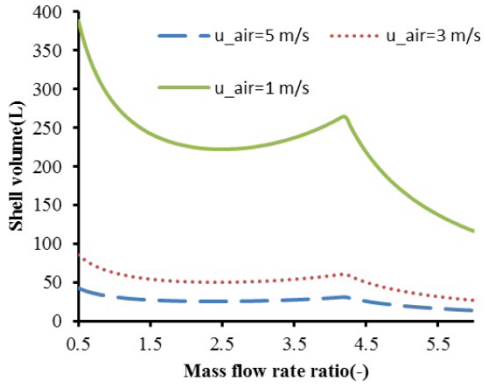

Figure 9. Effect of the air velocity on the shell volume (d=0.02 m).

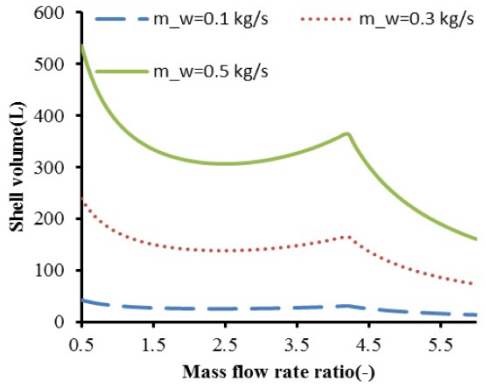

Figure 10. Effect of the mass flow rate of the seawater on the shell volume (d=0.02 m).

In Figure 10, changing the mass flow rate of the seawater is evaluated. As shown, increasing this input data extends the shell volume. Accordingly, the shell volume increased from 31.02 L ($\dot{m}_w$=0.1 kg/s) to 165.3 L ($\dot{m}_w$=0.3 kg/s) and 364.4 L ($\dot{m}_w$=0.5 kg/s) at the highest GOR points; therefore, there are 432.8 % and 1074.7 % relative change to the $\dot{m}_w$=0.1 kg/s case, respectively, which are massive changes. Thus, in this case, more amount of freshwater is produced; however, the size of the system increases (because of the rise in the area needed for heat transfer). Moreover, the allowable pressure loss in the coil section can be overshot by increasing the mass flow rate of the seawater.

3. RESULTS AND DISCUSSION

In this section, the momentous results of the previous parts are discussed in 3.1. Then, the optimization procedure and final results are presented and discussed in 3.2 and 3.3.

3.1. Key points about the useful parameters on GOR and the size of the system

- It should be noted that the last two inputs (i.e., the air velocity and the mass flow rate of the seawater) had no effects on GOR; the best quantity for each of them is set in Table 6 for optimization.
- Parametric studies for other input data can be done the same as above.
- Most essential parameters having a magnificent role in the size of the system and GOR are maximum temperature and both the effectiveness of humidifier and dehumidifier.

Table 8. Properties of the pattern search algorithm.

Property	Value
Mesh size	1
Mesh expansion factor	2
Mesh contraction factor	0.5
Max iterations	100 × number of variables
Tolerances	1e-6
Poll method	GPS positive basis 2N

3.2. Optimization procedure

The primary purpose of this article is to minimize the system volume and maximize GOR at the same time.

The pattern search optimization method was used as one of the most efficient methods for optimization [20-22]. Table 8 and Figure 11 show the properties and outline of this method, respectively.

Two objective functions were considered: GOR and the system volume. Five decision variables were selected to perform this optimization. Table 9 shows decision variables and their acceptable ranges known as constraints. Design parameters used in optimization are shown in Table 10.

One can optimize two or more objective functions by weighting each function and summing them all together in a multi-objective function. This new function is defined as follows:

$$\min (MOF = w_1 \times (-GOR) + w_2 \times TotalVolume) \qquad (43)$$

Note that the minus sign in Equation 43 is used to maximize GOR or, in other words, to minimize the negative GOR. For this purpose, six groups of weights (i.e., for w_1 and w_2) were given to the two functions, as mentioned above. These six weights, namely 90, 80, 70, 30, 20, and 10 percent for both of the objective functions with their results, are discussed in detail in the following section.

Table 9. Decision variables and their range of performance used for optimization.

Variable (unit)	Minimum value	Maximum value
T_{min} (°C)	30	40
T_{max} (°C)	60	80
e_h (-)	0.65	0.95
e_d (-)	0.65	0.95
MR (-)	0.5	6

Table 10. Design parameters for the optimization of the two functions simultaneously.

Variable (unit)	Value
φ_{a1} (-)	1
φ_{a2} (-)	1
S (ppm)	35000
u_s (m/s)	5
P (kPa)	101.325
D (m)	0.02
D (m)	0.2
$\dot{m}_w$ (kg/s)	0.1
T (m)	0.001
k_c (W/m.K)	386
p/d_e (-)	1.25
Humidifier_flux (kg.m^2/s)	2

3.3. Optimization results

Figure 12 shows a Pareto frontier curve, which was obtained to explain the conflict between the two objective functions clearer. Note that points A and B represent the least volume and the highest GOR that could be achieved, respectively. Their optimum value was 4.256 for the highest GOR and 13.12 L for the lowest volume.

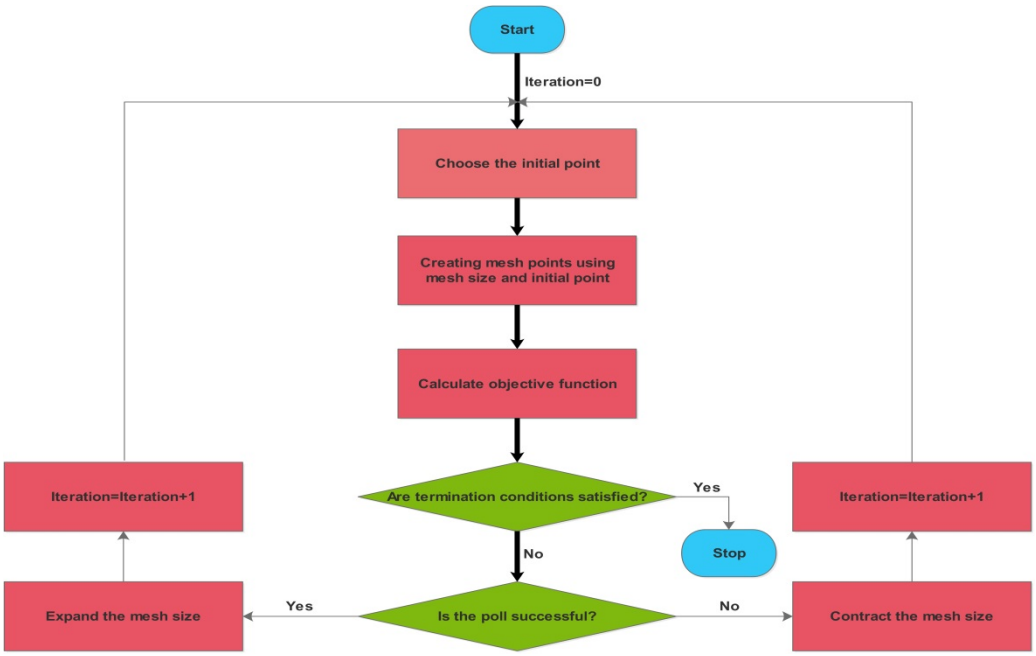

Figure 11. Flowchart of the pattern search optimization.

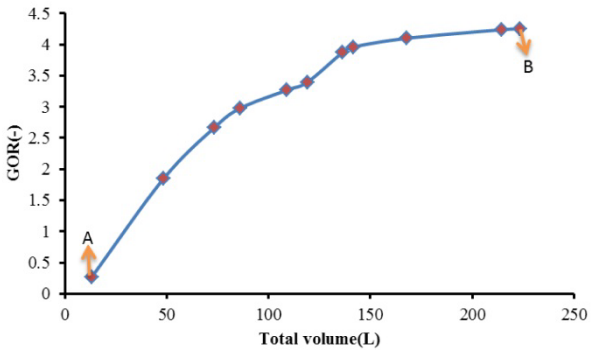

Figure 12. The Pareto curve for the objective functions.

Table 11. Optimized variables of objective functions.

Case	Weight of Volume in optimization (%)	GOR (-)	Volume (L)	Freshwater production (L/day)
1	10	4.239	214.5	216.95
2	20	4.101	167.9	216.17
3	30	3.96	141.5	215.22
4	70	2.98	86.19	303.09
5	80	2.67	73.47	336.18
6	90	1.844	48.36	379.47

Table 12. Optimized variables.

Case	T_{min} (°C)	T_{max} (°C)	e_h (-)	e_d (-)	MR (-)
1	40	60	0.95	0.95	3.162
2	40	60	0.95	0.95	3.427
3	40	60	0.95	0.95	3.722
4	39.03	70.37	0.93	0.93	5.682
5	36.5	71.81	0.91	0.93	5.900
6	30.9	74.56	0.88	0.93	5.992

According to the results of optimization shown in Tables 11 and 12, it can be seen that increasing the weight percentage of GOR caused an increase in its value; in addition, the volume of the system obviously increased. Following results were more interesting:

- Except for the mass flow rate ratio, all of the decision variables were constant at the high weights of the optimization for GOR; this means that this variable is of highest importance. The shift of the mass flow rate ratio is 6.3 % and 17.7 % compared to Case 1, resulting in 3.26 % and 6.58 % decreases in GOR (In Cases 2 and 3, respectively). Other variables are characterized by their best values to optimize GOR rather than volume.
- In Cases 4-6, other decision variables changed, too. Due to the lower effect of the minimum temperature, GOR was optimized with significant changes (6.4 % and 20.83 % for Cases 5 and 6 compared to Case 4, respectively). The maximum temperature varied at lower rates because of the results of the parametric study (Sections 2.2 and 2.5), i.e., the maximum temperature had more effects on the objective functions than the minimum temperature.
- Efficincy of the dehumidifier had significant effects as the mass flow rate ratio on the objective functions; therefore, it changed at a slow rate (in Case 6, it decreased by 1.1 % compared to Case 5). This pattern could be seen to be somewhat faster in the humidifier one (in Case 6, it decreased by 3.2 % compared to Case 5).
- At the higher weights of the optimization for GOR, higher GOR resulted in lower irreversibility and higher freshwater production; however, at the lower weights for GOR, there was higher irreversibility with higher freshwater production. This occurred because of the higher mass flow of the inlet water compared to the air (Mass flow rate ratio).

To sum up, one could find that:

- The minimum and maximum temperatures were separated from each other at lower weights of the optimization for GOR. This fact was correct based on the last part of the parametric study (Section 2.2).
- Because of the higher effects of the heat exchangers and the mass flow rate ratio, these variables could change at a lower rate; however, at least, one should change at a higher rate for producing different solutions in the optimization procedure. Fortunately, because of the ability to control the system by the mass flow rate ratio, this variable is the qualified one among them in this procedure.

Finally, a comparison between the optimized result of freshwater production (as an only objective function) and the results of previous work [23] with the same mass flows of water, air, and the maximum temperature was made, as reported in Table 13:

Table 13. Advantages of the optimization procedure.

Parameter	Present work	Dai et al. [23]
MR (-)	6.14	6.14
T_{max} (°C)	65-85	65-85
Maximum productivity (kg/h)	132	108

According to Table 13, productivity increased by 22 % in the same conditions through the optimization method, showing the advantage of the present work.

4. CONCLUSIONS

In this study, in addition to the thermodynamics and heat transfer analysis of the CAOW-HDH system, useful variables concerning the performance of the proposed system were optimized. One could find that some parameters only affected GOR (e.g., the minimum temperature) or size of the system (e.g., the mass flow rate of each flow and the air velocity in shell), while some others affected both GOR and the size of the system (e.g., the mass flow rate ratio, the maximum temperature, and effectiveness of the humidifier and dehumidifier). A Pareto frontier curve illustrated this conflict between the objective functions for optimized solutions, which were determined by choosing the weights of the multi-objective function. The highest achievable GOR was 4.239 (with 214.5 L for volume), and the lowest volume was 48.36 L (with 1.844 for GOR). The final system was small in

volume due to the type of its heat exchangers and, also, efficient due to its optimized decision variables. In addition, as a suggestion for future research, one can apply the iterative method for determining the size of the packed-bed humidifier according to the complete explanations in [9]; however, it also has to deal with the difficulties in its optimization process.

5. ACKNOWLEDGEMENT

We appreciate all the assistance and guidance that Mr. Faegh has offered to us during the course of this research.

NOMENCLATURE

A	Area
a	Effective surface area per unit volume
CR	Heat capacity ratio
C_p	Specific heat at constant pressure
D, d	Diameter
e	Effectiveness
F	Correction coefficient of heat transfer
f	Friction factor
flux	Water flux in packed-bed
H	Height of the packed-bed
h	Enthalpy (in thermodynamics), Convection heat transfer coefficient (in heat transfer)
h_d	Mass transfer coefficient
k	Thermal conductivity
L	Length
Me	Merkel number
$\dot{m}$	Mass flow rate
N	Number of coils
Nu	Nusselt number
P	Pressure
Pr	Prandtl number
p	Pitch in helical coils
$\dot{Q}$	Heat transfer rate
R	Helix radius of the helical coil heat exchanger
Re	Reynolds number
r	Internal radius of the coil of the heat exchanger
S	Salinity
s	Entropy
T	Temperature
t	Thickness of coils
U	Overall heat transfer coefficient
u	Velocity
V	Volume
w	Weight for the multi-objective optimization
Greek symbols	
μ	Dynamic viscosity
ω	Absolute humidity
φ	Relative humidity
ρ	Density
Subscripts	
in	Input
out	Output
eq	Equivalent
e	External
i	Internal
av	Available
d	Dehumidifier
da	Dry-air
gen	Generation
h	Humidifier
HS	Heat source
s	The shell of the dehumidifier
c	Coils of the dehumidifier
w	water
a1	Input air to the humidifier
a2	Output air from the humidifier
1	Inlet seawater
2	Outlet water from the dehumidifier
3	Inlet hot water to the humidifier
4	Brine
5	Freshwater produced
Abbreviations	
GOR	Gained output ratio
LMTD	Logarithmic mean temperature difference
MR	Mass flow rate ratio
MOF	Multi-objective function
NTU	Number of transfer units
HDH	Humidification dehumidification
CAOW-HDH	Closed air-open water HDH
OACW-HDH	Open air-closed water HDH
OAOW-HDH	Open air-open water HDH

APPENDICES

A. Equation A.8 from Ref. [18] is:

$$Me=2.049MR^{-0.779}\times H^{0.632} \quad (A.1)$$

where this relation is reported by the factory of Brentwood for CF1200MA Cross Fluted Film Fill Media (packing material). This equation relates the Merkel number with the mass flow rate ratio and height of the packing in meters [18].

B. Equation 11.29b from Ref. [19] is:

$$NTU=\left(\frac{1}{CR-1}\right)\times\ln\left(\frac{e-1}{e\times CR-1}\right) \quad (B.1)$$

where CR is less than one. This relation is used for counter flow heat exchangers in the ε-NTU method.

REFERENCES

1. Narayan, G.P., Sharqawy, M.H., Lienhard V.J.H. and Zubair, S.M., "Thermodynamic analysis of humidification dehumidification desalination cycles", ***Desalination and Water Treatment***, Vol. 16, No. 1-3, (2010), 339-353. (https://doi.org/10.5004/dwt.2010.1078).
2. Kabeel, A.E., Hamed, M.H., Omara, Z.M. and Sharshir, S.W., "Water desalination using a humidification-dehumidification technique—A detailed review", ***Natural Resources***, Vol. 4, No. 3, (2013), 286. (http://dx.doi.org/10.4236/nr.2013.43036).
3. Hou, S., Ye, S. and Zhang, H., "Performance optimization of solar humidification–dehumidification desalination process using Pinch technology", ***Desalination***, Vol. 183, No. 1-3, (2005), 143-149. (https://doi.org/10.1016/j.desal.2005.02.047).
4. He, W.F., Wu, F., Wen, T., Kong, Y.P. and Han, D., "Cost analysis of a humidification dehumidification desalination system with a packed bed dehumidifier", ***Energy Conversion and Management***, Vol. 171, (2018), 452-460. (https://doi.org/10.1016/j.enconman.2018.06.008).
5. Faegh, M., Behnam, P. and Shafii, M.B., "A review on recent advances in humidification-dehumidification (HDH) desalination systems integrated with refrigeration, power and desalination technologies", ***Energy Conversion and Management***, Vol. 196, (2019), 1002-1036. (https://doi.org/10.1016/j.enconman.2019.06.063).
6. He, W., Yang, H., Wen, T. and Han, D., "Thermodynamic and economic investigation of a humidification dehumidification desalination system driven by low grade waste heat", ***Energy Conversion and Management***, Vol. 183, (2019), 848-858. (https://doi.org/10.1016/j.enconman.2018.10.044).
7. Zubair, M.I., Al-Sulaiman, F.A., Antar, M.A., Al-Dini, S.A. and Ibrahim, N.I., "Performance and cost assessment of solar driven humidification dehumidification desalination system", ***Energy Conversion and Management***, Vol. 132, (2017), 28-39. (https://doi.org/10.1016/j.enconman.2016.10.005).
8. Niroomand, N., Zamen, M. and Amidpour, M., "Theoretical investigation of using a direct contact dehumidifier in humidification–dehumidification desalination unit based on an open air cycle", ***Desalination and Water Treatment***, Vol. 54, No. 2, (2015), 305-315. (https://doi.org/10.1080/19443994.2014.880157).
9. Dehghani, S., Date, A. and Akbarzadeh, A., "An experimental study of brine recirculation in humidification-dehumidification desalination of seawater", ***Case Studies in Thermal Engineering***, Vol. 14, (2019), 100463. (https://doi.org/10.1016/j.csite.2019.100463).
10. Elminshawy, N.A., Siddiqui, F.R. and Addas, M.F., "Experimental and analytical study on productivity augmentation of a novel solar

humidification–dehumidification (HDH) system", ***Desalination***, Vol. 365, (2015), 36-45. (https://doi.org/10.1016/j.desal.2015.02.019).

11. Gang, W., Zheng, H., Kang, H., Yang, Y., Cheng, P. and Chang, Z., "Experimental investigation of a multi-effect isothermal heat with tandem solar desalination system based on humidification–dehumidification processes", ***Desalination***, 378, (2016), 100-107. (https://doi.org/10.1016/j.desal.2015.09.024).
12. Yıldırım, C. and Solmuş, İ., "A parametric study on a humidification–dehumidification (HDH) desalination unit powered by solar air and water heaters", ***Energy Conversion and Management***, Vol. 86, (2014), 568-575. (https://doi.org/10.1016/j.enconman.2014.06.016).
13. Rajaseenivasan, T. and Srithar, K., "Potential of a dual purpose solar collector on humidification dehumidification desalination system", ***Desalination***, Vol. 404, (2017), 35-40. (https://doi.org/10.1016/j.desal.2016.10.015).
14. Deniz, E. and Çınar, S., "Energy, exergy, economic and environmental (4E) analysis of a solar desalination system with humidification-dehumidification", ***Energy Conversion and Management***, Vol. 126, (2016), 12-19. (https://doi.org/10.1016/j.enconman.2016.07.064).
15. Narayan, G.P. and Zubair, S.M., "Entropy generation minimization of combined heat and mass transfer devices", ***International Journal of Thermal Sciences***, Vol. 49, No. 10, (2010), 2057-2066. (https://doi.org/10.1016/j.ijthermalsci.2010.04.024).
16. Bonafoni, G. and Capata, R., "Proposed design procedure of a helical coil heat exchanger for an orc energy recovery system for vehicular application", ***Mechanics, Materials Science & Engineering Journal***, Vol. 1, (2015), 72-96. (doi:10.13140/RG.2.1.2503.5282).
17. Lazova, M., Huisseune, H., Kaya, A., Lecompte, S., Kosmadakis, G. and De Paepe, M., "Performance evaluation of a helical coil heat exchanger working under supercritical conditions in a solar organic Rankine cycle installation", ***Energies***, Vol. 9, No. 6, (2016), 432. (https://doi.org/10.3390/en9060432).
18. Sharqawy, M.H., Antar, M.A., Zubair, S.M. and Elbashir, A.M., "Optimum thermal design of humidification dehumidification desalination systems", ***Desalination***, Vol. 349, (2014), 10-21. (https://doi.org/10.1016/j.desal.2014.06.016).
19. Bergman, T.L., Incropera, F.P., DeWitt, D.P. and Lavine, A.S., Fundamentals of heat and mass transfer, ***John Wiley & Sons***, (2011).
20. Lewis, R.M., Torczon, V.J. and Kolda, T.G., "A generating set direct search augmented Lagrangian algorithm for optimization with a combination of general and linear constraints', (No. SAND2006-5315), ***Sandia National Laboratories***, (2006). (https://doi.org/10.2172/893121).
21. Conn, A.R., Gould, N.I. and Toint, P., "A globally convergent augmented Lagrangian algorithm for optimization with general constraints and simple bounds", ***SIAM Journal on Numerical Analysis***, Vol. 28, No. 2, (1991), 545-572. (https://doi.org/10.1137/0728030).
22. Conn, A., Gould, N. and Toint, P., "A globally convergent Lagrangian barrier algorithm for optimization with general inequality constraints and simple bounds", ***Mathematics of Computation of the American Mathematical Society***, Vol. 66, No. 217, (1997), 261-288. (https://doi.org/10.1090/S0025-5718-97-00777-1).
23. Dai, Y.J. and Zhang, H.F., "Experimental investigation of a solar desalination unit with humidification and dehumidification", ***Desalination***, Vol. 130, No. 2, (2000), 169-175. (https://doi.org/10.1016/S0011-9164(00)00084-9).

JREE: Vol. 7, No. 1, (Winter 2020) 12-17

Journal of Renewable Energy and Environment

Research Article

Journal Homepage: www.jree.ir

Maximizing Income of a Cascade Hydropower with Optimization Modeling

Hasan Huseyin Coban

Department of Electrical Engineering, Faculty of Engineering, Ardahan University, 75000, Ardahan, Turkey.

PAPER INFO

Paper history:
Received 09 September 2019
Accepted in revised form 23 March 2020

Keywords:
Optimization Based Electricity Market
Cascaded Reservoir Operating Rule
Hydroelectric Producer
Short-Term Hydro Scheduling
Nonlinear Optimization

ABSTRACT

This paper focuses on the short-term cascade hydro scheduling problem, especially in a competitive environment, namely in market conditions. A nonlinear stochastic optimization method is proposed to take into consideration the hydroelectric energy production as a function of hourly electricity market prices and water release rates. In order to solve a case study based on one of the Turkish cascaded hydropower facilities, the proposed method has been successfully applied to a wide variety of problems at a negligible computation time while providing a higher profit. The paper shows the benefits that could be achieved by applying a model based on the Quasi-Newton Method, which finds zeroes or local maxima and minima of solving a certain type of optimization functions because it can better handle the uncertainty, constraints, and complexity of the problem. Ten-year hourly water inflow data and electricity market prices were used as inputs, and the results of the cascade and single optimization were compared. A comparison study with the operation of each hydropower plant (HPP) separately showed that 18 % higher income was obtained with a cascade variant.

1. INTRODUCTION

Electrical energy has become one of the essential souls of developed and developing countries. Electricity can be generated from several kinds of energy sources that are basically listed into two groups as non-renewable and renewable. The efficient usage of renewable (clean and environmentally friendly energy option) energy resources these days is becoming considerably more important because of the limited non-renewable resources [1].

Hydropower is the most widely used renewable power source [2]. This paper aims to develop a control model scheme for cascade hydropower. The term cascade represents a series of hydropower plants (minimum two or more) located upwards the same river or in the same river basin. These energy facilities are hydraulically connected such that the water flows from the upstream powerhouse influencing the storage of the following downstream hydropower house. Therefore, the water flow rate from each power facility should be regulated to prevent needless discharge and overflow, keep the heads as high as possible, and manage reliable reservoir level and inflows.

Since many hydropower facilities are located on the main streams as a cascade, especially in a market environment, the operational optimization has turned into an important issue. During feasibility studies, the rate of return (IRR) is the main element of the initial investment selection and decision and, during the operation, the optimized use of sufficient water and related infrastructure is of great significance. From this perspective, instead of a random (classical) operation, a scheduled operation should consider uncertainties, and including defined constraints will increase the total income by the year-round electric energy production.

Because every hydropower facility and system can be different, each one has its own control schemes according to particular systems, regions, and operating objectives. There are various optimization functions and models that can be examined for various demands and purposes [3,4,5,6]. Mathematically solving the optimal control problems by means of nonlinear-programming (NLP) techniques and simulation for the purpose of investigating the effects of maximizing the income reviewed with reference to several kinds of literature. For a given purpose, they can have significantly differing abilities to perform and solve complexity [6]. In the literature, there are different optimization methods and algorithms available that have been successfully developed for solving optimization problems. It can be classified into two major categories of optimization algorithms widely used today: mathematical programming methods and heuristic search methods [7,8]. The first group covers mixed-integer linear programming [3,4,9,10,11], nonlinear programming [6,12], dynamic programming (DP) [13], and other methods. The second group includes genetic algorithm [4,14] and simulated annealing algorithm. After reviewing the literature, determining which variables are important and how those variables should be formed and optimized is an important designing decision and selection that diversifies in line with the scope of the suggested control strategy. Even though these methods have been shown to be successful in many different cases, there are certainly some disadvantages that cannot be neglected and programmers need to consider when resolving large and complicated HPP operation difficulties such as the incapability to address nonlinearity problems, long execution time, and high amount of memory utilization [9].

The main objective of this study is to maximize income by electricity generation for a cascade hydropower through a non-linear constrained optimization algorithm under the market conditions. From this point of view, the hydraulic design [15] of a cascade is investigated [5,6,16,17].

The data of the hourly water inflows to the reservoirs and electricity market prices [18] are studied. In this paper, a

*Corresponding Author's Email: huseyincoban@ardahan.edu.tr (H.H. Coban)

stochastic optimization approach is proposed for short-term operation planning of the power plant. The time-variant renewable generation based on conditional probabilities of the water inflow and electricity market price values are considered as stochastic variables. It has been proved that the problems of predicting random variables with multi-attributes can be solved better by Artificial Neural Network (ANN) than traditional methods [19].

On different types of hydro scheduling, for example in [20], a non-linear model represents the features of hydroelectric energy production more accurately and takes into account the head dependency of short-term optimal hydro generation scheduling, but water inflow uncertainty is entirely neglected as in most short-term optimization studies [21]; further, similarly, in [22], the determined linear programming model takes into account hourly water flow rates so that it can estimate the uncertainty limited by the volatility of electricity market prices.

In the previous work [23], on optimal hydro scheduling on a single dam operation and feasibility studies was established. Here, this study considered two or more dam operations at minimum and operation management.

The current section clarifies the scope and purpose of this study. Also, it presents the problem statement and compiles relevant literature sources in a review format. The structure of the remaining paper is organized as follows. The optimization process and the objective function formulation of the decision variables subject to constraints for power production and its formulation in MATLAB are explained in Section 2. The third section gives a brief description of chosen power plants as the case study with the optimization procedure. Also, this section shows the results of multi-objective optimization by the proposed algorithm for a real-world hydroelectric power plant (HPP). Finally, the last section concludes the paper and discusses and points out future challenges.

2. PROBLEM FORMULATION

The optimization scheme mainly pictures the efficiency degree, especially for the relationship among the head pond, turbine discharge, water inflow, and power plant generation in the market conditions by taking into account uncertainties. The profit has a stochastic nature and is subject to the electricity market price. Another important assumption is that these hydropower plants are hydraulically coupled cascade water storage systems, where the upstream power plant affects the water level of the reservoir of the downstream hydropower plant. Therefore, the size of reservoirs, as an essential factor in this study, is relatively not large, and the constraint concerning reservoir water level, both upstream and downstream, must be taken into account. Thus, in an overall case, energy generation is directly related to the structural and functional net effective head, where water level fluctuations affect the generating units.

The profit of each power plant can be expressed as follows:

$$\mathrm{Pr} = \sum_{t=1}^{T} c_t . p_t - o_t \quad (1)$$

where c_t is energy market price at time t ($/kWh); p_t is energy generated at time t (kWh); T and t is set and index of production hours in the scheduling horizon and o_t is variable operational costs.

It is assumed that the variable cost of production for HPP operation ranges from 1 % to 4 % of the investment costs per kW per year; in further calculations for our case study as small hydropower, operation cost is assumed to be 2.2 % of the annual income [24].

2.1. The objective function

The optimization process can be conducted after water inflow data, and the electricity market prices for the next day are known. A simplified structure of the power plant optimization algorithm is shown in Figure 1. Also, a model based on Artificial Neural Network (ANN) can be used to predict variables and the advantages of the ANN, making it highly suitable for certain problems [23]. In this study, the historical data including 10-year hourly water inflow data and electricity market prices were used as inputs, and results of the cascade and single optimization were compared.

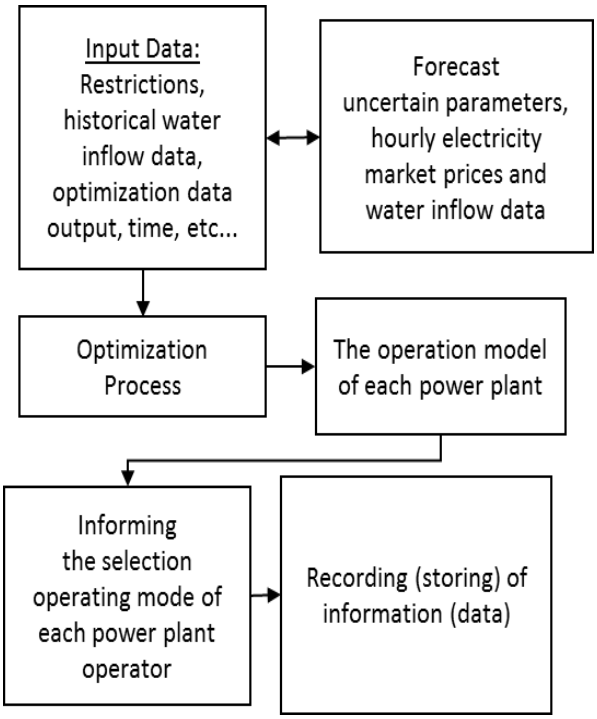

Figure 1. Structure of the cascade power plant optimization chart.

The objective of the hydropower plant is to maximize its own profit in an electricity market, where the total operating costs are subtracted from the revenues. The operating costs consist of generation costs and start-up costs. In this paper, the start-up costs and production/maintenance costs are fixed as 2.2 % of the annual income. Since the price of generated electricity is given on an hourly time scale, it is proposed that the objective function based on variables be considered on an hourly basis as follows:

$$\mathrm{R[f]} = \sum_{z=1}^{2} \mathrm{R}[f_z] \rightarrow \max \quad (2)$$

The mathematical formulation of the problem is summarized as the generated electric power P [W] is related to the potential energy of the (constant) water head H [m]; then, we have:

$$f_z = QgH\eta; \quad (W) \quad (3)$$

where

$$\eta = \eta_{trb} . \eta_{gen} . \eta_{trn} \quad (4)$$

Head is a vertical change in elevation defined as a function of storage.

$$H_t = L_t^{bgn} - Q_t^{usd} + w_t^{inflw} \quad (5)$$

$$L_t^{bgn} = L_{t-1}^{bgn} \sum_{u,\in U_t} Q_{ut}^{usd} + S_{ut}^{spl} \quad (6)$$

$$Pr = \sum_{t=1}^{24} c_t (P_t^A + P_t^B) \rightarrow max \quad (7)$$

Water storage constraints: note that we did not take into account evaporations from the reservoirs. The lower and upper reservoir bounds traditionally show the adequacy of available water.

$$h_z^{min} \leq h_{zt} \leq h_z^{max}; \qquad z \in Z \quad (8)$$

Water discharge constraints across the time horizon with lower and upper bounds:

$$q_z^{min} \leq q_{zt} \leq q_z^{max}; \qquad z \in Z \quad (9)$$

Generated power constraints: Generated power has minimum and maximum bounds:

$$0 \leq P_{zt} \leq P_z^{max}; \qquad z \in Z \quad (10)$$

Water spillage constraints: Environmental flow requirements are considered. The environmental flow determined and recommended by the State Hydraulic Works General Directorate is at least 10 % of the 10-year average lead [25,26].

$$s_{zt} \geq \%\,10.\, w_t^{inflw}; \qquad z \in Z \quad (11)$$

where Pr is profit; z is index of HPP in the cascade; t is hour; g is gravity acceleration (9.81 m/s^2); u is upstream power plant; η_{trb} is turbine (mechanical) efficiency; η_{gen} is generator (electrical) efficiency; η_{trn} is transformer (electrical) efficiency; H is the net head; c_i \$/MWh is the price for 1 MWh during the t^{th} hour; L_t^{bgn} is initial level of water in the reservoir; Q_t^{usd} is water through the turbine(s) for the t^{th} hour; w_t^{inflw} is water inflow rate in the river for the t^{th} hour; Q_{ut}^{usd} is water discharge of upstream plant at time t; S_{ut}^{spl} is the water spillage of the upstream reservoir at time t; P_i^A, P_i^B MW is unknown electrical powers of HPPs for the t^{th} hour; h_z^{min} is the minimum storage; h_z^{max} is the maximum storage; q_z^{min} is the minimum discharge; q_z^{min} is the maximum discharge, P_{zt} is generated power for the t^{th} hour; P_z^{max} is maximum producible power; s_{zt} is the water spillage for fish gate in hour t.

The travel time "t_z" between reservoir "z-1" and reservoir "z" is normalized by the optimization time step t_z. The distance between the HPPs is approximately 6 km. Due to the short distance and based on the information taken from operators in this work, it is implicitly set that t_z = 15 mins.

Herein, η is the total efficiency rate that consists of turbine, transformer, and generator efficiency; it is taken as η= 0,89 as a real data [27] and, in principle, these values for production are not so variable and, thus, an average is of little significance.

This paper poses a question to answer: "How to perform a cascade hydropower analysis using short-term optimization and ensure profit maximization?" The optimization goal is to maximize the benefit of produced energy according to electricity market conditions.

Many optimization techniques have been successfully performed in reservoir operation studies that are summarized and referenced in the first section. Meanwhile, linear [28,29] and non-linear optimization methods are extensively used and reported by researchers [30] as a powerful technique to optimize water resources. In this research, the Quasi-Newton method is used to optimize the cascade hydropower reservoir system; the objective of optimization is to maximize the income by power generation on a daily basis (24h). The necessary data for optimization are given below:

- Maximum and minimum reservoir levels/elevations (Equation 8)
- Power plant efficiency (Equation 4)
- HPP and unit(s) operation constraints and limitations (Equation 5)
- HPP maximum and minimum load (Equation 10)
- HPP restricted zones at different reservoir levels (Equation 11)
- Turbine discharge (Equation 9)
- Electricity market prices.

3. RESULTS AND DISCUSSION (CASE STUDY)

This section presents an effective scheme for real-time operation on the Turkish hydropower system. The system consists of two reservoir types of the hydropower plant along the Karaman River in Posof, Ardahan city. The aim of the research is to analyze performance improvements while optimizing real-time operations. The formulation of the objective function is to maximize the sum of income by each hydropower plant.

A real-world cascade power plant with separate dams as a case study is examined. Then, there is an opportunity to compare the results by a single dam operation. The operation of the HPPs is subject to several constraints due to safety and environmental issues. Table 1 below summarizes the technical specifications of the HPPs. During optimization studies, all these constraints are taken into account. Both power plants have 2 turbines, while the installed capacity of Sogutlukaya HPP is 6.1 MW/h, Merekler is 11.2 MW/h. Although the hydroelectric power plants are in the same river, the amount of energy to be produced is different due to the different levels of heads and Merekler HPP feeds by two rivers. The following table shows rated discharge as 4.5 m^3/s and rated head of turbine discharge as 11.1 m^3/s, with wicket gates in a fully open position to meet the rated power capacity.

Table 1. The characteristics of hydropower plants on River Karaman.

HPP	Number of units	Rated discharge	Rated power	The heads
Sogutlukaya (Posof III) HPP	2	4.5 m^3/s	6.1 MW/h	155 m
Merekler weir and Alagolu HPP	2	11.1 m^3/s	11.2 MW/h	115 m

An illustration of a cascade hydropower system is shown in Figure 2, where downstream reservoirs are fed by the release from the upstream reservoirs and, additionally, the second reservoir is also fed by an intermediate flow.

Generally, the highest observed electricity prices correspond to the hours when generation is at its highest capacity; it can only be influenced by reservoir size and level. It is a great opportunity that hydropower plants can be employed by increasing their energy generation during periods of peak

loads, reducing the need for the dispatch of expensive natural-gas power plants and reducing the overall system costs. In other words, HPPs represent the insurance for Turkey's electricity. Each power facility operates in line with the scheme shown in Figure 3. The optimization results and water level statistics in reservoirs are shown in Figures 4 and 5, respectively.

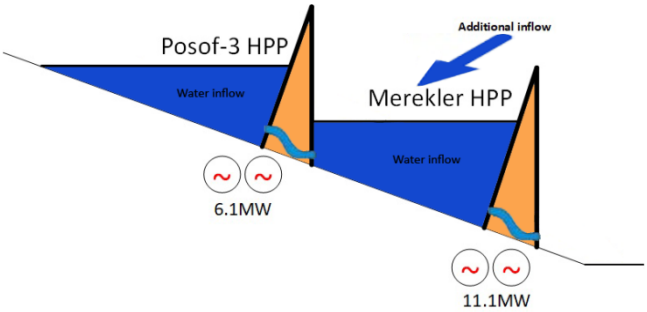

Figure 2. The illustration of the studied cascade HPPs.

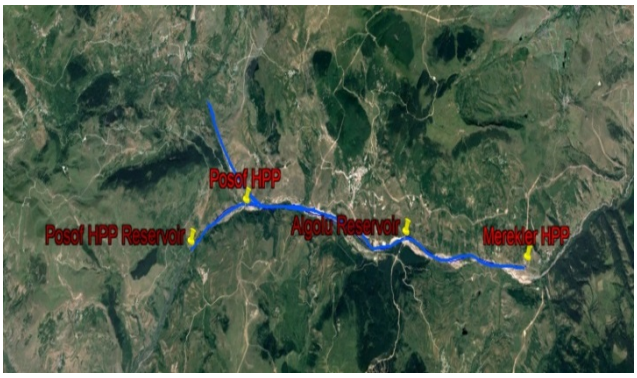

Figure 3. Disposition of the system of cascade HPPs on the lower part of the River Karaman.

Figure 4 shows the generated power (MW/h) in Posof HPP and Merekler HPP and electricity market prices (EUR/MWh). The method stores energy in the form of water in the reservoir during off-peak time. During the peak demand for electricity, the stored water is released from the reservoir through turbines. In this way, energy can be stored so that it can be released quickly when needed.

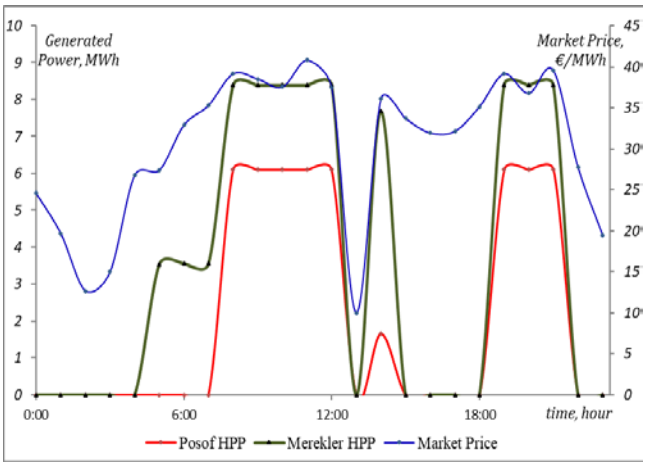

Figure 4. Dispatch schedule of the cascade HPPs.

Figure 5 represents the water evacuation of water in meters in Posof and Merekler dam.

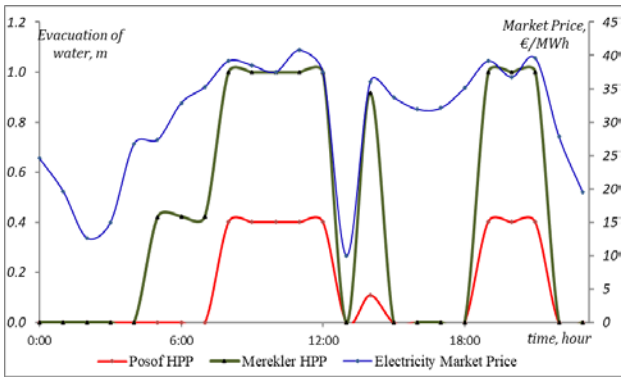

Figure 5. Evacuation of water schedule of the cascade HPPs.

Figure 6 shows optimized reservoir elevations for each hydropower plant. When there is low consumption (off-peak), the water existing in the accumulation reservoirs is used. When it is needed, this cumulated water could be used for electricity production. There is no overflow depending on the water levels in the reservoirs.

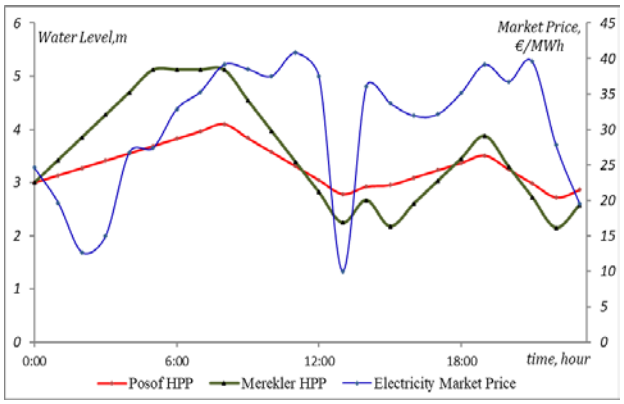

Figure 6. Water level in the reservoir basin.

A comparison of optimization performance can be made in terms of computational time and income rate. The results of the study showed that the revenue values of each HPP increased by approximately 18 %. Figure 7 shows the income comparison of HPPs. The results of optimization in real-life income and multi-reservoir system demonstrate that the use of the optimized HPPs would manage the system more efficiently in the multi-reservoir than in a single reservoir. It is very important to share information about the water level in reservoirs, the timing of water release, the planning produced power, etc.

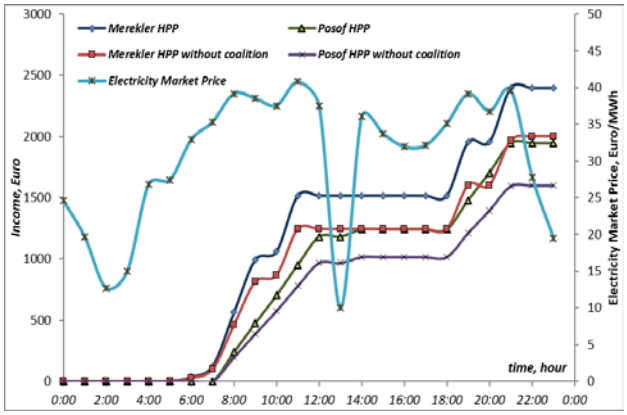

Figure 7. Pre- and post-optimized results versus electricity market price.

The results showed that the developed MATLAB script could approach an optimal solution that meets constraints and variables. The comparison made with individual runs of each power plant showed that 18 % higher income was attained with the cascade variant. The program was run for the cascade dam operation. Calculation time was approximately 46 seconds for the single runs in the 24-hour cascade case. This implies that runtime for the cascade case is within an order of magnitude and can easily be figured out with a regular office PC. The calculations were carried out on an Intel® Core™ 2 Duo CPU E7500 machine with 4GBs of RAM and Windows 10 operating system. A possible improvement can be achieved by submitting a more efficient algorithm with better performance for many decision variables.

4. CONCLUSIONS AND FUTURE WORK

This paper considered reservoir-based cascade hydropower to achieve the objective of maximizing the income from selling electricity in the day-ahead market. Within this scope, it supported a tool that allowed a power producer company to determine the short-term (24 h, but it can be easily extended) self-planning of its cascading facilities along a river basin. This paper proposed a dynamic non-linear programming model to account for each power plant based on the relationship among the head, the installed power capacity, and the water discharged, considering limitations. The mathematical model for the daily optimal scheduling of a hydropower plant cascade was successfully tested on a real-world case study. A MATLAB script was developed according to the electricity initial reservoir level and water inflow values as inputs, and the constructed script was used in the optimizer. The optimization method, used to solve the parametric equations, produced a stochastic optimization algorithm. As a result, it was found that hydroelectric power plants could increase their income by sharing information such as operation scheduling and reservoir levels.

As a future study, units might be divided, and the travel time between the upstream dam and downstream should be considered in a more detailed study. Additionally, the startup costs of implementing efficient algorithms should be considered as well. Further, any future work is advised to include the implementation of different objective functions for maximizing water use efficiency and assessment of the scheme based on various power generation and constraint scenarios.

5. ACKNOWLEDGEMENT

The present author would like to thank power plant operators and owners for their contribution to this paper and for their valuable technical support on this project. We appreciate the support given by the staff of Posof-3 and Merekler power plants and their help to collect the plant and river data and all the technicians who helped us handle the instruments.

REFERENCES

1. Application of non-conventional renewable energy sources, Bureau of Energy Efficiency, p 147.
2. World Energy Council, World Energy Resources Report, (2016), p 3.
3. Zicmane, I., Mahnitko, A., Kovalenko, S., Georgiev, G. and Kim, D., "Algorithmization in the task of optimization of cascade hydro power plants", ***Proceedings of 2017 IEEE Manchester PowerTech***, Manchester, UK, (2017), 1-6. (DOI: 10.1109 / PTC.2017.7980989).
4. Feng, Z.K., Liu, S., Jiang, Z.Q., Luo, B. and Miao, S.M., "Multi-objective operation of cascade hydropower reservoirs using TOPSIS and gravitational search algorithm with opposition learning and mutation", ***Water***, Vol. 11, No. 10, (2019), 2040. (DOI: 10.3390/w11102040).
5. Zhang, Y., You, J., Ji, C. and Wu, J., "Short-term operation optimization of cascade hydropower reservoirs with linear functional analysis", ***Proceedings of International Conference on Geo-Spatial Knowledge and Intelligence***, Springer, Singapore, (2017), 107-116.
6. Cuvelier, T., Archambeau, P., Dewals, B. and Louveaux, Q., "Comparison between robust and stochastic optimisation for long-term reservoir management under uncertainty", ***Water Resources Management***, Vol. 32, No. 5, (2018), 1599-1614.
7. Marko, V., "Value of stochasticity in hydropower planning optimization", Master Thesis, XR-EE-ES 2012:008, (2012).
8. Technical report, "Advanced algorithms for hydropower optimization", U.S. Department of the Interior, Bureau of Reclamation, Technical Service Center, Denver, Colorado, (2012), S&T-2011-486, (2011).
9. Chang, G.W., Aganagic, M., Waight, J.G., Medina, J., Burton, T., Reeves, S. and Christoforidis, M., "Experiences with mixed integer linear programming based approaches on short-term hydro scheduling", ***IEEE Transactions on Power Systems***, Vol. 16, No. 4, (2001), 743-749. (DOI: 10.1109/59.962421).
10. Belsnes, M.M., Wolfgang, O., Follestad, T. and Aasgard, E.K., "Applying successive linear programming for stochastic short-term hydropower optimization", ***Electric Power Systems Research***, Vol. 130, (2016), 167-180. (DOI: 10.1016/j.epsr.2015.08.020).
11. Grygier, J.C. and Stedinger, J.R., "Algorithms for optimizing hydropower system operation", ***Water Resources Research***, Vol. 21, No. 1, (1985), 1-10. (DOI: 10.1029/WR021i001p00001).
12. Arunkumar, R. and Jothiprakash, V., "Optimal reservoir operation for hydropower generation using non-linear programming model", ***Journal of The Institution of Engineers (India): Series A***, Vol. 93, No. 2, (2012), 111-120. (ISSN: 2250-2149, (Print) 2250-2157 (Online)).
13. Feng, Z.K., Niu, W.J., Cheng, C.T. and Wu, X.Y., "Optimization of hydropower system operation by uniform dynamic programming for dimensionality reduction", ***Energy***, Vol. 134, (2017), 718-730. (DOI: 10.1016/j.energy.2017.06.062).
14. Al-Aqeeli, Y.H., Lee, T.S. and Aziz, S.A., "Enhanced genetic algorithm optimization model for a single reservoir operation based on hydropower generation: Case study of Mosul reservoir, northern Iraq", ***SpringerPlus***, Vol. 5, No. 1, (2016), 797. (DOI: 10.1186/s40064-016-2372-5).
15. Rai, R. and Nagasaka, K., "Modeling and development of run-of-river cascade hydropower plants in Nepal", ***Journal of Clean Energy Technologies***, Vol. 5, No. 6, (2017), 469-474. (DOI: 10.18178/JOCET.2017.5.6.418).
16. Li, S., Li, Y. and Zhao, D., "Study on optimal operation of cascade hydropower stations under complex constraints", ***Journal of Residuals Science & Technology***, Vol. 13, No. 6, DEStech Publications Inc., (2016). (Doi: 10.12783/issn.1544-8053/13/6/58).
17. Wolf, A.J. and Lindber, P.O., " Optimal short-term operation of a cascade of hydropower Stations", ***Transactions on Ecology and the Environment***, Vol. 12, WIT Press, (1996). (ISSN 1743-3541).
18. Statistical data from Nordpool spot, (www.nordpoolspot.com).
19. Masters, T., Practical neural network recipes in C++, Morgan Kaufmann, (1993).
20. Xi, E., Guan, X. and Li, R., "Scheduling hydrothermal power systems with cascaded and head-dependent reservoirs", ***IEEE Transactions on Power Systems***, Vol. 14, No. 3, (1999), 1127-1132. (DOI: 10.1109/59.780941).
21. Guan, X., Svoboda, A. and Li, C.A., "Scheduling hydro power systems with restricted operating zones and discharge ramping constraints", ***IEEE Transactions on Power Systems***, Vol. 14, No. 1, (1999), 126-131. (DOI: 10.1109/59.744500).
22. Conejo, A.J., Arroyo, J.M., Contreras, J. and Villamor, F.A., "Self-scheduling of a hydro producer in a pool-based electricity market", ***IEEE Transactions on Power Systems***, Vol. 17, No. 4, (2002), 1265-1272. (DOI: 10.1109/TPWRS.2002.804951).
23. Coban, H.H., "Optimization techniques in short and long-term power production at small hydropower plants", Ph.D. Thesis, (2016).
24. Renewable energy technologies: Cost analysis series, Hydropower, Volume 1: Power sector, Issue 3/5, International Renewable Energy Agency(IRENA), (2012).

25. Yaşar, M., Baykan, N.O. and Bulbul, A., "Akişaşagisina Birakilmasi Gerekli Debi Yaklasimlari", ***Proceedings of II. Su Yapıları Sempozyumu, 16-18 Eylül 2011, Diyarbakır***, (2011), 211-218.
26. Karakoyun, Y. and Yumurtaci, Z., "Hidroelektrik Santral Projelerinde Çevresel Akis Miktarinin ve Çevresel Etkinin Değerlendirmesi", ***Tesisat Mühendisliği Dergisi***, (Kasim/Aralik, 2013), 1-16.
27. Datasheet of turbine, generator and transformer of Posof HPP and Merekler HPP.
28. Gullhamn, E., "Control of water content and retention in hydropower plant cascades", Master Thesis, IR-RT-EX-0410, Stockholm, Sweden, (2004).
29. Hamann, A. and Hug, G., "Real-time optimization of a hydropower cascade using a linear modeling approach", ***Proceedings of 2014 Power Systems Computation Conference***, IEEE, (2014), 1-7. (DOI: 10.1109/PSCC.2014.7038354).
30. Apostolopoulou, D. and McCulloch, M., "Cascade hydroelectric power system model and its application to an optimal dispatch design", ***Proceedings of IREP'2017-10th Bulk Power Systems Dynamics and Control Symposium***, Espinho, Portugal, (2017).

JREE: Vol. 7, No. 1, (Winter 2020) 18-32

Journal of Renewable Energy and Environment

Research Article

Journal Homepage: www.jree.ir

Economic Evaluation of Cooling Storage Warehouses in Hot and Dry Regions for Fruits Using Different Renewable Energies

Ali Mostafaeipour*, Afsaneh Nasiri

Department of Industrial Engineering, Yazd University, Yazd, Iran.

PAPER INFO

Paper history:
Received 17 October 2019
Accepted in revised form 28 March 2020

Keywords:
Renewable Energy
Energy Efficiency
Fruit Storage Warehouses
Solar Air Conditioner
Economic Evaluation

ABSTRACT

In hot and dry regions, air conditioning is used for many different applications like residential, industry, and agriculture and dairy products. This research studies the applicability of wind and solar energies for cooling fruit storage warehouse in the hot and dry region of Yazd in Iran. The studied case is a fruit warehouse with an area of 4240 m^2 resulting in a storage capacity of about 1000 tons. For this purpose, the heat gain of the warehouse is determined, and the obtained cooling load is then used to examine the solar and wind energy to power a conventional warehouse system. Different scenarios are examined for this research such as solar air conditioner, solar absorption chiller, wind catcher, and a combination of solar air conditioners and solar absorption chiller for cooling the fruit warehouse. Comparison and economic evaluation of different scenarios show that the solar air conditioning ranks first for this purpose. Results are then validated using value engineering methodology. Solar air conditioning with the highest net present value (NPV) of 4,865,040,418 Rials and the best internal rate of return (IRR) value of 182.98 % was determined to be the best approach among the studied methods. The results of this research can be applied to other regions with similar climatic conditions too.

1. INTRODUCTION

Fossil fuels such as oil and gas are nonrenewable sources of energy with detrimental pollution outputs. In addition, the depleting reserves of fossil fuels ensure that they will get more expensive in the future. These issues highlight the importance of the constant search for clean, permanent and cost-effective methods of energy supply. One such method is the effective use of renewable energy sources such as wind or the sun [1].

Today, fossil fuels are the main sources of energy in the world, but adverse global consequences like environmental pollution, global warming, and sea-level rise are considered as a common cause of these problems [2]. There have been numerous renewable energy researches in the literature, but solar and wind energies share more than other sources [3-6]. Global warming, adverse environmental impact, and limited resources of fossil fuel have resulted in discovering the importance of implementing alternative systems of energy [7-11]. Nowadays, many countries decided to begin paying more attention to replacing fossil fuels with different renewable energy sources [12]. Economic aspects of using electricity and high consumption have become an important concern of Iran for many years [8]. An important role of renewable energy technologies is its share in the energy production field, which must energy demands of industries [13, 14].

Iran is located on the radiation belt [15] which provides great potential for the use of solar power and is also positioned in a low pressure area relative to high pressure areas in north and northwest, which causes many winds in both winter and summer [16].

Distribution of water energy, wind energy, solar energy, and other resources in the world are illustrated in Table1. It shows that Asia shares 25 % of wind resource, and also 25 % of solar energy in the world and therefore provide good wind and solar energy potential [17]. Clearly, Africa has the highest capacity of wind and solar in the world.

Consumption of fossil fuel can be reduced by heating and cooling the buildings by renewable energies such as wind and solar which are not only permanent and clean but also cost effective. In recent years, engineers and architects have paid unparalleled attention to the use of these renewable energies to provide heating and cooling [18].

Solar radiation reaching unevenly to the earth's rough surface results in temperature and pressure variations that produce massive air flows known as wind. The wind is also a product of the earth's rotation, which causes heat transfer in the earth's atmosphere from warm regions to polar areas [19].

Wind energy can be used to produce electricity and provide cooling. One of the most basic cooling systems is air conditioning by drawing fresh air into the building and using the airflow to discharge the warm and polluted air out of it. The traditional system used for this purpose is known as wind catcher [18].

Wind catcher is an architectural element traditionally used for cooling and air conditioning in warm and dry regions [20]. A wind catcher causes the fresh air to flow into the building, which results in negative pressure on the other side pushing the warm air out of the building. Some wind catchers have a shelf with a wooden door to control airflow and works as a container like today's fridges. Based on the outer shape, wind catchers are divided into several groups: one-sided, two-sided, three-sided, four-sided, eight-sided, and double [21]. Figure 1 shows a typical four-sided wind catcher in Yazd, Iran [22].

Solar energy is a promising source of energy for the future needs of many sectors in different parts of the world. The earth relies on the sun to provide a majority of its required

*Corresponding Author's Email: mostafaei@yazd.ac.ir (A. Mostafaeipour)

energy. Wind energy, sea waves, and even fossil fuels stored within the earth are the results of the solar energy received by the earth. Solar energy can be converted into other forms of energy directly or via indirect measures. For example, solar energy can be converted to electricity using solar panels [23, 24].

Table 1. Distribution of water energy, wind energy, solar energy and other resources in the world [17].

Region	Water energy		Wind energy		Solar energy	
	Theoretical reserves (trillion of kwh/year)	Proportion (%)	Theoretical reserves (trillion of kwh/year)	Proportion (%)	Theoretical reserves (trillion of kwh/year)	Proportion (%)
North America	6	15	400	20	16500	11
South America	8	21	200	10	10500	7
Europe	2	5	150	8	3000	2
Asia	18	46	500	25	37500	25
Africa	4	10	650	32	60000	40
Oceania	1	3	100	5	22500	15
Total	39	100	2000	100	150000	100

Figure 1. A typical wind catcher in Yazd [22].

The solar energy map of the world is illustrated in Figure 2. In this map, the areas with a high solar energy potential are colored orange, and as can be seen, Iran falls in this category [25].

Figure 3 displays the solar energy map of Iran. In this map, the areas with a high solar energy potential are marked with a star. As this figure shows, Yazd is one of these areas [26].

This paper is structured as follows: In the next section, the literature review is presented in detail. Section 3 describes methodology. Section 4 presents the value engineering methodology. Case study is presented in section 5. Analysis is discussed in section 6. The economic evaluation is presented in section 7, and economic comparison is presented in section 8. Section 9 presents the validation, and finally conclusion is brought in section 10.

2. LITERATURE REVIEW

In this section, we will review the literature on the subject of study. There have been numerous research works which showed Iran is capable of using different sources of renewable energies [5,6,26-30].

Clark et al. [30] assessed the efficiency of a building's energy in two types of systems: standard and renewable. The building's required energy for cooling and heating was measured by two systems and the results showed that using solar energy and photovoltaic system increases the building's energy efficiency.

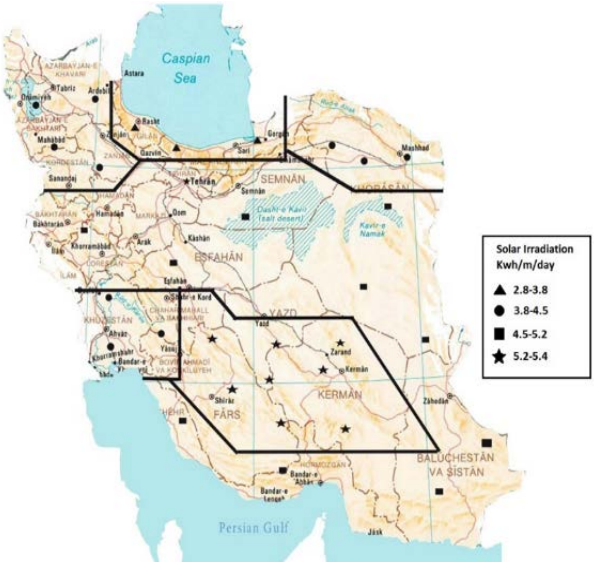

Figure 2. Solar energy map of Iran [25].

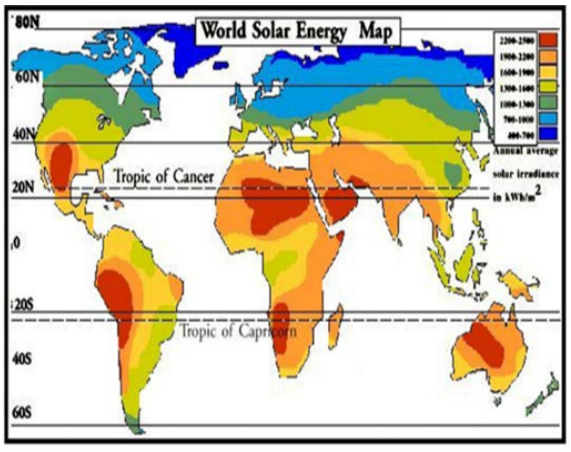

Figure 3. World solar energy map [26].

In a study by Hua and Shiu [31], where they investigated the use of renewable energies in Wangan Island of Taiwan, they found that using a wind-solar hybrid system can result in more than 50 % reduction in CO_2 emission and 23-27 % reduction in the cost of electricity consumed.

In an article by Danish and Wang [32] titled the "Role of renewable energy and non-renewable energy consumption on EKC: Evidence from Pakistan", it was reported that the use of

renewable energies can play a main in reducing CO_2 emissions and non-renewable energies use and that there is a bi-directional causality relationship between renewable energy use and CO_2 emission. It was also stated that to promote renewable energy use, the government has to increase investment in renewable energy projects.

Shahsavari and Akbari [33] studied the potential of developing countries in using solar energy to reduce greenhouse gas emissions. This study found that given the significant solar energy potential of many developing countries, the promotion of solar energy generation in these countries can be an effective strategy for reducing their greenhouse gas emissions. They added that to achieve this goal, governments of developing countries have to adopt a set of measures to support solar energy development and reduce dependence on fossil fuels and biomass resources; measures that may include restrictive laws and regulations, financial incentives, tax incentives, research and development programs, reduction or elimination of fossil fuel subsidies, and creation of a support program for investment in solar energy sector.

In an article by Lang et al. [34], they carried out a technical and economic analysis on the use of a grid-connected PV system for power generation in a residential unit. They also studied the geographical, technical and economical parameters of the study area and concluded that the PV system can be an attractive option in many areas; but the low cost of power (and fossil fuel subsidies) is a strong obstacle for further use of PV systems.

In an article by Askari et al. [35] titled "Energy management and economy of the system, solar PV, solar collector and fuel cost", they assessed the effect of solar panel, solar collector and fuel cost on the optimization of a cooler. The system was considered for supplying cooling and heating energy and power of a 5-story residential building. In the end, they concluded that removing the fuel subsidy would result in the PV system and generally all solar energy systems to become more attractive.

Daneshvar et al. [36] assessed the economic potential of using a solar air conditioner for reducing the peak loads in Gilan. They concluded that the allocation of government subsidies for the use of hybrid solar conditioners can be effective in all areas even in the clouded northern region of the country. Some of the mentioned effects included: reduced production costs, reduced peak load, reduced loss, increased reliability, reduced consumer cost, job creation, increased equipment lifetime, increased efficiency due to high efficiency of solar cells, environmental merits, etc.

Abdullah et al. [37] assessed the use of solar absorption chiller in three cities of Italy. They used the software TRNSYS17 for modeling and the software GenOpt for optimization. They concluded that using a solar chiller in these three cities increases energy efficiency and reduces power consumption.

In an article by Saffar [38], the author assessed the use of cooling apparatus such solar panels, wind catcher and solar chiller in a residential building in Bahrain, and concluded that using this cooling measures is significantly effective and results in reduced power consumption, reduced energy bill, and increased thermal comfort for residents.

In an article by Mostafaeipour & Bardel [22] titled "economic evaluation of surface and subsurface warehouses cooled with wind catcher: a case study", the authors assessed the use of cooling systems based on free natural energies such as wind and underground temperature gradient and carried out an economic analysis on the use of these measure in a medicine warehouse. The medicine warehouse with an absorption chiller was compared first with the one with a wind catcher and then with a warehouse built underground. For this purpose, heat gain and the costs associated with each project were calculated and then economic evaluation was carried out with the uniform annual cost method. The results showed that the warehouse with wind catcher is far more economical than the one with an absorption chiller, and in case of needing a new warehouse, constructing the facility underground would result in lower energy loss and would be more economical than constructing an ordinary warehouse with an absorption chiller.

3. METHODOLOGY

This study examines the use of free natural energies, wind and solar, for cooling a warehouse dedicated to fruit storage. For this purpose, first, the heat gain of facility is calculated; then the resulting cooling load is used to examine the utility of solar panels (to power a conventional warehouse), solar air conditioners, solar absorption chiller, wind catcher, and a combination of solar air conditioner and solar absorption chiller for cooling a typical fruit warehouse in Yazd. Finally, the method is evaluated economically by the software COMFAR as well as the value engineering technique.

3.1. Warehouse

Warehouses are stationary or mobile refrigerated spaces for storage of foodstuffs and operate with a mechanism similar to conventional refrigerators. A typical warehouse generally consists of a motor, compressor, condenser, nitrogen store, expansion valve, blower (fan) and connecting tubes [39].

3.2. Calculation of cooling load

The first step is to obtain the cooling load of the warehouse. To simplify the calculations, the total cooling load is divided by the heat source. Thus, the total cooling load is the sum of:

1. Wall, roof and floor gain load
2. Air change load
3. Product load
4. Respiration load
5. Miscellaneous load

The Equations used for calculation of these loads are described in the following:

3.2.1. Wall, roof, and floor gain load

The energy loss due to heat exchange through a wall is calculated by Equation (1) [22]:

$$Q = AU(T_i - T_0) \quad (1)$$

where A is the area of the wall, U is the overall heat transfer coefficient, T_0 is the temperature of the outer layer and T_i is the temperature of the inner layer.

Overall heat transfer coefficient (U) is obtained from Equation (2) [22, 40]:

$$U = \frac{1}{\frac{1}{f_i} + R_1 + R_2 + R_3 + R_4 + \cdots + \frac{1}{f_O}} \quad (2)$$

where R_i is the thermal resistance of the different layers of the wall, and is obtained by the following Equation [22]:

$$R = \frac{X}{K} \quad (3)$$

where X is the wall thickness, k_i is the wall conduction coefficient, $\frac{1}{f_i}$ is the surface conductance of the outside conductance of the inside wall, floor, or ceiling and $\frac{1}{f_o}$ is the surface conductance of the outside wall, floor, or ceiling. k_i depends on the material of the wall and is obtained from Table A (Appendix).

3.2.2. Air change load

Air change load is calculated by Equation (4) [40]:

$$\text{Air change load (KW)} = \text{Air infiltration rate } (\tfrac{l}{s}) \times (h_0 - h_i)\,\tfrac{kJ}{s} \quad (4)$$

where h_0 is the enthalpy of outside air and h_i is the enthalpy of the inside air. The enthalpy change coefficient for the incoming air is obtained from Table D (Appendix) according to its temperature and temperature and humidity of the warehouse. The approximate air infiltration rate is obtained from Table E (Appendix) according to the size of the warehouse.

3.2.3. Product load

The amount of heat released by the product is calculated by Equation (5) [40]:

$$Q\ (W) = \frac{(m)(c)(T_i - T_0)}{\text{chilling rate factor} \times \text{cooling time(s)}} \quad (5)$$

where m is the product weight, c is the specific heat above freezing (kj/kg/K), T_0 is the entering temperature (K), and T_i is the space temperature (K).

Space temperature refers to the temperature of the room where products are to be stored, entering temperature refers to the temperature of the space from which products are transferred to the warehouse, and chilling rate factor and c are obtained from Table F (Appendix) according to product type and storage temperature.

3.2.4. Respiration load

Respiration load is calculated by Equation (6) [40]:

$$Q\ (W) = \text{Weight of product (kg)} \times \text{Respiration heat } (^{W}/_{kg}) \quad (6)$$

where respiration heat is obtained from Table G (Appendix) according to product storage temperature. Respiration heat means oxidizing the six carbohydrates and converting them to carbon dioxide and water with the help of enzymes that release energy.

3.2.5. Miscellaneous load

The heat load due to lighting is obtained from Equation (7) [40]:

$$Q = \frac{P \times t}{24hr} \quad (7)$$

where P is the power of lights and t is the working time (hr).

Heat load due to the presence of people is calculated by Equation (8) [40]:

$$Q = \frac{n \times ph \times T}{24hr} \quad (8)$$

where n is the number of people, ph is the person's heat and T is working time (hr). hp is obtained from Table H (Appendix) according to the temperature of the point where the person stands.

Heat load due to operation of forklifts is obtained using Equation (9) [40]:

$$Q = \frac{n \times P \times t}{24hr} \quad (9)$$

where n is the number of forklifts and P is the Power of forklift and t is working time(hr).

Heat load due to boxes is obtained from Equation (10) [40]:

$$Q\ (kj) = \text{number of boxes} \times \text{Weight of each box (kg)} \times \text{Specific heat of each box} \times (T_i - T_0)(K) \quad (10)$$

where T_0 is the entering temperature (K) and T_i is the space temperature (K). Again, entering temperature refers to the temperature of the space from which products are transferred to the warehouse, and space temperature is the temperature of the room where products are to be stored.

3.3. Comfar software

Comfar is a software program developed by the United Nations Industrial Development Organization (UNIDO) for designing and evaluation economic development plans in developing countries [41]. This software can be used for estimating the revenue and cost of industrial, mining, agriculture, infrastructure, maritime, and many other types of projects [42].

3.4. Net Present Value (NPV)

Net Present Value (NPV) is a measure for the evaluation of returns of an investment with the time-variant value of the money taken into account. The present value of future cash flows can be determined by Equation (11):

$$NPV = NFC_0 + \frac{NFC_1}{(1+i)^1} + \frac{NFC_2}{(1+i)^2} + \ldots + \frac{NFC_t}{(1+i)^t} \quad (11)$$

where NPV is the net present value, i is the discount rate, and t is the time period. NPV may be positive, negative, or zero. The higher the discount rate is, the lower the present value of the future cash will be.

- IF: NPV> 0 → the project can be considered.
- IF: NPV = 0 → the project can also be considered.
- IF: NPV <0 → the project must be disregarded.

If, after applying a certain discount rate as the minimum rate to attract investment and taking into account the effect of inflation, calculations show that NPV of a project is positive, that project will have economic feasibility. Also, the larger the calculated NPV is the more attractive will be the investment [43].

3.5. Internal Rate of Return (IRR)

Internal rate of return (IRR) is another criterion for economics evaluation of projects and is commonly used to assess the desirability of an investment. In the NPV-discount rate plot, IRR of a project is the point where the curve intersects with the horizontal axis. For a project to be more desirable, the value of IRR, which is obtained by equating the project's NPV to zero, has to be greater than IRR of alternatives [44].

4. VALUE ENGINEERING METHODOLOGY

Value engineering is a systematic method of organizing creativity and teamwork to solve problems, reduce costs, and improve the performance and quality of projects, products and processes. Value engineering utilizes a wide range of expert knowledge and experience with a focus on the functions of the project, product or process to quickly provide applicable solutions for improving the results. The main procedure of value engineering consists of several phases: information phases, function analysis phase creativity phase, and evaluation phase, which are briefly described in the following.

4.1. Information phase

The purpose of this phase is to understand and define the current status of the project and the constraints affecting its outcomes as well as the objective of the effort. The activities to be done this phase include:

- Acquiring key data, information and documents, such as project scope and definitions, plans, specifications, reports, detailed project costs, and qualitative data.
- Provision of a main plan or design/product/process concepts by the project team.
- Defining the scope, schedule, budget, expenses, and non-financial performance criteria of the project.

4.2. Function analysis phase

The purpose of this phase is to understand the project from the functional perspective, in the sense that what functions the project should have rather than how it is now. The activities this phase include:

1. Determining the project functions by means such as random determination.
2. Classification of project functions.
3. Scaling the model with the parameters of cost, performance characteristics and user behavior in order to identify the value-incompatible functions and focus the creativity phase. The tools used in this phase include cost/function analysis (function matrix), and performance/function analysis.

4.3. Creativity phase

The objective of this phase is to produce a number of ideas regarding other methods of achieving the desired functions. In this stage, a group of usually 4 to 6 people with different specialties use techniques such as brainstorming to express their thoughts and ideas. In these sessions, people are encouraged to provide diverse views and no idea is criticized.

4.4. Evaluation phase

The purpose of this phase is to reduce the number of ideas to produce a shortlist of solutions with the highest potential for fulfilling the desired functions subject to quality requirements and resource constraints [45]. Some of the activities that should be carried out in this phase include:

1. Explaining and categorizing every idea to create a common understanding.
2. Discussing the impact of ideas on performance parameters and project cost with the help of tools such as T-Chart.
3. Prioritizing ideas for further development with the help of tools such as lifetime cost calculations.

In this paper, validation is performed by using Value Engineering (VE) technique. In VE, the criteria by which alternatives are to be evaluated are determined by brainstorming. Then options to reduce product prices to maintain its quality are obtained via creative analysis. The relative importance of the criteria is determined by pairwise comparison and the weight of each criterion equals the sum of all of the preference scores relative to other criteria. Finally, the weight of the criterion is multiplied by the normalized decision matrix to obtain the final score of each alternative, and the alternative with the highest score is determined to be as the best option [27].

5. CASE STUDY

5.1. Geoghraphic characteristics

The studied warehouse is located in the city of Yazd in Iran. This city is located at 37 ̊54' E and 31 ̊90' N on a desert valley between the mountains of Shirkooh and Kharanaq. The city has an area of 31539 m^2 and a mean height of 1200 meters above the sea level [46]. Figure 4 illustrates the location of Yazd [47].

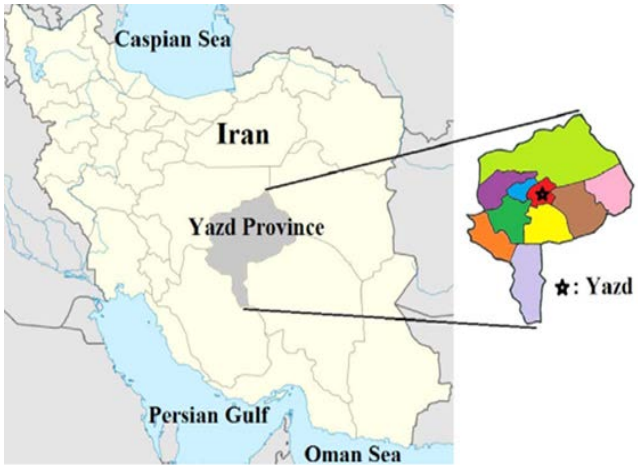

Figure 4. Location of Yazd [47].

Based on the information provided by the Meteorological Organization of Yazd, climatic conditions of the city are as follows (the following are the averages of previous years):

In Yazd, the average temperature is 18.9 °C; during warm months, the average temperatures is 30 °C and the diurnal temperature difference is 12 °C; strongest winds blow in spring and summer from the northwest; the average annual relative humidity is 30 %; the average sunshine hours is 3025 hours per year with the maximum of 345 hours in June and the minimum of 134 hours in January [22]. Table 2 shows the weather data of Yazd including Relative Humidity (%), Maximum Temperature (℃), Average Temperature (℃), Minimum Temperature (℃) and Sunlight Duration (hours) [47].

5.2. Specification of warehouse

The studied case is a fruit warehouse with an area of 4240 m^2

resulting in a storage capacity of about1000 tons. In this study, all calculations are performed for the summer.

5.2.1. Ceiling

The roof of all rooms is made of the 150 mm thick Reinforced Concrete (RC) slab covered with two layers of traditional waterproof (traditional tarpaper) with a total thickness of 60 mm. This floor is also coated with a layer of polyurethane insulation with a thickness of 150 mm.

Table 2. Average weather data of Yazd [47].

Monthly average	Jan.	Feb.	Mar.	Apr.	May	Jun.	Jul.	Aug.	Sep.	Oct.	Nov.	Dec.
Relative humidity (%)	44.5	30.3	20.6	20.5	13.1	9.7	9.0	9.5	11.6	18.7	34.2	45.6
Maximum temperature (℃)	12.8	17.1	22.8	27.6	33.5	38.4	40.5	38.8	35.0	29.3	20.2	14.2
Average temperature (℃)	6.8	11.2	15.7	20.7	26.4	31.1	33.4	31.2	27.1	21.6	13.5	8.0
Minimum temperature (℃)	0.8	4.0	8.6	13.8	19.3	23.8	26.2	23.7	19.2	14.0	6.9	1.9
Sunlight duration (hours)	215.4	919.3	257.4	258.9	316.0	345.7	352.8	353.1	320.4	296.5	229.5	213.9

5.2.2. Walls

All walls, both exterior and interior, are made of ordinary 500 mm thick brick walls covered with two layers of cement with a total thickness of 100 mm layer and coated on both sides with one layer of traditional tarpaper with a thickness of 30 mm. External walls are coated with polyurethane insulation with a thickness of 200 mm while internal walls are coated on both sides with polyurethane insulation with a thickness of 100 mm.

5.2.3. Floor

The floor of the warehouse is constructed with a 200 mm concrete slab (light pumice, cement) covered with 200 mm thick polyurethane insulation and coated with a 400 mm thick RC slab.

5.3. Warehouse size

The warehouse consists of six 25 m ×10 m rooms and a total area of 200 m^2 and a 30 m × 8 m corridor, all with a height of 4 meters. Each room can hold about 180 tons of fruits. The type, amount, and storage temperature of each fruit are shown in Table 3 [40].

Table 3. Type, amount, and storage temperature of fruits.

Room	Fruit	Ton (Quantity)	Degree (℃)
1	Peach	180	1
2	Plum	180	1
3	Apple	180	1
4	Watermelon	180	10
5	Melon	180	10
6	Cantaloupe	180	10

5.4. Miscellaneous specifications

1. The power required to light the room is considered to be 3-5 Watts per 1 m^2.
2. The workforce required to operate the warehouse is considered to be 1 person per 100 m^2.
3. Warehouse's equipment is considered to work 20 hours a day.
4. The temperature of the corridor is considered to be 25 °C.
5. Warehouse personnel are considered to work 8 hours a day.
6. The safety factor is 10 %.
7. Each room is equipped with an electric 4.17 KW forklift working 4 hours a day.
8. The cooling load due to products is calculated based on the amount entering the warehouse per day [29].
9. Fruits are stored in 0.5 m×0.3 m×0.25 m wooden boxes each holding about 15-20 kg of product. Given the amount of useful storage space, each room can store 34 boxes in the longitudinal direction, 12 boxes in the transverse direction and 11 rows in height, which amount to a total of 8976 boxes per room.
10. Total room space is 20 m×10 m. As shown in Figure 5, the useful storing space is divided into two 7 m×16 m rectangles.

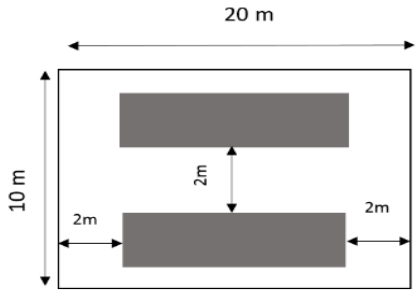

Figure 5. Useful storing space.

6. ANALYSIS

In this section, first, the cooling load of the described warehouse is calculated and then the cooling methods are evaluated with this cooling load acting as the basis of calculations.

6.1. Calculation of cooling load

As mentioned, the total cooling load is considered to be the sum of a number of separate cooling loads originating from different heat sources:

1. Wall, roof and floor gain load
2. Air change load
3. Product load
4. Respiration load
5. Miscellaneous loads

6.1.1. Wall, roof, and floor gain load

When calculating U for a warehouse, it is customary to only consider the effect of insulations and ignore the layers of air and other materials constituting the wall because of their considerably lower thermal resistance. Table 4 shows the parameter U based on the thickness of polyurethane insulation in walls, ceiling and floor of the warehouse [22]:

Table 4. Rate of U [22].

Title	Insulation thickness (mm)	U (m^2/k)
Outside walls	200	0.119
Inside walls	100	0.227
Roof	150	0.153
Floor	200	0.119

If the exterior walls of the refrigerator are exposed to direct sunlight, the temperature will rise as a result of this radiation, and this extra amount can depend on the color of the walls. Sun correction factor is presented in Table B of the Appendix.

The heat load of the wall, roof and floor is obtained from Equation (1). According to Table B (Appendix), the sun correction factor that is to be added to ΔT of the roof is 5. Using Table C (Appendix), the ground temperature is determined to be 24.4 °C. Since the overall heat transfer coefficient of the doors is much lower than the walls, all walls are considered to be monolithic (doors are disregarded). The outside temperature is 30 °C. Thus:

The heat load of the walls, roof and floor of the room dedicated to storing Peach at the temperature of 1 °C is shown in Table 5. According to this table, solar radiation has caused the heat load of the roof to be greater than all other surfaces.

Table 6 shows the heat load of the walls, roof and floor of the room dedicated to storing Plum at the temperature of 1 °C. As can be seen, the south and east walls have zero heat load.

The heat load of the walls, roof and floor of the room dedicated to storing Apple at the temperature of 1 °C is shown in Table 7. As shown in this table, only the east wall has zero heat load and the highest heat load is obtained for the roof (because of the sun).

Table 5. Heat load of the walls, roof and floor of room 1 dedicated to storing peach.

Title	A (m^2)	ΔT (°C)	U (m^2/K)	Solar correction factor	Q (w)
North wall	40	29	0.119	0	138.04
South wall	80	0	0.227	0	0
East wall	80	29	0.119	0	276.08
West wall	40	24	0.227	0	217.92
Roof	200	34	0.153	5	1040.4
Floor	200	23.4	0.119	0	556.92
Q_{total}	-	-	-	-	2229.36

Table 6. Heat load of the walls, roof and floor of room 2 dedicated to storing plum.

Title	A (m^2)	ΔT (°C)	U (m^2/K)	Solar correction factor	Q (w)
North wall	40	29	0.119	0	138.04
South wall	80	0	0.227	0	0
East wall	80	0	0.227	0	0
West wall	40	24	0.227	0	217.92
Roof	200	34	*0.*153	5	1040.4
Floor	200	23.4	0.119	0	556.92
Q_{total}	-	-	-	-	1953.28

Table 7. Heat load of the walls, roof and floor of room 3 dedicated to storing apple.

Title	A (m^2)	ΔT (°C)	U (m^2/K)	Solar correction factor	Q (w)
North wall	40	29	0.119	0	138.04
South wall	80	29	0.119	0	276.08
East wall	80	0	0.227	0	0
West wall	40	24	0.227	0	217.92
Roof	200	34	0.153	5	1040.4
Floor	200	23.4	0.119	0	556.92
Q_{total}	-	-	-	-	2091.32

Table 8 shows the heat load of the walls, roof and floor of the room dedicated to storing Watermelon at the temperature of 10 °C. Again, the east wall has zero and the roof has the highest heat load.

Table 9 shows the heat load of the walls, roof and floor of the room dedicated to storing Melon at the temperature of 10 °C. As can be seen, the east and south walls show the lowest and the roof shows the highest heat load.

The heat load of the walls, roof and floor of the room dedicated to storing Cantaloupe is shown in Table 10. As shown in this table, only the south wall has a heat load of zero and the heat load of the floor is lower than the walls.

Table 11 shows the heat load of the walls, roof and floor of the corridor with a temperature of 25 °C. As can be seen, heat loads of the floor, east wall, west wall and north wall are negative, and only the south wall has a positive heat load.

Table 8. Heat load of the walls, roof and floor of room 4 dedicated to storing watermelon.

Title	A (m^2)	ΔT (°C)	U (m^2/K)	Solar correction factor	Q (w)
North wall	40	15	0.227	0	136.2
South wall	80	20	0.119	0	190.4
East wall	80	0	0.227	0	0
West wall	40	20	0.119	0	95.2
Roof	200	25	0.153	5	765
Floor	200	14.4	0.119	0	342.72
Q_{total}	-	-	-	-	1529.52

Table 9. Heat load of the walls, roof and floor of room 5 dedicated to storing melon.

Title	A (m^2)	ΔT (°C)	U (m^2/K)	Solar correction factor	Q (w)
North wall	40	15	0.227	0	136.2
South wall	80	0	0.227	0	0
East wall	80	0	0.227	0	0
West wall	40	20	0.119	0	95.2
Roof	200	25	0.153	5	765
Floor	200	14.4	0.119	0	342.72
Q_{total}	-	-	-	-	1339.12

Table 10. Heat load of the walls, roof and floor of room 6 dedicated to storing cantaloupe.

Title	A (m^2)	ΔT (°C)	U (m^2/K)	Solar correction factor	Q (w)
North wall	40	15	0.227	0	136.2
South wall	80	0	0.227	0	0
East wall	80	20	0.119	0	190.4
West wall	40	20	0.119	0	95.2
Roof	200	25	0.153	5	765
Floor	200	14.4	0.119	0	342.72
Q_{total}	-	-	-	-	1529.52

Table 11. Heat load of the walls, roof and floor of the corridor.

Title	A (m^2)	ΔT (°C)	U (m^2/K)	Solar correction factor	Q (w)
North wall	24	-24	0.227	0	-136.2
South wall	160	5	0.119	0	95.2
East wall	160	-20	0.119	0	-26.4
West wall	24	-15	0.227	0	-81.72
Roof	240	-15	0.153	5	-550.8
Floor	240	-0.6	0.119	0	-17.13
Q_{total}	-	-	-	-	-717.05

6.1.2. Air change load

To calculate the air change load, the enthalpy coefficient is obtained based on the temperature and humidity of the room and the entering temperature. For this purpose, temperature of the rooms 1, 2, and 3 is determined to be 1 °C, temperature of the room 4, 5, and 6 is determined to be 10 °C; humidity is

determined to be 50 %; entering temperature is determined to be 25 °C for the rooms and 30 °C for the corridor (using Table D (Appendix)). Air infiltration rate is then obtained from Table E and these values are substituted into Equation (4). The results of these calculations are shown in Table 12.

6.1.3. Product load

To calculate the product load, first, the c-value and chilling rate factor of each fruit are obtained from Table F (Appendix), according to the type of fruit and its storage temperature, and the resulting values are then substituted into Equation (5). The results of these calculations are presented in Table 13.

6.1.4. Respiration load

To calculate the respiration load, the respiration temperature corresponding to each fruit is obtained from Table G (Appendix), according to the type of fruit and its storage temperature; then the resulting value and the weight of fruit stored in each room are substituted into Equation (6). Table 14 shows the results of these calculations.

6.1.5. Miscellaneous loads

Since the power required for lighting is considered to be 3-5 watts per 1 m^2, each room with an area of 200 m^2 needs about 1000 Watt and the corridor with the area of 240 m^2 needs about 1200 Watt of power for lighting. These values are substituted into Equation (7) to calculate the required power to provide 8 hours of lighting a day.

The workforce required for the warehouse is considered to be 1 person per 100 m^2, so each room with an area of 200 m^2 needs 2 workers and the corridor with the area of 240 m^2 needs 3 workers to be properly operated. The workers' heat in each room is determined using Table H (Appendix) and then the workers' heat load is obtained from Equation (8).

Each room is equipped with an electric 4.17 KW forklift working 4 hours a day, so substituting these values into Equation (9) gives the heat load generated by forklifts.

Calculations showed that each room can store 8976 boxes, each weighing 3 kg, and for each box c=2.5 [40]. Substituting these values into Equation (10) gives the heat load due to boxes. The final results of the above calculations are shown in Table 15.

The cooling load of each room is obtained by summing loads of walls, roof and floor, air exchange load, product load, respiration load, and miscellaneous loads using a safety factor of 10 % [40]. The cooling loads obtained for the room are shown in Table 16.

6.2. Valuation of cooling methods

Having the cooling load of the studied warehouse, we evaluate the performance of different methods for cooling this facility.

6.2.1. Cooling with solar panels

The average daily power consumption of the warehouse is 300 kW, so in this scenario, the cooling system is considered to consist of 300 KW solar panels and two 12 V 800 AH batteries and two 200 kW inverters.

Table 12. Air change load obtained for the studied warehouse.

Title	Room 1	Room 2	Room 3	Room 4	Room 5	Room 6	Corridor
Air infiltration rate (L/S)	24.7	24.68	24.7	24.7	24.68	24.7	26.57
Enthalpy rate (KJ/L)	0.0266	0.0266	0.0266	0.0472	0.0472	0.0472	0.0341
Air change load (KW)	1.165	0.252	1.165	0.788	0.787	0.787	0.908

Table 13. The product loads obtained for the studied warehouse.

Title	Peach	Plum	Apple	Watermelon	Melon	Cantaloupe
(kj/kg/k)C	3.81	3.68	3.72	3.81	3.81	3.81
Chilling rate factor	0.62	0.67	0.62	0.9	0.9	0.9
Product load (kw)	0.446	0.398	0.403	0.212	0.212	0.212

Table 14. The respiration loads obtained for the studied warehouse.

Title	Peach	Plum	Apple	Watermelon	Melon	Cantaloupe
(kj/kg/k)C	0.0166	0.021	0.0166	0.0656	0.0656	0.0656
Chilling rate factor	2.988	3.760	2.412	11.808	11.808	11.808

Table 15. Miscellaneous loads obtained for the studied warehouse.

Load	Room 1	Room 2	Room 3	Room 4	Room 5	Room 6	Corridor
Lights	0.333	0.333	0.333	0.333	0.333	0.333	0.4
People	0.179	0.179	0.179	0.141	0.141	0.141	0.181
Forklift	0.695	0.695	0.695	0.695	0.695	0.695	0.695
Box	18.7	18.7	18.7	27.115	27.115	27.115	-

Table 16. the Cooling load of the warehouse.

Room	Kw	TR	Btu/h
1	38.66	10.99	131880
2	39.24	11.16	133920
3	37.81	10.75	129000
4	37.62	10.69	128280
5	37.44	10.64	127680
6	37.62	10.69	128280
Corridor	2.206	0.627	7524

6.2.2. Cooling with solar air conditioner

Considering the calculated cooling load, in this scenario, the rooms 1, 2, 3, 4, 5 and 6 are considered to be cooled with twelve 60000 Btu/h solar air conditioners (2 per each) and the corridor is considered to be cooled with one 9000 Btu/h solar air conditioner.

6.2.3. Cooling with solar absorption chiller

The choice of chiller is usually based on two-thirds of the total cooling capacity. Therefore, in this scenario, rooms 1, 2, 3, 4, 5 and 6 are cooled with six 7-ton solar absorption chillers (1 per each) and the corridor is cooled with one 1-ton solar absorption chiller.

6.2.4. Cooling with solar air conditioner and solar absorption chiller

In this scenario, the rooms 1, 2, and 3 are considered to be cooled with three 7-ton solar absorption chillers (1 per each) while the rooms 4, 5, and 6, are cooled with six 60000 Btu/h solar air conditioners (2 per each) the corridor is cooled with one 9000 Btu/h solar air conditioner.

6.2.5. Cooling with wind catcher

A wind catcher can reduce the temperature by 8-16 °C at low relative humidity (10 %-30 %) and by 4-5 °C when relative humidity is higher (65 %-70 %) [42]. Thus, wind catcher by itself cannot meet the fruit storage cooling requirements. The other issue of this method is the discharge of cold air through outlet vents, which make the wind catcher completely unsuitable for this application.

7. ECONOMIC EVALUATION

In the economic evaluation, the NPV of every project is obtained and the project with the greatest positive NPV is identified. In the economic analysis:

1. All projects are evaluated with the software Comfar.
2. The discount rate is considered to be 18 % [48].
3. The inflation rate is considered to be 9 % [48].
4. The lifetime of solar energy systems is considered to be 20 years [27].
5. The fixed investment cost is considered to be the system price plus the cost of installation [43].

7.1. Cost of cooling warehouse by fossil power

Here, fossil power refers to the electricity provided by the conventional power grid. According to the Ministry of Energy, the cost per kilowatt-hour of fossil power for the warehouse is 208, 416, and 832 respectively for low, medium, and high peak hours [49].

Thus, the annual cost of electricity and NPV of fossil power consumed by the warehouse with an average daily consumption of 300 kw is calculated according to Table 21. The results of this calculation shown that annual electricity cost and NPV are 1,114,214,400 Rials (Iranian currency unit) and 9,538,837,442 Rials respectively.

7.2. Revenue by solar power

Assuming that the state purchases the solar electricity with a price of 4900 Rials [50], annual revenue and NPV of the solar power system are calculated to be 546,840,000 Rials and 15,276,856,284 Rials respectively.

7.3. Economic evaluation of cooling methods

Table 17 shows the list of costs associated with solar power systems.

7.3.1. Economic evaluation of cooling by solar panels

As mentioned, in this scenario, the warehouse is considered to be cooled with the power produced by 300 KW solar panels, supported by two batteries and two inverters. Thus, the initial cost of this method is 2,837,409,600 Rials, maintenance and repair cost of 500,000 Rials, and NPV of 2,513,794,655 Rials. The internal rate of return would then be 29.34 %.

Table 17. List of costs associated with solar power systems.

Title	Capacity	Price (Rials)	Installation cost (Rials)	Annual maintenance & repair costs (Rials)
Solar panel	300 kw	9357 (per watt)	10,000,000	500,000
Battery	12 V 800 AH	7,592,880		
Inverter	200 kw	5,061,920		
Solar air conditioner	60000 (Btu/h)	24,727,200	2,000,000	800,000
	9000(Btu/h)	13,343,400		
Solar absorption chiller	7 TR (Ton of Refrigeration)	97,785,500	100,000,000	10,000,000
	1 TR	60,190,300		

7.3.2. Economic evaluation by solar air conditioner

In this scenario, the warehouse is cooled with twelve 60000 Btu/h solar air conditioners (2 per room) and one 9000 Btu/h solar air conditioner for the corridor. Thus, the initial cost of this method is 336,069,800 Rials, maintenance and repair cost of 10,400,000 Rials, and NPV of 4,865,040,418 Rials. The internal rate of return would then be 182.98 %.

7.3.3. Economic evaluation by solar absorption chiller

In this scenario, the warehouse is cooled with six 7-ton solar absorption chillers (1 per room) and one 1-ton solar absorption chiller for the corridor. Therefore, the initial cost of this method is 1,351,903,300 Rials, materials, maintenance and repair cost of 70,000,000 Rials, and NPV of 3,433,476,659 Rials. The internal rate of return would then be 47.42 %.

7.3.4. Economic evaluation by solar air conditioner and solar absorption chiller

In this scenario, the rooms 1, 2, and 3, are cooled with three 7-ton solar absorption chillers (1 per room), the rooms 4, 5, and 6, are cooled with six 60000 Btu/h solar air conditioners (2 per room), and the corridor is cooled with one 9000 Btu/h solar air conditioner. Therefore, the initial cost of this method is 694,881,500 Rials, materials, maintenance and repair cost of 35,600,000 Rials and NPV of 4,327,869,138 Rials. The internal rate of return would then be 89.19 %.

8. ECONOMIC COMPARISON OF METHODS

The total cost and NPV and IRR of the methods evaluated in this study are shown in Table 18. According to Table 18, all methods have a positive NPV and thus economic justification, but among these methods, the ones with the highest NPV and IRR would be the most desirable. As can be seen, the method that is based on solar air conditioner has yielded the highest NPV and IRR among the evaluated methods, so it can be considered as the most economically desirable method.

Table 18. Economic comparison of evaluated methods.

Method	NPV (Rials)	IRR (%)
Solar panel	2,513,794,655	29.34
Solar air conditioner	4,865,040,418	182.98
Solar absorption chiller	3,433,476,659	53.70
Solar air conditioner & Solar absorption chiller	4,327,869,138	89.19

Also, the NPV of cost of solar air conditioning, 402,815,886 Rials, is lower than the NPV of the cost of fossil power, which indicates that the use of solar air conditioning is more economically feasible than the use of fossil power.

9. VALIDATION BY VALUE ENGINEERING

The results obtained in previous sections are validated by the use of value engineering. As mentioned, the procedure of value engineering consists of several phases: information phase, function analysis phase, creativity phase, and evaluation phase.

9.1. Information phase

The studied case is a warehouse with the capacity to store 1000 tons of fruit in six rooms. The cooling method considered for this warehouse includes solar panels (to power conventional cooling), solar air conditioner, solar absorption chiller, and combined use of solar air conditioner and a solar absorption chiller. We show methods with M (method). Thus, there are 4 M values as shown in Table 19.

Table 19. Information phase.

Methods	M
Solar panel	M1
Solar air conditioner	M2
Solar absorption chiller	M3
Solar air conditioner & Solar absorption chiller	M4

9.2. Function analysis phase

The parameters considered important include cooling power, ease of installation, ease of maintenance, ease of implementation, low weight, low space usage, availability, climatic limitations, low power consumption, low emissions, and low price.

9.3. Creativity phase

In this phase, the methods are shown in Table (23) are considered for cooling the warehouse.

9.4. Evaluation phase

In this phase, M is selected and prioritized, the evaluation criteria of alternatives are obtained by brainstorming, and then options for selecting the best cooling method are determined by creative analysis. The description and categorization of each idea developed to create a common understanding are shown in Table 20.

Table 20. Desired criteria.

A = Cooling power
B = Ease of installation
C = Ease of maintenance
D = Ease of implementation
E = Low weight
F = Low space usage
G = Availability
H = Climatic limitations
I = Low power consumption
J = Low emissions
K = Low price

The ideas were then compared with the help of a matrix known as a pairwise comparison matrix. For this comparison, the ideas of Table 20 were placed in the top row of the matrix, and then pairwise comparison was made by brainstorming and the total score points of every row were obtained in the corresponding column. All these operations are illustrated in Table 21.

The weight of ideas of Table 21 was written in the top row of the decision matrix and then each M was given a score by

the analyst in view of the associated parameters. These scores were then multiplied by each weight, and the values obtained for each M were summed together. The method with the highest score was selected as the best method for cooling the warehouse. The above calculations are presented in Table 22.

As can be seen, cooling with solar air conditioner has earned the highest score among the studied methods, so it is the best method for this particular application.

Table 21. Matrix of pairwise comparisons.

	B	C	D	E	F	G	H	I	J	k	SCORE
A	A3	A1	A1	A3	A3	A2	A3	A1	A1	A1	**19**
	B	C2	D3	B3	B3	G1	B3	I2	J1	K1	**9**
		C	D1	C3	C3	C1	C2	I1	C1	K1	**12**
			D	D3	D3	D3	D2	D1	D1	D1	**19**
				E	E1	G2	H1	I3	J3	K3	**1**
					F	G2	F1	I3	J3	K3	**1**
						G	G2	I3	J2	K3	**7**
							H	H1	J3	K3	**2**
								I	I1	K1	**12**
									J	K1	**12**
										k	**16**

Comparison	Pts.
Major Difference	3
Minor Difference	2
Minor Difference	1
No Difference	0

Table 22. Decision matrix**.**

Value Engineering Analysis	**Desired criteria**	**Cooling power**	**Ease of installation**	**Ease of maintenance**	**Ease of implementation**	**Low weight**	**Low space usage**	**Availability**	**Climatic limitations**	**Low power consumption**	**Low emissions**	**Low price**	
Excellent=5 **Very Good=4** **Good=3** **Fair=2** **Poor=1**													
Proposal	Weightage for criteria	**A**	**B**	**C**	**D**	**E**	**F**	**G**	**H**	**I**	**J**	**K**	**Total Score**
		19	9	12	19	1	1	7	2	12	12	16	
Solar panel		5	5	5	5	5	3	5	4	5	5	1	**482**
		95	45	60	95	5	3	35	8	60	60	16	
Solar air conditioner		5	4	4	4	4	2	3	3	5	5	4	**472**
		95	36	48	76	4	2	21	6	60	60	64	
Solar absorption chiller		5	3	3	4	2	2	5	3	5	5	2	**431**
		95	27	36	76	2	2	35	6	60	60	32	
Solar air conditioner & Solar absorption chiller		5	3	3	4	2	1	3	3	5	5	3	**432**
		95	27	36	76	2	1	21	6	60	60	48	

10. CONCLUSIONS

Today, the rising prices of fossil power and the resulting increase in the energy costs of business operations, and more importantly, the environmental pollution resulting from fossil fuels motivate the efforts toward cheaper and cleaner energy solutions like the use of renewable energy such as solar and wind. The good potential of Iran for the exploitation of wind and solar energy provide ample opportunities for such efforts, one example of which could be in cooling applications based on renewable energies. In this paper, the use of wind and solar energies via solar panels (to power a conventional cooling system), solar air conditioner, solar absorption chiller, wind catcher, and a combination of solar air conditioners and solar absorption chillers was subjected to techno-economic study. In the economic analysis, as shown in Table 18, solar air conditioning with the highest NPV of 4,865,040,418 Rials, and the best IRR value of 182.98 % was determined to be the best approach among the studied methods. Above result was validated using value engineering technique, as shown in Table 22, cooling with solar air conditioner earned the highest score of 489, and is found to be the best option in this respect. Considering the rising price of fossil power in Iran, the availability of less expensive solar cooling equipment such as solar chillers and solar air conditioners and better incentives for the use of solar power can make these systems more economically attractive.

The approach of this paper can be used in the examination of cooling systems for any other similar applications in other regions.

11. ACKNOWLEDGEMENT

Authors would like to thank all the organizations for providing data for this research, also specialists who participated in brainstorming sessions for value engineering techniques.

APPENDIX

Table A. Thermal conductivity of the materials used in the walls of warehouse [40].

Material	Thermal conductivity (k) (w/m k)	Thermal conductance (c) (w/m^2 k)
Polyurethane	0.025	-
Cement	0.72	-
Brick, common	0.72	-
Brick, face	1.30	-
Tile	-	5.11

Table B. Sun radiation correction factor [40].

Type of surface	East wall	South wall	West wall	Flat roof
Dark-colored surfaces such as: Slate roofing, Tar roofing, Black paint	5	3	5	11
Medium-colored surfaces such as: Unpainted wood, Brick, Red title, Dark cement, Red, gray or green paint	3	2	3	8
Light-colored surfaces such as: White stone, Light-colored, Cement, White paint	2	1	2	5

Table C. Ground temperature for warehouse [40].

Design outside temperature for winter	Design ground temperature
-40	7
-35	10
-30	
-25	15
-20	17
-15	20
-10	22
-5	25
0	27

Table D. Heat due to one liter of air (kJ) for above zero warehouse [40].

Storage room temperature (℃)	Inlet air temperature (℃)					
	25 ℃			30 ℃		
	50	60	70	50	60	70
15	0.0441	0.0357	0.0281	0.0246	0.186	0.0128
10	0.0574	0.0491	0.0319	0.0382	0.0323	0.0266
5	0.0693	0.0610	0.0536	0.0502	0.0445	0.0388
0	0.0794	0.0713	0.0639	0.0606	0.0550	0.0493

Table E. Air infiltration rate (in liters per second) due to opening and closing of door [40].

Infiltration rate (L/S)	
Room volume (m^3)	Room (℃)
700	24.3
800	25.9
900	27.1
1000	28.9

Table F. Design data for storing vegetables [40].

Fruits	Rate factor	Special heat
Apple	0.62	3.72
Plum	0.67	3.68
Peach	0.62	3.81
Watermelon	0.90	3.81
Melon	0.90	3.81
Cantaloupe	0.90	3.81

Table G. Respiration temperature of fruits and vegetables [40].

Commodity	Temperature (℃)	Watts per kilogram
Apples	0 5 10	0.012 0.019 0.075
Pulm	0 16	0.010 0.149
Peach	0 5 16	0.015 0.023 0.110
Watermelon Melon Cantaloupe	0 5 16	0.016 0.026 0.113

Table H. Heat due to people [40].

Cooler temperature (℃)	Heat equivalent/Person Kw
10	0.211
5	0.242
0	0.275
-5	0.305
-10	0.347
-15	0.378
-20	0.407

REFERENCES

1. Huang, Y., "Drivers of rising global energy demand: The importance of spatial lag and error dependence", ***Energy***, Vol. 76, (2014), 254-263. (DOI: 10.1016/j. Energy. 2014.07.093).
2. Ramazankhani, M., Mostafaeipour, A., Hosseininasab, H. and Fakhrzad, M., "Feasibility of geothermal power assisted hydrogen production in Iran", ***International Journal of Hydrogen Energy***, Vol. 41, (2016), 18351-18369. (DOI: 10.1016/j.ijhydene.2016.08.150).
3. Sedaghat, A., Hassanzadeh, A., Jamali, J., Mostafaeipour, A. and Chen, W.H., "Determination of rated wind speed for maximum annual energy production of variable speed wind turbines", ***Applied Energy***, Vol. 205, (2017), 781-789. (DOI: 10.1016/j.apenergy.2017.08.079).
4. Goudarzi, H. and Mostafaeipour, A., "Energy saving evaluation of passive systems for residential buildings in hot and dry regions", ***Renewable and Sustainable Energy Reviews***, Vol. 68, (2017), 432-446. (DOI: 10.1016/j.rser.2016.10.002).
5. Fereidooni, M., Mostafaeipour, A., Kalantar, V. and Goudarzi, H., "A comprehensive evaluation of hydrogen production from photovoltaic

power station", ***Renewable and Sustainable Energy Reviews***, Vol. 82, (2018), 415-423. (DOI: 10.1016/j.rser.2017.09.060).

6. Zarezade, M. and Mostafaeipour, A., "Identifying the effective factors on implementing the solar dryers for Yazd province, Iran", ***Renewable and Sustainable Energy Reviews***, Vol. 57, (2016), 765-775. (DOI: 10.1016/j.rser.2015.12.060).
7. Jahangiri, M., Haghani, A., Alidadi Shamsabadi, A., Mostafaeipour, A. and Pomares, L.M., "Feasibility study on the provision of electricity and hydrogen for domestic purposes in the south of Iran using grid-connected renewable energy plants", ***Energy Strategy Reviews***, Vol. 23, (2019), 23-32. (DOI: 10.1016/j.esr.2018.12.003).
8. Moein, M., Pahlavan, S., Jahangiri, M. and Alidadi Shamsabadi, A., "Finding the minimum distance from the national electricity grid for the cost-effective use of diesel generator-based hybrid renewable systems in Iran", ***Journal of Renewable Energy and Environment (JREE)***, Vol. 5, (2018), 8-22.
9. Jahangiri, M., Rizi, R.A. and Alidadi Shamsabadi, A., "Feasibility study on simultaneous generation of electricity and heat using renewable energies in Zarrin Shahr, Iran", ***Sustainable Cities and Society***, Vol. 38, (2018), 647-661. (DOI: 10.1016/j.scs.2018.01.043).
10. Jahangiri, M., Haghani, A., Mostafaeipour, A., Khosravi, A. and Raeisi, H.A., "Assessment of solar-wind power plants in Afghanistan: A review", ***Renewable and Sustainable Energy Reviews***, Vol. 99, (2019), 169-190. (DOI: 10.1016/j.rser.2018.10.003).
11. Ebrahimi, S., Jahangiri, M., Raiesi, H.A. and Rahimi Ariae, A., "Optimal planning of on-grid hybrid microgrid for remote island using HOMER software, Kish in Iran", ***International Journal of Energetica***, Vol. 3, (2018), 13-21.
12. Mostafaeipour, A., Saidi Mehrabad, M., Qolipour, M., Basirati, M., Rezaei, M. and Golmohammadi, A., "Ranking locations based on hydrogen production from geothermal in Iran using the Fuzzy Moora hybrid approach and expanded entropy weighting method", ***Journal of Renewable Energy and Environment (JREE)***, Vol. 4, (2017), 9-21.
13. Kuhe, A., Terhemba Achirgbenda, V. and Agada, M., "Global solar radiation prediction for Makurdi, Nigeria using feed forward backward propagation neural network", ***Journal of Renewable Energy and Environment (JREE)***, Vol. 5, (2018) 51-55.
14. Ameri, M. and Salimi, K., "Techno-economic and life-cycle cost assessment of the CCHP/PV hybrid system application", ***Journal of Renewable Energy and Environment (JREE)***, Vol. 4, (2017), 1-8.
15. Najafi, G., Ghobadian, B., Mamat, R., Yusaf, T. and Azmi, W.H., "Solar energy in Iran: Current state and outlook", ***Renewable and Sustainable Energy Reviews***, Vol. 49, (2015), 931-942.) DOI: 10.1016/j.rser.2015.04.056).
16. Alamdari, P., Nematollahi, O. and Mirhosseini, M., "Assessment of wind energy in Iran: A review", ***Renewable and Sustainable Energy Reviews***, Vol. 16, (2012), 836-860. (DOI: 10.1016/j.rser.2011.09.007).
17. Yang, B., Yao, L., Yan, S., Li, N., Cao, Y., Cui, H. and Ge, X., "Comprehensive benefits assessment of different new energy generation technologies for global energy Internet development", ***Materials Science and Engineering***, Vol. 452, (2018), 2-3. (DOI: 0.1088/1757-899X/452/3/032036).
18. Kalantar, V., "Numerical simulation of cooling performance of wind tower in hot and arid region", ***Renewable Energy***, Vol. 34, (2009), 246-254. (DOI: 10.1016/j.renene.2008.03.007).
19. http://moe.gov.ir, (Accessed 14-03-2019), In Farsi language.
20. Bahadori, M.N., "Passive cooling systems in Iranian architecture", ***Scientific American***, Vol. 10, (1978), 144-278. (DOI: 10.1038/scientificamerican0278-144).
21. Mahdinejad, M.J. and Javanrudi, K., "Comparative examination of effects of air flow on Yazdi and Kermani wind catchers", ***The Journal of Fine Arts - Architecture***, Vol. 48, (2012), 69-76. (In Farsi language).
22. Mostafaeipour, A., Bardel, B., Mohammadi, K., Sedaghat, A. and Dinpashoh, Y., "Economic evaluation for cooling and ventilation of medicine storage warehouses utilizing wind catchers", ***Renewable and Sustainable Energy Reviews***, Vol. 38, (2014), 12-19. (DOI: 10.1016/j.rser.2014.05.087).
23. Mostafaeipour, A. and Sadeghi Sedeh, A., "Investigation of solar energy utilization for production of hydrogen and sustainable chemical fertilizer: A case study", ***International Journal of Energy Research***, Vol. 43, No. 14, (2019), 1-23. (DOI: 10. 1002/er.4829).
24. Qasemifard, M., "Prioritization of the cities of Yazd province for the use of solar energy", Dissertation for the master's degree in Industrial Engineering, Yazd University, (2013), In Farsi language.
25. http://www.satba.gov.ir/br/sun/potential, (Accessed 6-3-2019), In Farsi language.
26. https://www.google.com/search?sxsrf=ACYBGNTJ3rqJQqebL8vBFK20QNHW7hFv8Q:1569678467076&q=The-world-solar-energy-map-Zhang-et-al-2013&tbm=isch&source=univ&client=firefox-b-d&sxsrf=ACYBGNTJ3rqJQqebL8vBFK20QNHW7hFv8Q:1569678467076&sa=X&ved=2ahUKEwiI5sP70_PkAhWEJFAKHThzCJwQsAR6BAgJEAE; 2019, (Accessed 5-3-2019).
27. Rezaei-Shouroki, M., Mostafaeipour, A. and Qolipour, M., "Prioritizing of wind farm locations for hydrogen production: A case study", ***International Journal of Hydrogen Energy***, Vol. 42, No. 15, (2017), 9500-9510.
28. Mostafaeipour, A., Qolipour, M. and Goudarzi, H., "Feasibility of using wind turbines for renewable hydrogen production in Firuzkuh, Iran", ***Frontiers in Energy***, Vol. 13, No. 3, (2019), 494-505.
29. Mostafaeipour, A. and Sadeghi Sedeh., A., "Investigation of solar energy utilization for production of hydrogen and sustainable chemical fertilizer: A case study", ***International Journal of Energy Research***, Vol. 43, No. 14, (2019), 8314-8336.
30. Clark, J.A. and Stachan, P.A., "Simulation of conventional and renewable building energy systems, Energy systems research unit University of Strathclyde", ***Renewable Energy***, Vol. 5, (2009), 1178-1189. (DOI: 10.1016/0960-1481(94)90148-1).
31. Hua, J. and Shiu, H.-G., "Sustainable development of renewable energy on Wangan Island, Taiwan", ***Utilities Policy***, Vol. 55, No. C, (2018), 200-208. (DOI: 10.1016/j.jup.2018.10.003).
32. Danish, Zhang, B., Wang, B. and Wang, Z., "Role of renewable energy and non-renewable energy consumption on EKC: Evidence from Pakistan", ***Journal of Cleaner Production***, Vol. 156, (2017), 855-864. (DOI: 10.1016/j.jclepro.2017.03.203).
33. Shahsavari, A. and Akbari, M., "Potential of solar energy in developing countries for reducing energy-related emissions", ***Renewable and Sustainable Energy Reviews***, Vol. 19, (2018), 275-291. (DOI: 10.1016/j.rser.2018.03.065).
34. Lang, T., Gloerfeld, E. and Girod, B., "Don't just follow the sun – A global assessment of economic performance for residential building photovoltaics", ***Renewable and Sustainable Energy Reviews***, Vol. 42, (2015), 932-951. (DOI: 10.1016/j.rser.2014.10.077).
35. Askari, I., Sadegh, M. and Ameri, M., "Energy management and economics of a trigeneration system considering the effect of solar PV, solar collector and fuel price", ***Energy for Sustainable Development***, Vol. 26, (2015), 43-55. (DOI: 10.1016/j.esd.2015.03.002).
36. Daneshvar, H., Honarmand, M.I. and Talebi, J., "The potential of hybrid solar air conditioners to reduce peak load", ***Proceedings of The 25th International Conference on Electricity***, Gilan, Iran, (2011), Source file is in Farsi.
37. Abdullah, G., Saman, W. and Whaley, D., "Optimization of standalone solar heat fired absorption chiller for typical Australian homes", ***Energy Procedia***, Vol. 91, (2016), 692-701, (DOI: 10.1016/j.egypro.2016.06.232).
38. Saffar, A.," Passive cooling strategies in greening existing residential building in hot dry climate: Case study in Bahrain", ***Journal of Environmental Science and Engineering***, Vol. 4, (2015), 233-240. (DOI: 10.17265/2162-5298/2015.05.003).
39. Gholamnejad, N., "Economic and feasibility analysis of a solar cold room in desert regions", Dissertation for the bachelor's degree in Mechanical Engineering, Yazd University, (2013), Source file is in Farsi.
40. Dossat R.J. and Horan T.J., Principles of refrigeration, 5th Edition, published by Pearson, (2001).
41. https://fa.wikipedia.org/w/index.php?search=%2F%E2%80%8E%E2%80%8Fcomfar&title=%D9%88%DB%8C%DA%98%D9%87%3A%D8%AC%D8%B3%D8%AA%D8%AC%D9%88&go=%D8%A8%D8%B1%D9%88&ns0=1, (Accessed 09-11-2018).
42. Valipour, M., A practical guide to COMFAR, Daneshparvar Publications, Tehran, (2014), Source file is in Farsi.
43. Oskunejad, M.M., Engineering economics, Amirkabir University of Technology Publications, Tehran, (1997), Source file is in Farsi.

44. Pazhuyan, J., Money, currency, and banking (for the students of Accounting and Business Administration), Payam Noor University Press, (2015), Source file is in Farsi.
45. PourReza, M., Zolforian, M.H. and Atri, I., Introduction to value engineering, Training unit of Iran's value engineering comprehensive reference, Tehran, (2014), Source file is in Farsi.
46. Labs, K., Regional analysis of ground and above-ground climate, Oak Ridge National Laboratory,)1981).
47. Mostafaeipour, A., Zarezade, M., Goudarzi, H., Rezaei-Shouroki, M. and Qolipour, M., "Investigating the factors on using the solar water heaters for dry arid regions: A case study", ***Renewable and Sustainable Energy Reviews***, Vol. 78, (2017), 157-166. (DOI: 10.1016/j.rser.2017.04.102).
48. https://www.cbi.ir, (Accessed 30-12-2018), Source file is in Farsi.
49. http://barghnews.com/fa/news/8305, (Accessed 30-12-2019), Source file is in Farsi.
50. http://www.satba.gov.ir/fa/guidances, (Accessed 30-12-2019), Source file is in Farsi.

JREE: Vol. 7, No. 1, (Winter 2020) 33-39

Journal of Renewable Energy and Environment

Research Article

Journal Homepage: www.jree.ir

Optimization the Performance and Emission Parameters of a CI Engine Fueled with Aviation Fuel-Biodiesel-Diesel Blends

Alireza Shirneshan[a,b*], Mohammad Mostofi[a]

[a] *Department of Mechanical Engineering, Najafabad Branch, Islamic Azad University, Najafabad, Iran.*
[b] *Aerospace and Energy Conversion Research Center, Najafabad Branch, Islamic Azad University, Najafabad, Iran.*

PAPER INFO

Paper history:
Received 28 December 2019
Accepted in revised form 28 March 2020

Keywords:
Optimization
Aviation Fuel
Emission
Performance
Diesel Engine

ABSTRACT

The determination of the optimum engine working conditions plays an important role in increasing engine performance and reducing exhaust emissions. The main objective of this study is to optimize the performance and emission characteristics of a CI engine fueled with aviation fuel-biodiesel-diesel blends at various engine speeds and loads using Mixture-RSM. According to the experimental tests carried on a 4-cylinder engine, the mathematical models were developed. Then, the optimization processes were defined as the six scenarios containing the consideration of performance or emission parameters or both of them. Scenario 1 shows that the higher percentage of diesel and jet fuel can improve the performance parameters of the engine; however, Scenario 2 shows that only higher percentage of diesel can improve the engine emission due to negative effect of biodiesel on the NOx emissions and negative impact of aviation fuel on the CO and HC emissions that limit the amount of biodiesel and aviation fuel in the fuel mixture. The results also show that Scenario 3 does not vary compared to Scenario 2. The optimized point for both of engine performance and emission parameters presented in Scenario 6 was calculated as D48.9B32.7J18.4 at 2526 RPM and full engine load to obtain 88.4 (kW), 337 (N.m), 255 (gr/Kw.hr), 0.0268 (%), 469 (ppm), 7.7 (%) brake power, torque, BSFC, CO, NOx, and HC emission, respectively.

1. INTRODUCTION

To analyze engine behavior, linear and non-linear algorithms such as genetic algorithm, artificial neural network, Taguchi method, factorial design, and response surface methodology are used. This algorithm has reduced the number of experimental trials, search time, and expenditure, and it becomes an effective tool for rapid optimization [1].

The optimum working conditions with binary blends based on engine operating parameters by design of experiments (DOE) are established by response surface methodology (RSM) [2,3] provides a high level of information with fewer experiments and data and can transform parameters concurrently throughout optimization [4].

Recently, the optimization of SI engine parameters based on the Taguchi approach was performed by Anand and Karthikeyan [5]. Further, on the performance optimization of diesel particulate filter (DPF) based on adaptive mutative scale chaos optimization algorithm, Zhang et al. [6] found this method very suitable in achieving large filtration efficiency, small pressure drop, low microwave energy consumption, and better emission performance.

In another study [7], the artificial intelligence method was combined with KIVA-3V code to optimize the performance and emission characteristics of a dual-fuel engine. In this research, the operating parameters and chamber shape were optimized, and the regression analysis of the engine parameters was conducted.

Krishnamurthy et al. [8] considered the compression ratio, speed, and load as input factors for diesel engine optimization. This investigation is done through a combination of experimental data analysis and artificial neural network modeling. In this study, the RSM optimization was applied to minimize engine emissions and maximize engine performance. Overall, the results conclude that the application of ANN for prediction and RSM optimization plays an important role in increasing engine performance and reducing exhaust emissions.

Saxena et al. [9] carried out an experimental and statistical analysis on a diesel engine to determine the optimal doping rate of nanoparticles and engine operating parameters applying response surface methodology and desirability function approach. The results showed that the optimal value, TiO_2 doping rate of 150 mg/liter, injection timing of 22.5 °CA bTDC, and 82.37 % engine load would constitute the most suitable combination. This was obtained with an overall high desirability value of 0.707.

In another research [10], the optimization was done for the effect of fuel injection pressure, injection timing, and compression ratio by applying the desirability approach of the RSM. In this paper, the input parameters were taken as 210 bar, 230 bar, and 250 bar for injection pressure, 16, 17, 18 for compression ratios, and 21°, 23°, 25° bTDC for injection timing. The results showed that the maximum BTE of 30.05 % was found at a bar injection pressure of 230 and a compression ratio of 18 with 23° bTDC injection timing. Minimum carbon monoxide of 0.41 % was observed at an injection pressure of 230 bar and a compression ratio of 18 with the injection timing of 25° bTDC, and the oxide of nitrogen of 205.7 ppm was found at an injection pressure of 250 bar and a compression ratio of 16 with 25° bTDC injection timing.

*Corresponding Author's Email: arshirneshan@yahoo.com (A. Shirneshan)

Singh et al. [11] performed an RSM-based optimization of cassia tora oil blends. In this research, the optimum fuel blends were determined based on diesel engine operating conditions, and biodiesel blends, engine load, injection timing, and injection pressure were as the input parameters. The best combination of the four input parameters was obtained as follows: 15° bTDC fuel injection timing, 221 bar fuel injection pressure, B40 as the fuel blend, and 47 % engine load, resulting in the corresponding output parameters of BTE to be 29.48 % and 43 ppm and 507.60 ppm for HC and NOx emissions, respectively.

In another research [12], the optimized RCCI and DDFS engines fueled with methanol and diesel at low loads were investigated by the multiple-objective optimization. The results showed that the optimization of operating parameters, the fuel properties of methanol, could also be utilized to improve the engine performance, and the co-optimization of operating parameters and fuel properties offers a promising approach to the development of advanced internal combustion engines to meet more stringent requirements on both engine efficiency and engine-out emissions in the future.

Cho et al. [13] performed a multi-objective Pareto optimization to minimize both BSFC and BSNOx. The injection timing and air-fuel ratio were selected as parameters for optimization, and it was possible to improve both variables. The method selects optimum conditions for a given purpose due to the NOx emissions and fuel economy to involve a tradeoff. The results showed that engine-makers could thus minimize fuel consumption when meeting emission criteria.

Niu et al. [14] proposed a novel online optimization approach using NSGA-II coupled with a machine learning method. The optimization approach was conducted based on an engine physical model, which was calibrated and validated carefully using experimental data. The results showed that, based on the Pareto-optimal solutions obtained by the proposed optimization approach, by combining the maps, the solving process of multi-objective optimization problems will be significantly facilitated.

Millo et al. [15] applied random optimization methods and surrogate models to generate a population of engine calibrations, which then served as an initial population to a specifically conceived Genetic Algorithm (GA) based optimizer. It was finally applied to a real data set for a particular engine operating point. The results showed that a large number of optimized calibrations were scattered along with the complete model domain while providing a significant reduction in NOx (20 %) and BSFC (1 %).

Considering that there has not been any research on the use of JP-4 blended with biodiesel in the diesel engines and that this aviation fuel, JP-4, is one of the most important products in Iran by NIOPD Company, this study turned to the optimization of performance and emission characteristics of a CI engine fueled with aviation fuel-biodiesel-diesel blends at different engine speeds and loads using Mixture-RSM.

2. METHODS

2.1. Optimization

One of the important abilities of the Mixture-RSM method is the optimization of complex processes and the evaluation of interactive effects among the variables.

According to the experimental tests based on the matrix obtained from Mixture-RSM, the mathematical models were developed. In this study, the ranges of fuel variables were considered as 0 to 100, 0 to 100, and 0 to 20 for biodiesel, diesel, and Jet Propellant (JP -4) percentage in the fuel mixture, respectively. Moreover, the ranges of 20 to 100 % and 1200 to 2600 RPM were determined for engine loads and speeds, respectively. The specifications of the engine on which experimental tests were carried out are presented in Table 1. In this way, the number of dependent variables was predicted by developed mathematical models.

Table 1. The test engine specifications.

Model	OM364
Number of cylinders	4
Stroke (mm)	133
Bore (mm)	97.5
Compression ratio	17:1
Maximum power	92 kW at 2400 RPM
Maximum torque	455 N.m at 1450 RPM
Cooling system	Water

After that, the optimization of the performance and emission characteristics of the engine was performed according to the results optioned from extracted models.

In the present research, the desirability approach was applied to optimize the independent variables (diesel, biodiesel, and JP-4 percentages in the fuel blend and engine load and speed) for the measured properties of responses (brake power and torque, BSFC, NOx, HC, and CO) [16]. The optimization analysis that was performed by Design Expert version 7 and the responses of brake power and brake torque were selected to be maximized, and HC, CO, NOx, and BSFC were considered to be minimized in the software.

The optimization process in this research is included in six scenarios:

- Scenario 1: Determination of the optimized area considering the performance parameters of the engine (the limits of optimization criteria were defined as the half value of the brake power and torque as the lower limit and the maximum value of these parameters as the upper limit; in addition to BSFC, the limits were defined as the minimum value of this parameter as the lower limit and the half value of it as the upper limit).
- Scenario 2: Determination of the optimized area considering the emission parameters of the engine (the limits of the optimization criteria were defined as the minimum value of the emission parameters as the lower limit and the half value of the emission parameters as the upper limit).
- Scenario 3: Determination of the optimized area considering both performance and emission parameters of the engine (the limits of the optimization criteria were defined as the combination of the lower and upper limits of Scenarios 1 and 2).
- Scenario 4: Determination of the optimized point with the higher importance weight of the performance parameters of the engine (the optimization criteria were defined with an importance weight of 5 for the performance parameters and an importance weight of 3 for emission parameters).
- Scenario 5: Determination of the optimized point with the importance of the emission parameters of the engine (the optimization criteria was defined with an importance

weight of 3 for the performance parameters and an importance weight of 5 for emission parameters).

- Scenario 6: Determination of the optimized point with the importance of the both of performance and emission parameters of the engine (the optimization criteria were defined with an importance weight of 5 for both of performance and emission parameters).

3. RESULTS AND DISCUSSION

3.1. The maximum and minimum value of parameters

According to the extracted models, the maximum and minimum values of the performance and emission parameters are shown in Table 2.

Table 2. The maximum and minimum values of parameters.

Variable	Data	
	Minimum	Maximum
Brake power (Kw)	5.6	95.6
Brake torque (N.m)	41.9	435.5
BSFC (gr/kw.hr)	207	476
CO (%)	0.015	0.062
HC (ppm)	2	25
NO_x (ppm)	138	841

3.2. Optimized area with consideration of performance parameters

The optimized area (red color) with the consideration of performance parameters is presented in Figures 1 and 2.

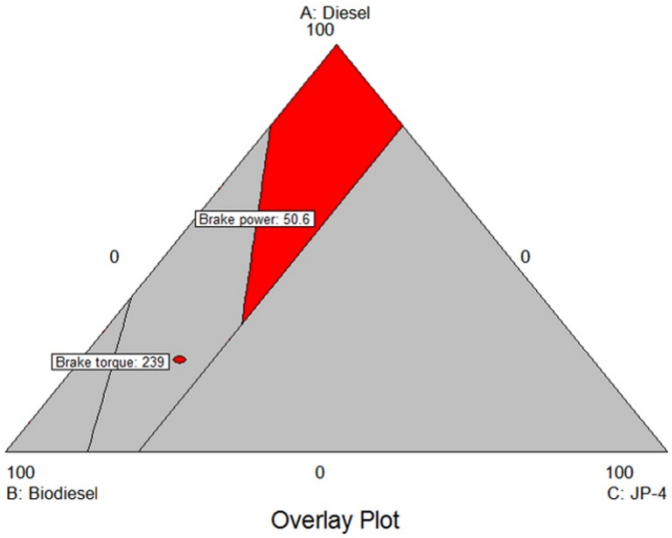

Figure 1. Optimized area with the consideration of performance parameters at a speed of 1900 RPM and an engine load of 60 %.

According to Figure 1, the optimized area at a speed of 1900 RPM and an engine load of 60 % belongs to the fuel blends including 30 to 50 % biodiesel. In addition, in this area, the percentage of diesel and jet fuel changes from 75 to 100 % and 0 to 20 %, respectively. This issue shows that a higher percentage of diesel and jet fuel can improve the performance parameters of the engine.

Based on Figure 2, the optimized area for fuel mixture D50B40J10 belongs to an engine speed of more than 1300 RPM and an engine load of more than 55 %.

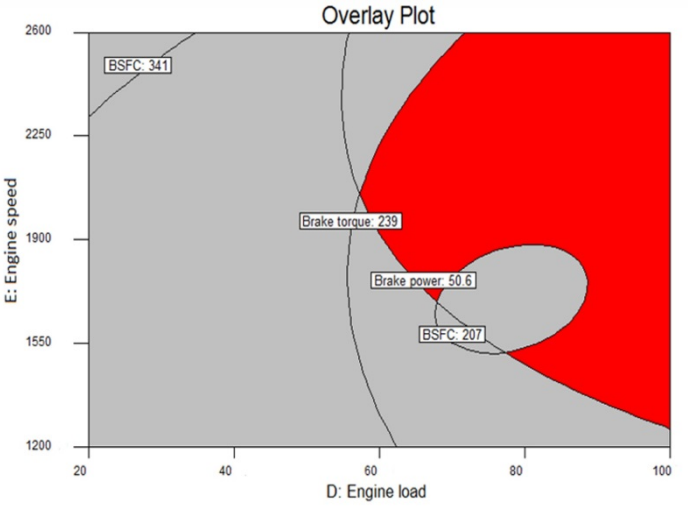

Figure 2. Optimized area with the consideration of engine performance parameters for fuel mixture D50B40J10.

3.3. Optimized area with consideration of emission parameters

The optimized area (red color) with the consideration of emission parameters is presented in Figures 3 and 4.

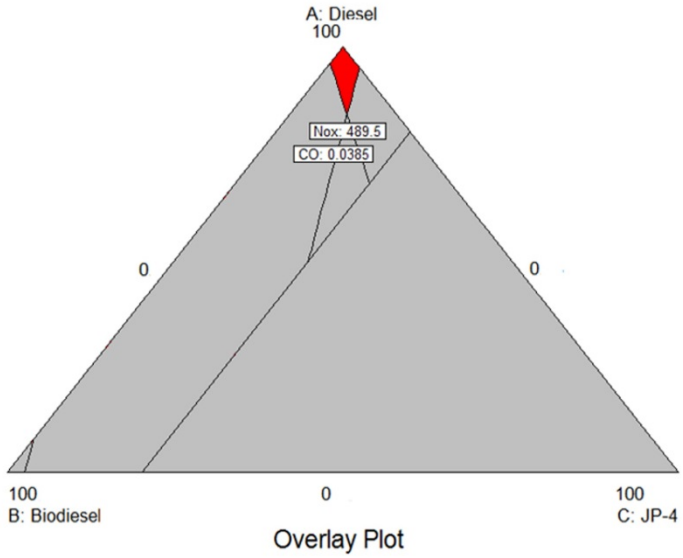

Figure 3. Optimized area with consideration of emission parameters at a speed of 1900 RPM and an engine load of 60 %.

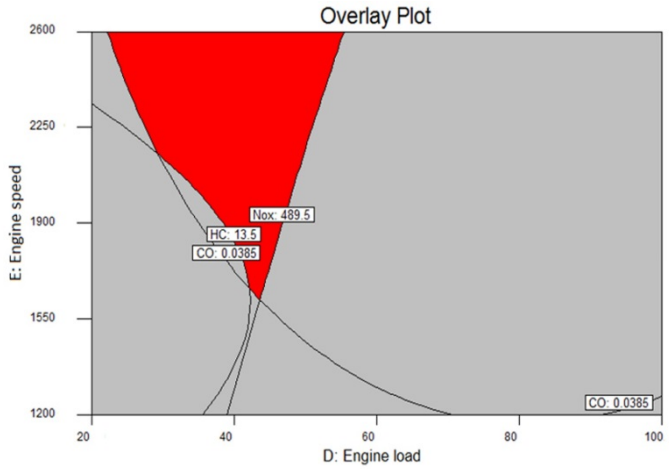

Figure 4. Optimized area with consideration of emission parameters for a fuel mixture of D50B40J10.

According to Figure 3, the optimized area at a speed of 1900 RPM and an engine load of 60 % belongs to the fuel blends including 0 to 10 % biodiesel. In addition, in this area, the percentage of diesel and jet fuel changes from 85 to 100 % and from 0 to 7 %, respectively. This issue shows that only a higher percentage of diesel can improve the engine parameters of the engine. This is due to the important role of biodiesel that has a negative effect on NOx emissions [17-20]. On the other hand, the negative impact of JP-4 on the CO and HC emissions limits the amount of aviation fuel in the fuel mixture [21-26]. Based on Figure 4, the optimized area for fuel mixture D50B40J10 belongs to an engine speed of more than 1600 RPM and an engine load lower than 45 %. This scenario showed that the optimum values of emission parameters overall occurred at lower engine loads in contrast with the optimum values of performance parameters that belonged to higher engine loads.

3.4. Optimized area with the consideration of both performance and emission parameters

The optimized area (red color) with the consideration of performance and emission parameters is presented in Figures 5 and 6.

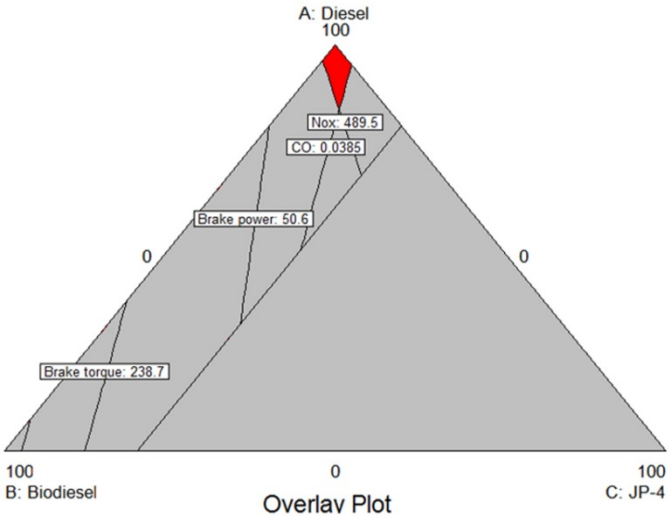

Figure 5. Optimized area with the consideration of both performance and emission parameters at a speed of 1900 RPM and an engine load of 60 %.

According to Figure 5, the optimized area at a speed of 1900 RPM and an engine load of 60 % belongs to the fuel blends including 0 to 10 % biodiesel. In addition, in this area, the percentage of diesel and jet fuel changes from 85 to 100 % and from 0 to 7 %, respectively. This issue shows that this plot did not change compared with the optimization scenario that included the consideration of the emission parameters. This is due to the negative effect of biodiesel on the NOx emission and negative impact of JP-4 on the CO and HC emissions.

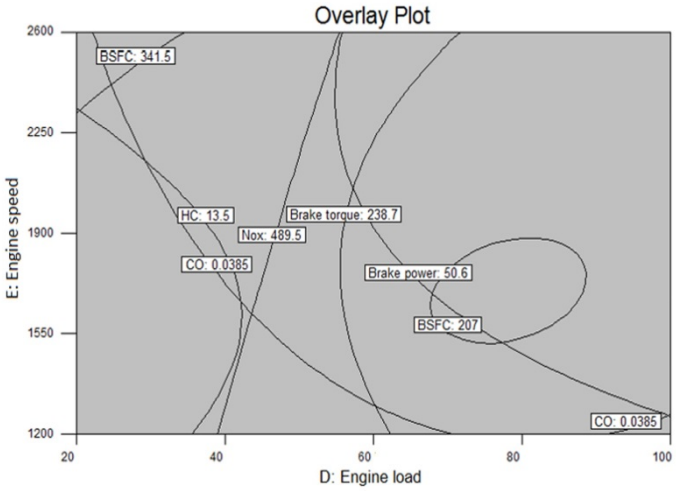

Figure 6. Optimized area with the consideration of both of performance and emission parameters for the fuel mixture of D50B40J10.

Based on Figure 6, there is no overlapped area as the optimized area for the fuel mixture D50B40J10 to satisfy the condition of both performance and emission parameters.

3.5. Optimized point with the higher importance for the performance parameters of the engine

The criteria for the optimization (weights and importance of the parameters, lower and upper limits, and the target of the responses) are presented in Table 3. Different solutions were achieved by the desirability-based approach, and the solution with high desirability was utilized.

The optimized point of the following independent parameters is fuel blend including 100 % diesel at 2344 RPM and full (100 %) engine load by obtaining the maximum desirability of 0.98. In this condition, the optimized values include 89.1 (kW), 371.2 (N.m), 230.9 (gr/Kw.hr), 0.03 (%), 435 (ppm), and 9.4 (%) for brake power, torque, BSFC, CO, NOx, and HC emissions, respectively.

Table 3. The criteria of the optimization.

Variable	Weights		Importance	Criterion
	Lower	Upper		
Diesel percentage in fuel mixture (%)	-	-	-	In-range
Biodiesel percentage in fuel mixture (%)	-	-	-	In-range
JP-4 percentage in fuel mixture (%)	-	-	-	In-range
Engine speed (RPM)	-	-	-	In-range
Engine load (%)	-	-	-	In-range
Brake power (Kw)	0.1	1	5	Minimize
Brake torque (N.m)	0.1	1	5	Minimize
BSFC (gr/kw.hr)	1	0.1	5	Minimize
CO (%)	1	0.1	3	Minimize
HC (ppm)	1	0.1	3	Minimize
NO_x (ppm)	1	0.1	3	Minimize

3.6. Optimized point with the higher importance of the emission parameters of the engine

The criteria for the optimization (weights and importance of the parameters, lower and upper limits, and the target of the responses) are presented in Table 4. Different solutions were achieved by the desirability-based approach, and the solution with high desirability was utilized.

Table 4. The criteria of the optimization.

Variable	Weights		Importance	Criterion
	Lower	Upper		
Diesel percentage in fuel mixture (%)	-	-	-	In-range
Biodiesel percentage in fuel mixture (%)	-	-	-	In-range
JP-4 percentage in fuel mixture (%)	-	-	-	In-range
Engine speed (RPM)	-	-	-	In-range
Engine load (%)	-	-	-	In-range
Brake power (Kw)	0.1	1	3	Minimize
Brake torque (N.m)	0.1	1	3	Minimize
BSFC (gr/kw.hr)	1	0.1	3	Minimize
CO (%)	1	0.1	5	Minimize
HC (ppm)	1	0.1	5	Minimize
NO_x (ppm)	1	0.1	5	Minimize

The optimized point for the following independent parameters was fuel blend including 31 % diesel, 50.7 % biodiesel, 18.3 % JP-4 at 2600 RPM and full engine load by obtaining the maximum desirability of 0.968. In this condition, the optimized values include 87 (kW), 320 (N.m), 268 (gr/Kw.hr), 0.0236 (%), 505 (ppm), and 5.9 (%) for brake power, torque, BSFC, CO, NOx, and HC emissions, respectively.

3.7. Optimized point with the same importance of the performance and emission parameters of the engine

The criteria for the optimization (weights and importance of the parameters, lower and upper limits, and the target of the responses) are presented in Table 5. Different solutions were achieved by the desirability-based approach, and the solution with high desirability was utilized.

Table 5. The criteria of the optimization.

Variable	Weights		Importance	Criterion
	Lower	Upper		
Diesel percentage in fuel mixture (%)	-	-	-	In-range
Biodiesel percentage in fuel mixture (%)	-	-	-	In-range
JP-4 percentage in fuel mixture (%)	-	-	-	In-range
Engine speed (RPM)	-	-	-	In-range
Engine load (%)	-	-	-	In-range
Brake power (Kw)	0.1	1	3	Minimize
Brake torque (N.m)	0.1	1	3	Minimize
BSFC (gr/kw.hr)	1	0.1	3	Minimize
CO (%)	1	0.1	3	Minimize
HC (ppm)	1	0.1	3	Minimize
NO_x (ppm)	1	0.1	3	Minimize

The optimized point of the following independent parameters was fuel blend including 48.9 % diesel, 32.7 % biodiesel, and 18.4 % JP-4 at 2526 RPM and full engine load by obtaining the maximum desirability of 0.97. In this condition, the optimized values are 88.4 (kW), 337 (N.m), 255 (gr/Kw.hr), 0.0268 (%), 469 (ppm), and 7.7 (%) for brake power, torque, BSFC, CO, NOx, and HC emissions, respectively.

4. CONCLUSIONS

The main objective of this study was the optimization of the performance and emission characteristics of a CI engine fueled with aviation fuel-biodiesel-diesel blends at different engine speeds and loads using Mixture-RSM. According to the results, it was concluded that:

a) The optimized area in Scenario 1 showed that a higher percentage of diesel and jet fuel could improve the performance parameters of the engine.
b) The optimized area in Scenario 1 for fuel mixture D50B40J10 showed that the higher performance of the engine occurred at higher engine speeds and loads.
c) The optimized area in Scenario 2 showed that only a higher percentage of diesel could improve the engine parameters of the engine. This is due to the negative effect of biodiesel on the NOx emissions and negative impact of JP-4 on the CO and HC emissions limiting the amount of biodiesel and aviation fuel in the fuel mixture.
d) The optimized area in Scenario 2 for fuel mixture D50B40J10 showed that the better emission values of the engine occurred at higher engine speeds and lower engine loads.
e) The optimized area in Scenario 3 did not change compared with Scenario 2 due to the negative effect of biodiesel on the NOx emission and negative impact of JP-4 on the CO and HC emissions.
f) There was no overlapped area as the optimized area for the fuel mixture D50B40J10 to satisfy the condition of both performance and emission parameters.
g) In Scenario 4, the optimized point was D100 at an engine speed of 2344 RPM and full engine load to obtain 89.1 (kW), 371.2 (N.m), 230.9 (gr/Kw.hr), 0.03 (%), 435 (ppm), and 9.4 (%) for brake power, torque, BSFC, CO, NOx, and HC emission, respectively.
h) In Scenario 5, the optimized point was D31B50.7J18.3 at 2600 RPM and full engine load to obtain 87 (kW), 320 (N.m), 268 (gr/Kw.hr), 0.0236 (%), 505 (ppm), and 5.9 (%) for the brake power, torque, BSFC, CO, NOx, and HC emissions, respectively.
i) In Scenario 6, the optimized point was D48.9B32.7J18.4 at 2526 RPM and full engine load to obtain 88.4 (kW), 337 (N.m), 255 (gr/Kw.hr), 0.0268 (%), 469 (ppm), and 7.7 (%) for brake power, torque, BSFC, CO, NOx, and HC emission, respectively.

It is recommended that other optimization methods be used and compared with Mixture-RSM method. Moreover, the fuel mixture included diesel-biodiesel-alcohol-aviation that could be evaluated and optimized for the diesel engine.

5. ACKNOWLEDGEMENT

The authors would like to thank the Aerospace and Energy Conversion Research Center at Najafabad Branch, Islamic Azad University for partly supporting this study.

REFERENCES

1. Krishnamoorthi, M. and Malayalamurthi, R., "Engine characteristics analysis of chaulmoogra oil blends and corrosion analysis of injector nozzle using scanning electron microscopy/energy dispersive spectroscopy", ***Energy***, Vol. 165, (2018), 1292-1319. (https://doi.org/10.1016/j.energy.2018.10.112).
2. Sivaramakrishnan, K. and Ravikumar, P., "Optimization of operational parameters on performance and emissions of a diesel engine using biodiesel", ***International Journal of Environmental Science and Technology***, Vol. 11, No. 4, (2014), 949-958. (https://doi.org/10.1007/s13762-013-0273-5).
3. Raheman, H. and Phadatare, A.G., "Diesel engine emissions and performance from blends of karanja methyl ester and diesel", ***Biomass and Bioenergy***, Vol. 27, No. 4, (2013), 393-397. (https://doi.org/10.1016/j.biombioe.2004.03.002).
4. Hirkude, B.J. and Padalkar, S.A., "Performance optimization of CI engine fuelled with waste fried oil methyl ester- diesel blend using response surface methodology", ***Fuel***, Vol. 119, (2014), 266-273. (https://doi.org/10.1016/j.fuel.2013.11.039).
5. Anand, G. and Karthikeyan, B., "An investigation and engine parameters optimization of a spark ignition engine with gaseous fuels", ***Proceedings of 4th Dessau Gas Engine Conference***, Germany, (2005).
6. Zhang, B., JQ, E., Gong, J.K., Yuan, W.H., Zuo, W. and Li, Y., "Multi disciplinary design optimization of the diesel particulate filter in the composite regeneration process", ***Applied Energy***, Vol. 181, (2016), 14-28. (https://doi.org/10.1016/j.apenergy.2016.08.051).
7. Liu, J., Ma, B. and Zhao, H., "Combustion parameters optimization of a diesel/natural gas dual fuel engine using genetic algorithm", ***Fuel***, Vol. 260, (2020), 116365. (https://doi.org/10.1016/j.fuel.2019.116365).
8. Krishnamoorthi, M., Malayalamurthi, R. and Sakthivel, R., "Optimization of compression ignition engine fueled with diesel-chaulmoogra oil-diethyl ether blend with engine parameters and exhaust gas recirculation", ***Renewable Energy***, Vol. 134, (2019), 579-602. (https://doi.org/10.1016/j.renene.2018.11.062).
9. Saxena, V., Kumar, N. and Saxena, V.K., "Multi-objective optimization of modified nanofluid fuel blends at different TiO_2 nanoparticle concentration in diesel engine: Experimental assessment and modeling", ***Applied Energy***, Vol. 248, (2019), 330-353. (https://doi.org/10.1016/j.apenergy.2019.04.091).
10. Krishnamoorthi, M., Malayalamurthi, R. and Shameer, P.M., "RSM based optimization of performance and emission characteristics of DI compression ignition engine fuelled with diesel/aegle marmelos oil/diethyl ether blends at varying compression ratio, injection pressure and injection timing", ***Fuel***, Vol. 221, (2018), 283-297. (https://doi.org/10.1016/j.fuel.2018.02.070).
11. Singh, Y., Sharma, A., Tiwari, S. and Singla, A., "Optimization of diesel engine performance and emission parameters employing cassia tora methyl esters-response surface methodology approach", ***Energy***, Vol. 168, (2019), 909-918. (https://doi.org/10.1016/j.energy.2018.12.013).
12. Li, Y., Jia, M., Xu, L. and Bai, X., "Multiple-objective optimization of methanol/diesel dual-fuel engine at low loads: A comparison of reactivity controlled compression ignition (RCCI) and direct dual fuel stratification (DDFS) strategies", ***Fuel***, Vol. 262, (2020), 16673. (https://doi.org/10.1016/j.fuel.2019.116673).
13. Cho, J., Park, S. and Song, S., "The effects of the air-fuel ratio on a stationary diesel engine under dual-fuel conditions and multi-objective optimization", ***Energy***, Vol. 187, (2019), 115884. (https://doi.org/10.1016/j.energy.2019.115884).
14. Niu, X., Wang, H., Hu, S., Yang, C. and Wang, Y., "Multi-objective online optimization of a marine diesel engine using NSGA-II coupled with enhancing trained support vector machine", ***Applied Thermal Engineering***, Vol. 137, (2018), 218-227. (https://doi.org/10.1016/j.applthermaleng.2018.03.080).
15. Millo, F., Arya, P. and Mallamo, F., "Optimization of automotive diesel engine calibration using genetic algorithm techniques", ***Energy***, Vol. 158, (2018), 807-819. (https://doi.org/10.1016/j.energy.2018.06.044).
16. Montgomery, D.C., Design and analysis of experiments, John Wiley & Sons, (2008).
17. Shirneshan, A., Samani, B.H. and Ghobadian, B., "Optimization of biodiesel percentage in fuel mixture and engine operating conditions for diesel engine performance and emission characteristics by Artificial Bees Colony Algorithm", ***Fuel***, Vol 184, (2016), 518-526. (https://doi.org/10.1016/j.fuel.2016.06.117).
18. Buyukkaya, E., "Effects of biodiesel on a DI diesel engine performance, emission and combustion characteristics", ***Fuel***, Vol. 89, (2010), 3099-3105. (https://doi.org/10.1016/j.fuel.2010.05.034).
19. Mistri, G.K., Aggarwal, S.K., Longman, D. and Agarwal, A.K., "Performance and emission investigations of Jatropha and Karanja biodiesels in a single-cylinder compression-ignition engine using endoscopic imaging", ***Journal of Energy Resources Technology***, Vol. 138, (2015), 011202-011213. (https://doi.org/10.1115/1.4031317).

20. Hess, M.A., Haas, M.J., Foglia, T.A. and Marmer, W.N., "Effect of antioxidant addition on NOx emissions from biodiesel", ***Energy & Fuels***, Vol. 19, (2005), 1749-1754. (https://doi.org/10.1021/ef049682s).

21. Lee, J. and Bae, C., "Application of JP-8 in a heavy duty diesel engine", ***Fuel***, Vol. 90, (2011), 1762-1770. (https://doi.org/10.1016/j.fuel.2011.01.032).

22. Lee, J., Lee, J., Chu, S., Choi, H. and Min, K., "Emission reduction potential in a light-duty diesel engine fueled by JP-8", ***Energy***, Vol. 89, (2015), 92-99. (https://doi.org/10.1016/j.energy.2015.07.060).

23. Uyumaz, A., Solmaz, H., Yılmaz, E., Yamık, H. and Polat, S., "Experimental examination of the effects of military aviation fuel JP-8 and biodiesel fuel blends on the engine performance, exhaust emissions and combustion in a direct injection engine", ***Fuel Processing Technology***, Vol. 128, (2014), 158-165. (https://doi.org/10.1016/j.fuproc.2014.07.013).

24. Labeckas, G. and Slavinskas, S., "Combustion phenomenon, performance and emissions of a diesel engine with aviation turbine JP-8 fuel and rapeseed biodiesel blends", ***Energy Conversion and Management***, Vol. 105, (2015), 216-229. (https://doi.org/10.1016/j.enconman.2015.07.065).

25. Spadaccini, L.J. and Tevelde, J.A., "Autoignition characteristics of aircraft-type fuels", ***Combustion and Flame***, Vol. 46, (1982), 283-300. (https://doi.org/10.1016/0010-2180(82)90022-0).

26. Spadaccini, L.J., "Autoignition characteristics of hydrocarbon fuels at elevated temperatures and pressures", ***Journal of Engineering for Power***, Vol. 99, (1977), 83-87. (https://doi.org/10.1115/1.3446256).

JREE: Vol. 7, No. 1, (Winter 2020) 40-50

Journal of Renewable Energy and Environment

Research Article

Journal Homepage: www.jree.ir

Electrochemical Modeling and Techno-Economic Analysis of Solid Oxide Fuel Cell for Residential Applications

Sadegh Safari[a], Hassan Ali Ozgoli[b*]

[a] *School of the Environment and Energy, Islamic Azad University, Science and Research Branch, Daneshgah Blvd., Simon Bolivar Blvd., P. O. Box: 1477893855, Tehran, Iran.*

[b] *Department of Mechanical Engineering, Iranian Research Organization for Science and Technology (IROST), Sh. Ehsani Rad St., Enqelab St., Parsa Sq., Ahmadabad Mostoufi Rd., Azadegan Highway, P. O. Box: 3313193685, Tehran, Iran.*

PAPER INFO

Paper history:
Received 20 January 2020
Accepted in revised form 28 March 2020

Keywords:
Solid Oxide Fuel Cell
Electrochemical Model
Sensitivity Analysis
Economic Evaluation

ABSTRACT

In this paper, an electrochemical model was developed to investigate the performance analysis of a Solid Oxide Fuel Cell (SOFC). The curves of voltage, power, efficiency, and the generated heat of cell have been analyzed to accomplish a set of optimal operating conditions. Further, a sensitivity analysis of major parameters that have a remarkable impact on the economy of the SOFC and its residential applications has been conducted. The results illustrate that the current density and cell performance temperature have vital effects on the system efficiency, output power and heat generation of cell of the SOFC. The best system efficiency is approached up to 53.34 % while implementing combined heat and power generation might be further improved up to 86 %. The economic evaluation results indicate that parameters such as overall efficiency, natural gas price and additional produced electricity that has prone to be sold to the national power grid, have a significant impact on the SOFC economy. The results indicate the strong reduction in the purchasing cost of the SOFC, i.e. not more than $2500, and improving the electrical efficiency of SOFC, i.e. not less than 42 %, can be the breakeven points of investment on such systems in residential applications. Also, it is found that the target of this SOFC cogeneration system for residential applications in Iran is relying on considerable technological enhancement of the SOFC, as well as life cycle improvement; improvement in governmental policies; and profound development in infrastructures to mitigate legal constraints.

1. INTRODUCTION

Although a variety of co-generation technologies are available to provide residential buildings demands, individually heating and lighting, employing clean energy generation is still a significant source of energy supply.

Co-generation systems are able to produce two or more forms of useful energy using a primary energy source such as Natural gas. If properly designed and operated, these systems have prone to save energy due to their higher efficiency and lower emissions in comparison to parallel systems. Some systems such as Micro Gas Turbines, Internal Combustion Engines, Stirling Engines, and Fuel cells are considered as Combined Heat and Power (CHP) systems [1-4].

Renewable energy production techniques have been intensively studied in recent years. Since fuel cells inherently produce both electricity and heat simultaneously, they are thoroughly fitted to use in CHP applications. Among these existing technologies, solid oxide fuel cells (SOFC) have been extensively developed. Since SOFC work at high temperatures, this provides the opportunity of the CHP concepts employment and leading to a considerable improvement of the overall system efficiency. This technology also offers special benefits such as the ability to internal fuel conversion and the potential of efficient utilization of the generated heat energy. There are growing appeals for using the SOFC systems applications in small scale and residential buildings in recent years [5-8].

A techno-economic model for both Polymer Membrane Fuel Cell (PMFC) and SOFC for CHP applications in residential buildings that have been analyzed by Napoli, et al. It has suggested for reducing electricity network dependency, employing PEMFC is more suitable while using SOFC is more appropriate to decrease initial energy consumption [8]. Optimal design and operation of a SOFC cogeneration system for residential applications which was fed by syngas fuel have been evaluated by Yang, et al. in the mentioned study, the ability and capability of a SOFC system for supplying required energy demand of a residential building have examined thoroughly [9]. Longo, et al. [10], have studied the life cycle energy and environmental performances of a SOFC system for residential applications, their results revealed that eco-design solutions of the assessed system can be traced in the improvement of the energy system efficiency and reduction of emissions during the operation, and in the increase of the durability of the system components, thus reducing the number of their substitutions. The results also clarified that in order to avoid concurrent energy generation from conventional sources the recovery of the thermal energy generated by the SOFC is significantly useful [10]. Besides, [11-13] have investigated other applications of SOFC CHP systems in both commercial and residential buildings, as well as employment hybrid concept with Gas Turbine (GT) and Gasifier. Although, the SOFC systems are usually supplied by natural gas, which is converted by means of an internal reformer. This will dramatically reduce the system capital cost since any external fuel processing will be no longer required [12], Employing SOFC and gas turbine (GT), the gaseous fuel

*Corresponding Author's Email: a.ozgoli@irost.org (H.A. Ozgoli)

can be turned into heat and power. However, the combination of SOFC and GT has yielded higher performance [13, 14]. Ghadamian, et al. [15], proposed a novel hybrid pressurized SOFC/ GT power generation system, fed by biomass to serve in a small-scale industrial application. This hybrid system will provide superior utilization of natural resources that considerably decreases harmful impacts on the environment as well as making higher profit. The results have revealed, employing a decent cooling system such as an absorption chiller for cooling the inlet air will enhance the overall efficiency of combined cycle meaningfully [15].

Although this is now a mature field that is now being spun out into commercial, it has not developed in Iran's energy supplying sector suitably neither in small scale nor power plants.

However, addressing the fundamental challenges of the SOFC such as its cost and life-cycle have a crucial impact on nurturing and mastering this technology in Iran's energy sector which makes it able to compete with existing systems, some impediments such as high investment cost, natural gas price as well as the sale price of surplus electricity to the government are adding fuel to this challenge, too. To our knowledge, there are a variety of studies aimed to analyze SOFC cost, power or efficiency while a few studies might have examined economy of the SOFC versus efficiency, however, this study investigates the impacts of some operating parameters such as the efficiency of the system on the SOFC's economy, thoroughly.

As discussed earlier, a variety of the previous literature has focused solely on the technical aspects of the SOFC technology, whereas the technical and economic aspects of technology are firmly coupled to each other. For this study, it was of interest to investigate a sensitivity analysis on key performance parameters of the SOFC aimed to achieve the best operating conditions, further some pivotal parameter on the economy of the system such as fuel cell purchase cost, operational life-cycle, sell price of surplus electricity to government, and the effect of feeding fuel of the SOFC will be examined and evaluated. Since not all prevailing factors have been comprehensibly studied, it is still necessary to apply a tailored approach. Therefore, this work intends to develop a parametric investigation of a SOFC performance to assist in obtaining appropriate operating conditions and a more sophisticated analysis of the economy of the SOFC system to apply this technology in Iran's energy sector individually in residential sectors.

The main objectives of the present study can be summarized as follows:

(1) development of a validated model depicting a SOFC system behavior to form a basis of economic evaluations.
(2) investigation of the effects of all three polarization losses on the voltage regard to various working conditions.
(3) performing a parametric investigation of the system on key performance parameters of the SOFC aimed to assist finding the best-operating conditions.
(4) study the impact of some pivotal parameters on the economy of the system using in residential applications.

2. MATERIAL AND METHODS

2.1. SOFC system

The schematic diagram of the electrochemical processes occurring in a tubular SOFC system is illustrated in Figure 1. As can be seen, The SOFC system consists of two Anode and Cathode electrodes separated by a ceramic electrolyte. To conduct negative oxygen ions within the cathode electrode and the anode electrode a solid oxide electrolyte is facilitated. Further, the electrons created at the anode side pass within an external circuit and will introduce to the cathode electrode. Then electrical circuit will be completed and electricity will be generated [16].

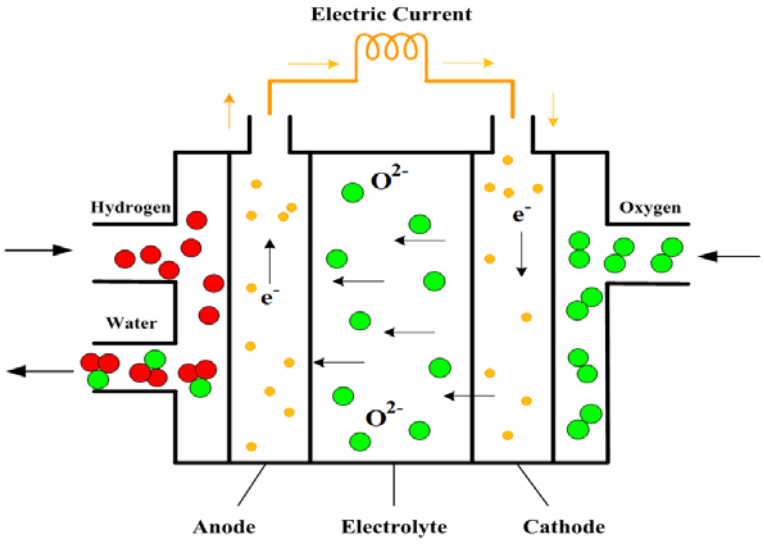

Figure 1. The schematic of SOFC system.

2.2. Model assumption

Principal assumptions of developing the SOFC system are listed as follows [16, 17]:

- All gases are considered as ideal gas.
- Internal distribution of temperature and pressure is assumed uniform through the SOFC.
- The fuel supplied to the system is assumed to be Natural gas with a composition of 97 % CH_4, 1.5 % CO_2, and 1.5% N_2.
- The air composition, provided for the cathode side is assumed to consist 79 % N_2 and 21 % O_2.
- By using internal reformer, the fuel inside of the SOFC will be formed into hydrogen.

These assumptions are employed throughout the analysis to derive the corresponding equations of each the SOFC system[16, 17].

2.3. System modeling

Among all developed electrochemical models of the SOFC, a zero-dimensional model that has employed in the present study is considered as the most suitable option for analyzing the system performance in terms of both integrity and fast response [16].

One of the key intentions of the developed model is acquiring the voltage variations and current density with an acceptable fluctuation. Briefly, the developed model should comprise the following features:

- Calculation process must be precise and reliable;
- The developed model must provide a vast operating range and running sensitivity analysis;
- The model can be easily integrated into the economic model;

In the present study, some of the influential factors such as the Nernst equation, Activation, Ohmic, and Concentration polarization have taken into consideration. In the economic sector, first and foremost, the mathematical correlation between SOFC investment cost, operation, and maintenance costs with its power generation have examined. Moreover, the financial index will be examined regarding the vital economic parameters of the system. To simulate the model MATLAB environment is used.

2.3.1. Electrochemical model of SOFC

In order to analyze the SOFC system parameters, it is crucial to consider a model that is capable of predicting the performance based on its operating condition. The proposed SOFC is built on a tubular design which has been designed and demonstrated by Siemens-Westinghouse [18].

The gas flow will enter the pre-reformer, then reforming and shifting reactions occur, i.e. ($CH_4 + H_2O \leftrightarrow 3H_2 + CO$) and ($CO + H_2O \leftrightarrow H_2 + CH_4$), respectively. As a result, a portion of methane will be turned into hydrogen.

The exhaust gas composition of the internal reformer may be obtained from k_r, and k_s constants as follows:

$$k_r = e^{(\Delta G_T/RT)} = \frac{(p_{H_2})^3 . p_{CO}}{p_{CH_4} . p_{H_2O}} \quad (1)$$

$$k_s = e^{(\Delta G_s/RT)} = \frac{p_{H_2} . p_{CO_2}}{p_{CO} . p_{H_2O}} \quad (2)$$

here the subscripts s and r denote the shifting and reforming reactions, respectively, R is the universal gas constant, ΔG indicates Gibbs free energy at standard conditions for the electrochemical reaction, and the partial pressures of the reacted gas streams is presented by p_i [17].

The fuel utilization factor, U_f, is an important parameter that represents the ratio of hydrogen amount consumed in the SOFC to the amount of supplied fuel may be formulated as [17]:

$$U_f = \frac{\dot{z}}{4.\dot{n}_{CH_4} + \dot{n}_{H_2} + \dot{n}_{CO}} \quad (3)$$

where ż indicates the hydrogen amount that reacted at the electrochemical reaction [17].

The reversible voltage of the SOFC can be obtained by the Nernst equation, as following while the Nernst voltage can be calculated as follows [16]:

$$V_{nernst} = -\frac{\Delta G^0}{2F} - \frac{RT}{2F} \ln \left[\frac{p_{H_2} . p_{O_2}{}^{1/2}}{p_{H_2 0}} \right] \quad (4)$$

where F refers to Faraday's constant (96485.33 C mol^{-1}), cell temperature is introduced by T and p indicates the partial pressure of respective species.

The operating voltage drops when the electric current is drawn from the cell, mainly because of some loss such as ohmic, activation and concentration polarization, which are individually categorized as electrochemical reaction activation, V_{act} ohmic polarization, V_{ohm} and concentration depletion, V_{Con}. Operating cell voltage, V_{Cell}, can be calculated as following [16]:

$$V_{cell} = V_{nernst} - (V_{act} + V_{ohm} + V_{con}) \quad (5)$$

Chemical reactions, comprising electrochemical reactions, consist of energy restrictions that must be addressed by reacting species. This energy barrier is named the activation energy and appears in activation polarization, the main reason behind this is charges transferring between the electronic and ionic conductors.

Activation polarization can be calculated by the Butler-Volmer equation, expressed as [16]:

$$j = j_0 \left[\exp\left(\frac{\beta n_e F V_{act}}{RT} \right) - \exp\left(-(1-\beta) \left(\frac{n_e F V_{act}}{RT} \right) \right) \right] \quad (6)$$

where j indicates the current density, β refers to transfer coefficient, and j_0 refers to exchange current density [16].

$$j_0^{an} = \gamma^{an} \left[\left(\frac{p_{H2}}{P^0} \right) \left(\frac{p_{H2O}}{P^0} \right) \exp\left(\frac{E_{act}^{an}}{RT} \right) \right] \quad (7)$$

$$j_0^{ca} = \gamma^{ca} \left[\left(\frac{p_{O2}}{P^0} \right)^m \exp\left(-\frac{E_{act}^{ca}}{RT} \right) \right] \quad (8)$$

here γ is denoted pre-exponential coefficient, P is ambient pressure, E refers to activation energy.

Moreover, ohmic polarization which is related with electron and ion transmission processes is determined by the following equations based on ohm's law [16]:

$$V_{Ohm} = i \sum_k r_k \quad (9)$$

$$r_k = \sum_k \frac{\rho_k \delta_k}{A} \quad (10)$$

$$\rho_k = \sum_k a_k \exp^{(b_k/T)} \quad (11)$$

where r_k is ohmic resistance, δ_k refers to the current flow length and ρ_k indicates the material resistivity. The coefficients of a and b are the characteristics of component materials [16].

The concentration loss which is a result of the transport of gases to the electrodes will be calculated as [16]:

$$V_{con} = \frac{RT}{2F} \ln \left(1 + \frac{p_{H_2} . j}{p_{H_2} . j_{lim}} \right) - \frac{R.T}{2F} Ln \left(1 - \frac{j}{j_l} \right) \quad (12)$$

while j_l is the limiting current density and j refers to the current density that will be estimated by the following electrochemical reaction [16]:

$$j = \frac{n_e . F . \dot{z}}{A_c} \quad (13)$$

where n_e is the number of electrons that are produced per hydrogen mole by electro-chemical reactions, i.e. ($H_2 + \frac{1}{2} O_2 \rightarrow H_2O$), A_c is the cell activation area and z refers to the number of hydrogen moles per second, which reacts in the electrochemical reaction.

The electrical power generated from the SOFC can be calculated as [16]:

$$\dot{W}_{SOFC} = N . V_{Cell} . j . A_C \quad (14)$$

where N indicates number of cells. Also, the net electrical power of the SOFC can be given as:

$$\dot{W}_{SOFC,net} = \dot{W}_{SOFC} . \eta_{inv} \quad (15)$$

where η_{inv} (0.98) is the inverter efficiency [17].

The heat generated from SOFC electrochemical reactions can be calculated by following equation [16]:

$$\dot{Q}_{SOFC} = (\dot{m}_f * U_f * LHV) \quad (16)$$

Overall efficiency of the SOFC can be determined as following [16]:

$$\eta = \frac{\dot{W}_{net}}{\dot{Q}_{tot}} \quad (17)$$

2.3.2. Economic model of SOFC

Regarding the investment, operating, maintenance costs, the total annual cost of the system can be calculated by equation (18) [19]:

$$C_t = C_c + C_f + C_m \quad (18)$$

where, C_t is total investment cost, C_c annual investment cost, C_f operation cost and, C_m is maintenance cost.

Also, the annual investment cost, regardless of the cost of replacing the cells over the life-span of the SOFC, can be obtained from the following equation [19]:

$$C_c = C_{FC}\left(\frac{i_r(1+i_r)^n}{(1+i_r)^n - 1}\right) \quad (19)$$

here, C_{FC} is SOFC purchase cost regardless of the cost of replacing cells over the its life- span n, and i_r is annual interest rate (%).

Since thermal energy is considered as a by-product of the SOFC and is producing at a constant rate of electrical energy, the cost of production can be formulated as the following equation [19]:

$$C_f = \left(\frac{\gamma_{Ng} . E_{ep}}{\eta}\right) \quad (20)$$

where, γ_{Ng} is natural gas price $\$kWh^{-1}$ and η is electrical efficiency.

Although repair and maintenance costs of the SOFC are highly dependent on its technology, in the previous literature is recommended 4 % to 10 % of the SOFC's cost accordingly in this study is assumed 10 % [19].

$$C_f = \left(\frac{\gamma_{Ng} . E_{ep}}{\eta}\right) \quad (21)$$

Further, the cost of each unit of electrical energy production $\$kWh^{-1}$ is calculated by the following equation [19]:

$$\gamma_p = \left(\frac{C_t}{E_P}\right) \quad (22)$$

where, E_p is annual energy production.

In residential applications, part of produced electricity will be consumed, which is signified by E_{ec} and surplus electricity will be sold to the government which is denoted by E_{es} as indicated following [19]:

$$E_p = E_{ec} + E_{es} + E_{th} \quad (23)$$

In this paper, it is assumed that surplus energy produced can be contracted to the government by γ_{es} ($), while there is not any appropriate infrastructure for selling the surplus thermal energy to the government, only can be stored in the user home by fascinating a thermal storage energy tank.

The economic value between thermal energy and electrical energy cannot be treated equally as they are priced differently in the market. Assuming consistent energy generation, the annual profit can be calculated from the following equation [19]:

$$B = E_{es}(\gamma_{es} - \gamma_p) + E_{ec}(\gamma_{ec} - \gamma_p) + E_{th}(\gamma_{th} - \gamma_p) \quad (24)$$

where B is the annual profit, γ_{es} is the electricity sale price and γ_{ec} is the electricity purchase price from the network.

Moreover, the Net Present Value (NPV), which is considered as a significant parameter in the economic evaluations of an energy system can be calculated as follows [19]:

$$NPV = \left(\sum_{t=1}^{n} \frac{B}{(1+i_r)^t}\right) \quad (25)$$

where t is operation period and i_r is annual interest rate.

NPV can be interpreted as some kind of income the owner of the SOFC generator can get during the whole lifespan of the SOFC, discounted by an interested rate. For example, for a family with a yearly income of $12,000, the $2000 NPV from the SOFC generation means 2 months' additional income for the family.

It should be noted that when the NPV of proposed system is bigger than zero, the economic feasibility of the system can be considered acceptable, otherwise the plan has not offered an economic justification [19].

2.4. Solution procedure

The calculation methodology is to first to determine the cell current at a given current density value. The amounts of hydrogen and oxygen required for the electrochemical reaction can be calculated at this identified current amount. Later, the value of utilization factor can be calculated by equations (1-3), then inlet molar flow rates of anode and cathode can be determined. Then, the cell voltage can be found by Nernst equation (4) and then voltage equation (5) at given operating cell temperature and pressure. Finally, heat and electrical power and efficiency will be calculated. More details about calculation procedures of voltage, polarizations and current density may be found in [15, 16].

2.5. Simulation and validation

The proposed model developed in the preceding sections is employed to determine and assess the performance of the SOFC system. Input parameters for simulation of SOFC

system is presented in Table 1, also more detailed may be found in [16, 17, 19].

Temporal variations of energy demand concerning various factors such as climate, building insulation, and consumption patterns are considered as a principal measure in designing a CHP system. In order to choose an appropriate capacity for the CHP system, it is necessary to determine the electricity and heat demand. On this basis, it is crucial to obtain the electrical and thermal demand curves of a residential building.

Table 1. Model input parameters and operating condition [16].

Parameter	Unit	Value
Pressure	bar	1
Temperature	K	1273
Fuel utilization factor	%	85
Air utilization factor	%	16.7
Anode energy activation	kJ $kmol^{-1}$	110,000
Cathode energy activation	kJ $kmol^{-1}$	155,000
Porosity	%	30

Therefore, in this study it is assumed that the electricity consumption profile for a typical household is alike in Figure 2, similarly the heat consumption profile is given by Figure 3 [19].

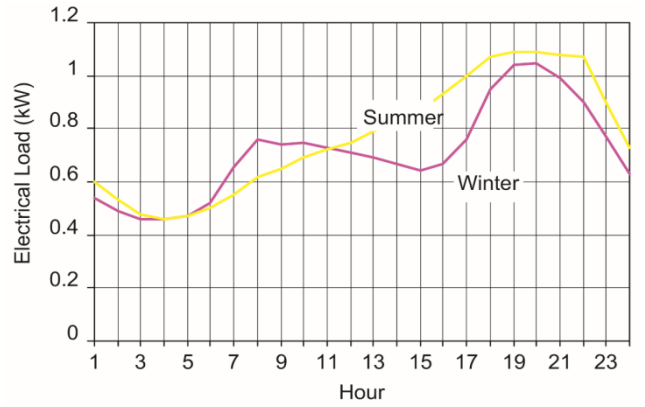

Figure 2. Electrical consumption profile a residential building [19].

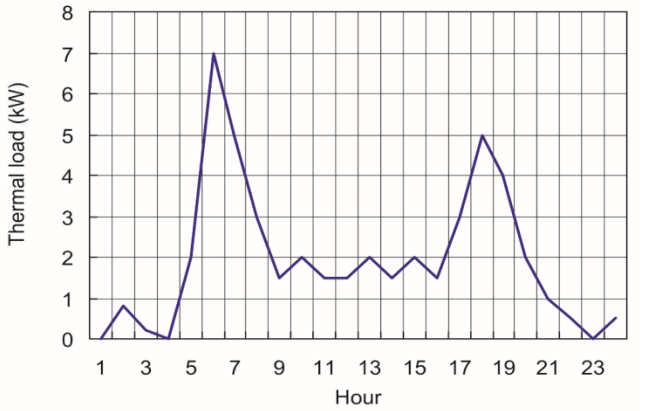

Figure 3. Thermal consumption profile of a residential building [19].

In Table 2, some basic economic information of SOFC that use natural gas as fuel is provided.

It is assumed that during the winter season, the recovered thermal energy is used to heat the environment while in the summer season, the SOFC's heat recovered, will be used to produce cold water through a lithium bromide-water absorption cycle, which is fed by hot water.

Table 2. Economic model input parameters [19].

Economic parameter	Value	Unit
SOFC purchase cost	4000	$
Natural gas purchase price	0.065	$\$kWh^{-1}$
Thermal energy purchase price	0.05	$\$kWh^{-1}$
Electrical energy purchase price	0.13	$\$kWh^{-1}$
Electrical energy sale price	0.16	$\$kWh^{-1}$
Cost of energy production	0.136	$\$kWh^{-1}$
Interest rate	5	%
Operating period	5	Year
Reference Net Present Value	-4239	$

In Table 3, in order to indicate the model validation and accuracy, some simulation results of the proposed model are compared to existing studies [16]. Our results are in a reasonable agreement with counterparts in literature.

Table 3. Simulation results of the present study compared to literature [16].

Parameter	literature	Simulation results	Relative error (%)
Cell voltage (V)	0.678	0.617	-9.8
DC electrical power (kW)	187	187.53	0.28
AC electrical power (kW)	176	175.2	-0.45
Electrical Efficiency (%)	57	58.47	2.57

After simulating, the results are compared for cell voltage and power in Figures 4 and 5, respectively. Power at the current density range of 1500-6500 Am^{-2} shows excellent compliance with reference model [16].

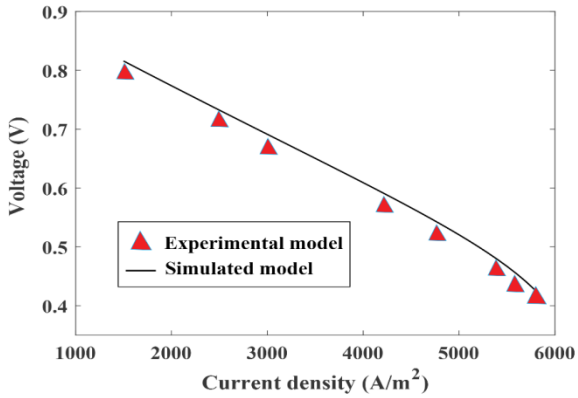

Figure 4. Cell voltage comparison of experimental model and simulated model.

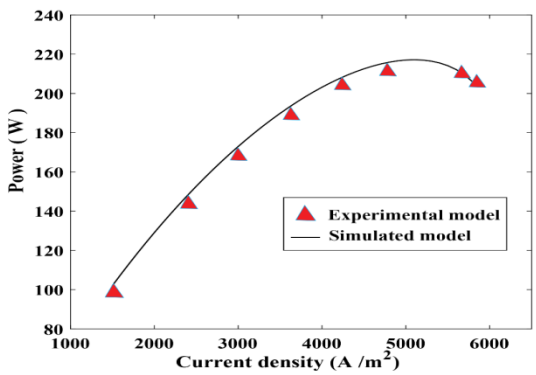

Figure 5. Cell power comparison of experimental model and simulated model.

As a result, it can be said that the model demonstrates good capability in evaluating SOFC performance.

3. RESULTS AND DISCUSSION

The results of modeling are given first to prove the impact of the operating parameters. Then, sensitivity analysis has been performed on some key operating parameters to determine a situation that makes the SOFC system an affordable and attractive system for residential applications.

3.1. Effect of the cell operating temperature variation on ohmic polarization

The influence of the cell operating temperature on ohmic polarization regard to different electrolyte thicknesses is illustrated in Figure 6. Current density is considered as fix parameter with value of 3000 Am^{-2}. As shown in Figure 6, increasing temperature leads to decrease ohmic potential loss which is mainly because of the reduction in ohmic resistance. Besides, the increase in electrolyte thickness, will raise the ohmic polarization drop, for example at a constant temperature of 1050 K, the ohmic drop values regard to the thicknesses of 10, 40 and 100 microns are 0.05, 0.09 and 0.2 V, respectively.

As indicated, increasing the electrolyte thickness will affect the length of the current, thus the ohmic resistance will be increased consequently, while its growth rate will be decreased when the temperature has increased. Accordingly, it can be concluded that higher operating temperatures as well as a lower electrolyte thickness will enhance the SOFC performance by reducing ohmic polarization drop.

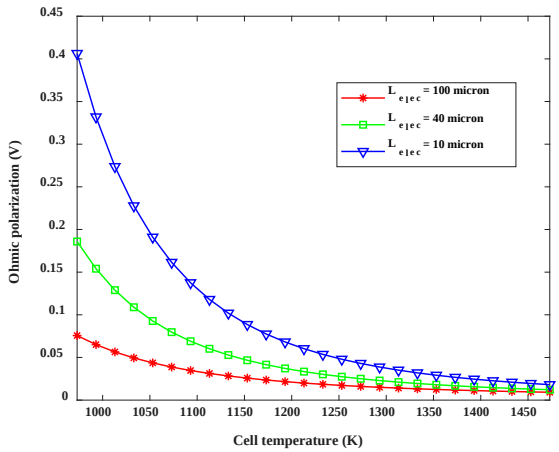

Figure 6. The cell operating temperature on ohmic polarization.

3.2. Effect of the cell operating temperature variation on activation polarization

The impact of cell operating temperature on activation polarization regard to different activation energy is determined in Figure 7. As it can be observed from Figure 7, activation polarization voltage will be decreased when the operating cell temperature is increasing, particularly in lower activation energy.

Activation energy depends on the cell's temperature and the properties of the material that is used in the electrolyte. In this model, the various values of activation energy from 12000 to 16000 (kJ/kmol) are investigated. As it can be seen, at a constant current density of 3000 Am^{-2}, by decreasing cell operating temperature, the activation loss will be raised while increasing cell temperature, will result in activation loss reduction significantly. This occurs mainly because the exchange current will be improved when the cell operating temperature is enhanced. Since higher exchange current density brings a more powerful electrochemical reaction rate, the activation loss will be reduced desirably.

Regarding the above analysis, to reach an improvement in the operating performance of the SOFC, materials with lower activation energy should be practiced for manufacturing purposes.

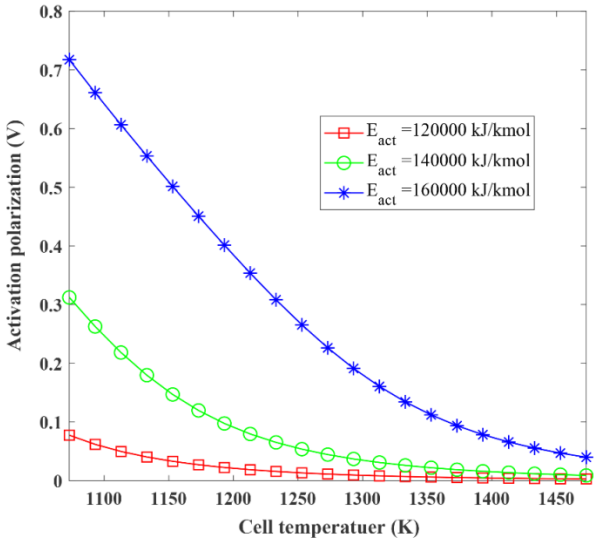

Figure 7. The cell operating temperature on activation polarization.

3.3. Effect of current density variation on diffusion polarization

The impact of the current density on diffusion polarization with respect to various pore size is examined and the results is shown in Figure 8. Since in concentration polarization, one of the most significant parameters is anode and cathode pore size, concentration polarization is examined concerning different pore sizes. The results prove that under atmospheric conditions, the concentration polarization drop will rise when the pore size diameter increased. For instance, in atmospheric condition and a constant value of 3000 Am^{-2}, for current density diffusion polarization is equal to 0.15, 0.25 and 0.5 V for thicknesses of 1.5, 1 and 0.5 microns, respectively.

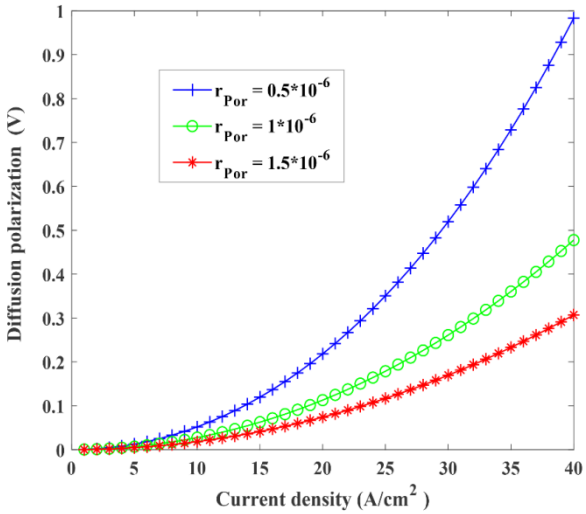

Figure 8. The current density variation on diffusion polarization.

3.4. Effect of current density variation on polarizations

To observe the variation of each polarization loss over the cell voltage, under standard operating conditions, the polarization of each loss for a given range of current density has been examined and illustrated in Figure 9.

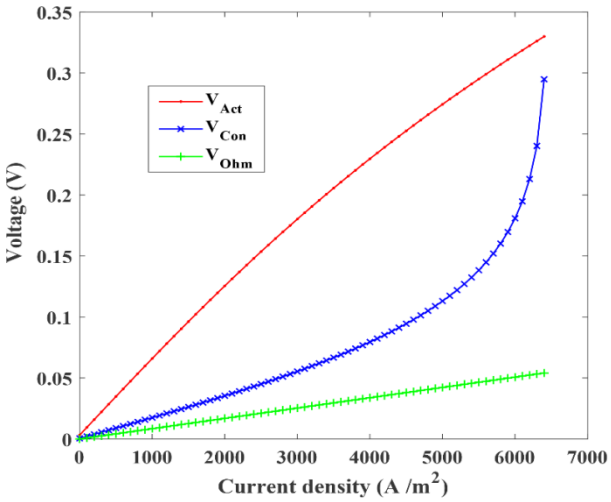

Figure 9. The current density variation on polarizations.

All polarization losses have risen when the current density has increased however, the most striking drop in the upward trend is the activation loss in which at a current density of 3000 Am^{-2}, its value is approximately 0.18 V. On the flip side, when the current density is approaching the limiting current density, the diffusion polarization is considerably increased at that point, which is even greater than the activation loss. Although the ohmic drop decreases linearly with the current density, it does not exceed 0.05 V even in the limiting current density range.

Therefore, by considering the above analysis it can be concluded that for a better voltage performance, the SOFC should be operating at a lower current density and this will lead to more power generation, too. However, for achieving this aim the cell surface must increase which will result in increasing SOFC's cost.

3.5. Effect of current density variation on voltage and power generation

The effect of the current density on voltage and power is examined, simultaneously and the results is shown in Figure 10.

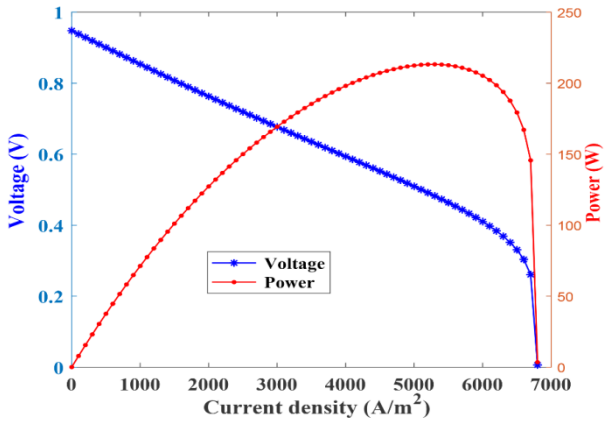

Figure 10. The current density variation on voltage and power.

The effect of the current density on voltage and power is examined, simultaneously and the results is shown in Figure 10. As indicated, the voltage and power curves intersect in the current density range of 3200 Am^{-2}, in which the voltage value is about 0.7 V and power generated at corresponding voltage is approximately 175 W. It can be observed that the maximum power of the cell obtains in the current density range of 5200 and has a value of about 210 W, at this point the cell voltage value is 0.48 V. Although the cell power improves when current density increase, the best operating region should be determined while both power and voltage best performance are taking into consideration. Therefore, it can be noticed that the best current density operating range has laid slightly lower than maximum power generation current density.

3.6. Effect of current density variation on voltage in different temperatures

The effect of the current density on voltage in different temperatures is investigated and the results is shown in Figure 11. It can be observed that higher working temperature leads to a lower Nernst potential.

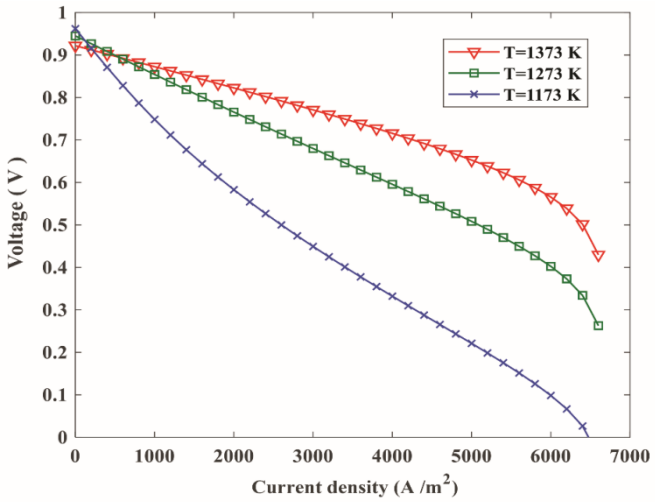

Figure 11. The current density variation on voltage in different temperatures.

For example, at the current density of 3200 Am^{-2}, at temperatures of 1173 K, 1273 K, and 1373 K the cell voltage value is approximately equal to 0.37, 0.65, 0.74 V. The main reason behind it is that there is a significant decrease in both the ohmic and the activation polarization will occur while the operating temperature is rising. Moreover, it can be seen that higher working temperatures will result in better power generation as well as limiting current density.

3.7. Effect of current density variation on power in different temperatures

In Figure 12, the impact of temperature variation on the power output has examined. As shown in Figure 12, at a constant value of current density of 3200 Am^{-2}, at temperatures of 1173, 1273, and 1373 K, the cell power generation will reach 110, 170, and 210 W, respectively.

From the above analysis, it can be concluded that a higher temperature provides a higher maximum power. Besides, it can be observed that by increasing temperature, the amount of maximum power agrees with the increase of the limiting

current density. For example, by increasing cell temperature from 1173 to 1373 K in a fix current density, the maximum power generation improves about 100 %.

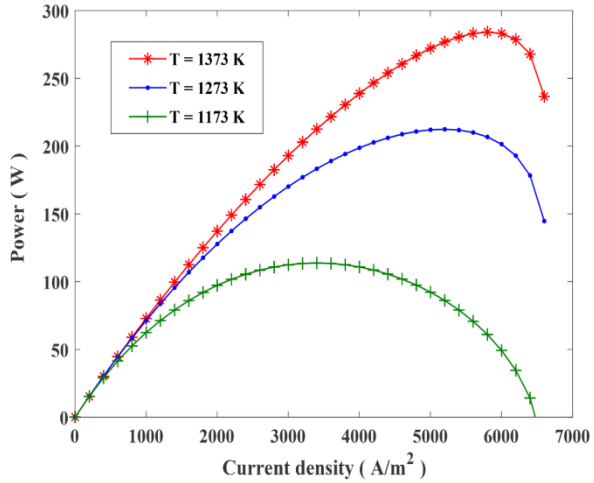

Figure 12. The current density variation on power in different temperatures.

3.8. Effect of the cell temperature Variation on the heat generation and efficiency

As discussed earlier, heat generated from the cell as well as cell efficiency are two crucial factors for predicting SOFC performance. In Figure 13, the cell efficiency is considered as an independent variable and the values of heat generation and cell efficiency at the constant current density of 3200 Am^{-2}, have investigated. The results prove that, since a lower operating temperature leads to more polarization losses, consequently heat generation of the cell will be enhanced considerably.

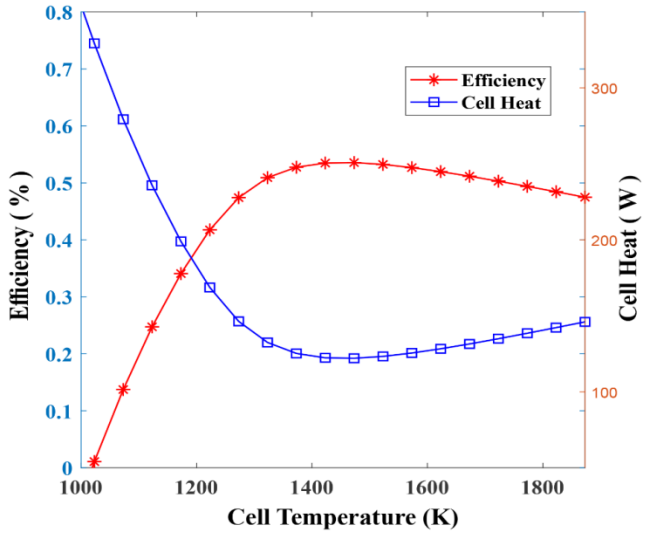

Figure 13. Cell temperature variations versus efficiency and cell's heat.

The heat generated by the SOFC electrochemical reactions declines while the temperature is increased to approximately 1430 K, later this value its trend turns to down. This is mainly because, the entropy-generated heat will be greater than the polarization-induced heat that will lead to a slight increment in the generated heat.

This individual characteristic of SOFC may provide the best opportunity to develop hybrid concepts and employing this technology as a CHP system in residential buildings. In this way, the user will be able to enhance the overall system efficiency by using heat recovery equipment.

4. ECONOMIC SCENARIO ANALYSIS

Sensitivity analysis has been performed on some key parameters of SOFC to make it an affordable and attractive system for residential applications.

4.1. Effect of SOFC efficiency improvements

The economic feasibility of the SOFC is strongly coupled with its efficiency somehow, developing technology and the internal design of SOFC leads to finished product cost reduction and make it economically viable and attractive. In Figure 14, the NPV variations regard to different efficiency range between 38 % and 46 % and the SOFC purchase price is evaluated. As it is shown, the NPV of the system will rise while the system efficiency has enhanced, and a similar trend can be seen while the purchase price of the SOFC is reducing.

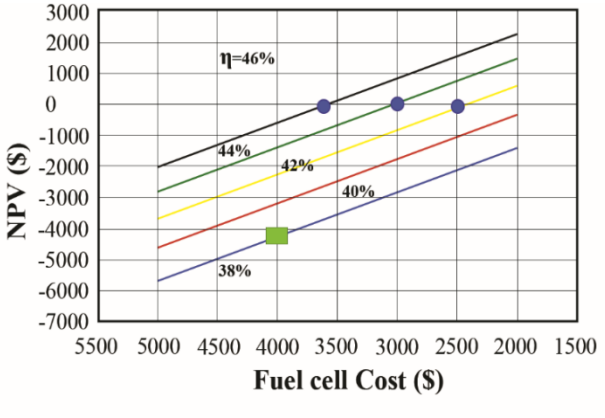

Figure 14. NPV variations regard to different efficiency.

In Figure 14, the reference status is shown with a green square. It can be seen, at the reference point with efficiency of 38 % and SOFC cost around $4000 the system provides a minimum economy attractiveness in which the NPV value is about -4200.

The first scenario could drastically fall in the purchase price of the SOFC, at least to less than $2,500 and improving efficiencies above 42 %, simultaneously. From another point of view, lowering prices below $3600 and advancing efficiencies above 46 % will lead to more attractive values of NPV and could make the SOFC system feasible for residential application purposes.

To accomplish this target, extensive research, and development program is required to address technical barriers and reach a more desirable efficiency and operating performance.

4.2. Effect of electricity sale price to the government

Increasing the purchase price of electricity, which is generated by a green or environmentally friendly power generation system, is considered as one of the most promising and efficient policies which are practiced by some developed countries.

As illustrated in Figure 15, at the reference point that is denoted with a green square, the grid sale price of $0.16 the fuel cell cost of $4000 the NPV value is about -4200 which is not desirable for any investment purposes.

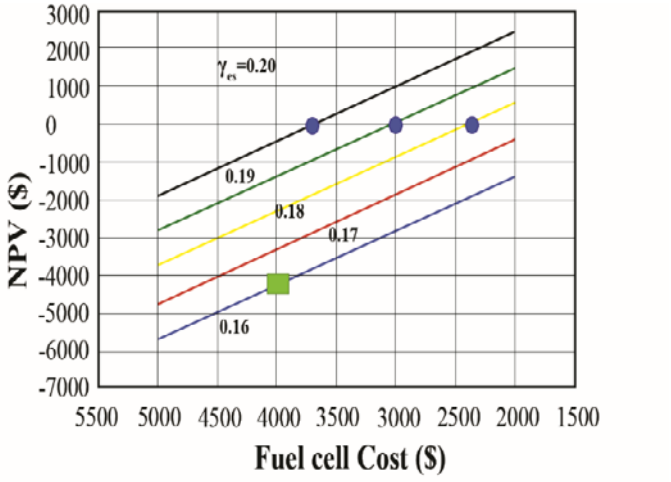

Figure 15. NPV variations versus different sale price of surplus electricity.

The effect of the sale price of surplus electricity in the range of \$0.16 to \$0.20 per kWh has demonstrated by Figure 15. As can be seen, the breaking even point will appear while the purchase price is lower than \$2400, and the sale price of electricity is \$0.18 per kWh.

As indicated, the increase in government electricity sale price has a significant impact on the economy of the system, with electricity purchasing at around \$0.20 per kWh, even at prices below \$3700 the system economy will reach to the break-even point. To provide ground for investment on mentioned technology, the governmental support in terms of guaranteed renewable electricity purchase tariffs is a vital action.

4.3. Effect of SOFC feed price

The income of a SOFC cogeneration system also is highly dependent on other factors such as the price of natural gas, consumed in the SOFC. Feed price is considered as one of the main concerns of SOFC -CHP application in residential buildings. Increasing the Natural gas rate will lead to a higher electricity price, which is generated by the SOFC system, and the economic feasibility of the CHP system might be endangered, significantly.

As depicted in Figure 16, the reference green square has demonstrated a \$0.065 price for the Natural price and \$4000 as the cost of SOFC. These conditions lead to NPV values of -4200 which is not attractive for investment.

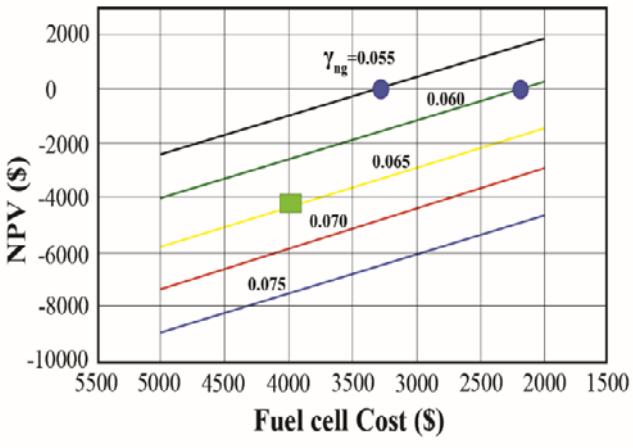

Figure 16. NPV variations versus different Natural gas price.

As is illustrated in Figure 16, the considered range of the Natural gas price is from \$0.05-\$0.055 per kWh. By assuming all variables fix, with a purchase price of less than \$2400, the break-even point will appear at prices below \$0.06 per kWh.

From the above analysis it can be concluded that to develop residential applications of the SOFC system, it is highly advisable to the government that may be reforming energy incentive policies can lead to spreading the SOFC cogeneration application, particularly in residential buildings.

4.4. Efficiency improvement in combined heat and power

Since the SOFC is operating at high temperatures, one way to improve efficiency is to recycle heat output from it. Applications of this heat recycling include space heating and supplying hot water for residential applications. In this study, at the best working point of electricity generation, the efficiency of the system 53.34 % at 1400 K working temperature. At this point, assuming the whole of thermal energy generated by the cell, the efficiency reaches 86.12 %. It should be noted that, whenever the electrical efficiency is decreased, the heat generation by the SOFC will be increased, as result by employing the CHP applications, the overall efficiency will be improved while this leads to a more fuel-efficiently and consequently a more economically efficient system.

5. CONCLUSIONS

In the present study, an electrochemical model has developed and the results concerning the economy of the proposed SOFC system have investigated. The chemical reactions within the SOFC have considered in which the SOFC performance investigation regard to some principal variables such as temperature, pressure and current density have discussed. The system polarization losses variation versus some key parameters such as the cell performance temperature have analyzed. Similarly, some functional properties of the SOFC such as anode and cathode pore size, activation energy and electrolyte thickness, have studied and analyzed. To accomplish this goal, the operating parameters have been modified to reach the best performance characteristics in both the technical aspect and financial attractiveness of the SOFC system. As analyzed above, the SOFC economy is highly dependent on its efficiency, therefore the NPV value will improve as efficiency being enhance. Further, simulation results were employed in economic evaluations. Economic analysis shows that the target cost of a SOFC residential application usage is about \$2400 regard to current Iranian network price in which in today's energy market, a 1 kW SOFC purchase price with an efficiency of about 38 % to 46 % has a purchase price of around \$6,000-\$7,000, therefore for economizing on the use of mentioned technology in residential applications, it requires a significant reduction in finished cost (at least \$2400>) and remarkably enhancement of efficiency. The present study is established to examine the possibility of the SOFC cogeneration system in hope of seeking a new resolution to employ this technology in residential building applications. Concerns have raised with regard to the technical issues and the economic viability of the system. In brief, destiny of this SOFC cogeneration system for residential usage in Iran is relying on: (1) considerable technological enhancement to improve the affordability of the

SOFC; (2) improvement in governmental policies in terms of guaranteed renewable electricity purchase tariffs; (3) improvement in life cycle of SOFC systems and (4) Profound development in infrastructures to mitigate legal constraints and address distributed generation systems barriers for network connection.

By considering the above aspects, this technology application will be more affordable and reliable for residential applications in Iran.

6. ACKNOWLEDGEMENT

We thank our colleagues who provided insight and expertise that greatly assisted the research.

NOMENCLATURE

A	Area (m^2)
A_c	Cell activation area
D_{eff}	Effective gas diffusion factor ($m^2\ s^{-1}$)
E	Activation energy (kJ $kmol^{-1}$)
F	Faraday's constant ($kmol^{-1}$)
i	Current (A)
j	Current density (Am^{-2})
J_o	Exchange current density (Am^{-2})
j_L	Limiting current density (Am^{-2})
L	Electrode thickness (m)
M	Molecular weight ($kgkmol^{-1}$)
n	Molar flow rates ($kmol^{-1}$)
ne	Number of electrons
p	Partial pressure (bar)
P	Operating pressure (bar)
Q_{Cell}	Heat generation rate (W)
r	Ohmic resistance (Ω)
r_{Por}	Average pore radius
R	Universal gas constant (8.134 $Jmol^{-1}k^{-1}$)
k	Fuel cell components
T	Cell temperature (K)
U_f	Fuel utilization factor
V_{Cell}	Cell voltage (V)
V_{nerst}	Nernst potential (V)
V_{Act}	Activation polarization (V)
V_{Con}	Concentration polarization (V)
V_{Loss}	Voltage losses (V)
V_{Ohm}	Ohmic polarization (V)
W_{el}	Electrical power (W)
z	Reacted hydrogen molar follow rate ($kmols^{-1}$)
NPV	Net Present Value

Greek letters

β	Transfer coefficient
δ	Current flow length (m)
ε	Porosity
γ	Pre-exponential coefficient
η	Efficiency
ρ	Material resistivity (Ωm)
τ	Tortuosity

Superscripts

an	Anode
ca	Cathode
e	Exit
i	Inlet

REFERENCES

1. Ozgoli, H.A., "Exergy analysis of a molten carbonate fuel cell-turbo expander-steam turbine hybrid cycle", ***Iranian Journal of Hydrogen & Fuel Cell***, Vol. 3, (2017), 267-279. (DOI: 10.22104/ijhfc.2017.480).
2. Ozgoli, H.A. and Ghadamian, H., "Energy price analysis of a biomass gasification-solid oxide fuel cell-gas turbine power plant", ***Iranian Journal of Hydrogen Fuel Cell***, Vol. 3, No. 1, (2016), 45-58. (DOI: 10.22104/IJHFC.2016.327).
3. Ozgoli, H.A., Ghadamian, H. and Hamidi, H., "Modeling SOFC & GT integrated-cycle power system with energy consumption minimizing target to improve comprehensive cycle performance (Applied in pulp and paper, case studied)", ***GSTF Journal of Engineering Technology***, Vol. 1, No. 1, (2012). (DOI: 10.5176/2251-3701_1.1.1).
4. Ahmadi, N., Dadvand, A., Mirzaei, I. and Rezazadeh, S., "Modeling of polymer electrolyte membrane fuel cell with circular and elliptical cross-section gas channels: A novel procedure", ***International Journal of Energy Research***, Vol. 42, No. 8, (2018), 2805-2822. (DOI: 10.1002/er.4069).
5. Pellegrino, S., Lanzini, A. and Leone, P., "Techno-economic and policy requirements for the market-entry of the fuel cell micro-CHP system in the residential sector", ***Applied Energy***, Vol. 143, (2015), 370-382. (DOI: 10.1016/j.apenergy.2015.01.007).
6. Ozgoli, H.A., Ghadamian, H., Roshandel, R. and Moghadasi, M., "Alternative biomass fuels consideration exergy and power analysis for a hybrid system includes PSOFC and GT integration", ***Energy Sources, Part A: Recovery, Utilization, and Environmental Effects***, Vol. 37, (2015), 1962-1970. (DOI: 10.1080/15567036.2012.654898).
7. Kupecki, J., "Off-design analysis of a micro-CHP unit with solid oxide fuel cells fed by DME", ***International Journal of Hydrogen Energy***, Vol. 40, No. 35, (2015), 12009-12022. (Doi: 10.1016/j.ijhydene. 2015.06.031).
8. Napoli, R., Gandiglio, M., Lanzini, A. and Santarelli, M., "Techno-economic analysis of PEMFC and SOFC micro-CHP fuel cell systems for the residential sector", ***Energy Buildings***, Vol. 103, (2015), 131-146. (DOI: 10.1016/j.enbuild.2015.06.052).
9. Yang, W., Zhao, Y., Liso, V. and Brandon, N., "Optimal design and operation of a syngas-fuelled SOFC micro-CHP system for residential applications in different climate zones in China", ***Energy Buildings***, Vol. 80, (2014), 613-622. (DOI: 10.1016/j.enbuild.2014.05.015).
10. Longo, S., Cellura, M., Guarino, F., Brunaccini, G. and Ferraro, M., "Life cycle energy and environmental impacts of a solid oxide fuel cell micro-CHP system for residential application", ***Science of The Total Environment***, Vol. 685, (2019), 59-73. (DOI: 10.1016/j.scitotenv. 2019.05.368).
11. Brown, J., Hajilounezhad, T., Dee, N.T., Kim, S., Hart, A.J. and Maschmann, M.R., "Delamination mechanics of carbon nanotube micropillars", ***ACS Applied Materials***, Vol. 11, No. 38, (2019), 35221-35227. (DOI: 10.1021/acsami.9b09979).
12. Marcoberardino, G.D, Chiarabaglio, L., Manzolini, G. and Campanari, S., "A techno-economic comparison of micro-cogeneration systems based on polymer electrolyte membrane fuel cell for residential applications", ***Applied Energy***, Volume 239, (2019), 692-705. (DOI: 10.1016/j.apenergy.2019.01.17).
13. Ozgoli, H.A., Moghadasi, M., Farhani, F. and Sadigh, M., "Modeling and simulation of an integrated gasification SOFC–CHAT cycle toimprove power and efficiency", ***Environmental Progress & Sustainable Energy***, Vol. 36, (2017), 610-618. (DOI: 10.1002/ep.12487).
14. Ozgoli, H.A., Ghadamian, H. and Farzaneh, H., "Energy efficiency improvement analysis considering environmental aspects in regard to biomass gasification PSOFC/GT power generation system", ***Procedia Environmental Sciences***, Vol. 17, (2013), 831-841. (DOI: 10.1016/j.proenv.2013.02.101).
15. Ghadamian, H., Hamidi, A., Farzaneh, H. and Ozgoli, H.A., "Thermo-economic analysis of absorption air cooling system for pressurized solid oxide fuel cell/gas turbine cycle", ***Journal of Renewable Sustainable Energy***, Vol. 4, No. 4, (2012), 043115. (DOI: 10.1063/1.4742336).
16. Akkaya, A.V., "Electrochemical model for performance analysis of a tubular SOFC", ***International Journal of Energy Research***, Vol. 31, No. 1, (2007), 79-98. (DOI: 10.1002/er.1238).

17. Akkaya, A.V., Sahin, B. and Erdem, H.H., "An analysis of SOFC/GT CHP system based on exergetic performance criteria", ***International Journal of Hydrogen Energy***, Vol. 33, No. 10, (2008), 2566-2577. (DOI: 10.1016/j.ijhydene.2008.03.013).

18. George, R.A., "Status of tubular SOFC field unit demonstrations", ***Journal of Power Sources***, Vol. 86, No. 1-2, (2000), 134-139. (DOI: 10.1016/S0378-7753(99)00413-9).

19. Bompard, E., Napoli, R., Wan, B. and Orsello, G., "Economics evaluation of a 5 kW SOFC power system for residential use", ***International Journal of Hydrogen Energy***, Vol. 33, No. 12, (2008), 3243-3247. (DOI: 10.1016/j.ijhydene.2008.04.017).

20. Ahmadi, N. and Rostami, S., "Enhancing the performance of polymer electrolyte membrane fuel cell by optimizing the operating parameter", ***Journal of the Brazilian Society of Mechanical Sciences and Engineering***, Vol. 41, No. 220, (2019). (DOI: 10.1007/s40430-019-1720-0).

21. Hajilounezhad, T., Ajiboye, D.M. and Maschmann, M.R., "Evaluating the forces generated during carbon nanotube forest growth and self-assembly", ***Materialia***, (2019), 100371. (DOI: 10.1016/j.mtla. 2019.100371).

JREE: Vol. 7, No. 1, (Winter 2020) 51-61

Journal of Renewable Energy and Environment

Research Article

Journal Homepage: www.jree.ir

Energy, Exergy, and Environmental Analysis and Optimization of Biodiesel Production from Rapeseed Using Ultrasonic Waves

Bahram Hosseinzadeh Samani[a*], Marziyeh Ansari Samani[a], Rahim Ebrahimi[a], Zahra Esmaeili[a], Ali Ansari Ardali[b]

[a] *Department of Mechanical Engineering of Biosystem, Shahrekord University, Shahrekord, Iran.*
[b] *Department of Applied Mathematics, Faculty of Methematical Sciences, Shahrekord University, Shahrekord, Iran.*

PAPER INFO

Paper history:
Received 28 January 2020
Accepted in revised form 31 March 2020

Keywords:
Exergy
Energy Consumption
Rapeseed
Biodiesel
Renewable Energy

ABSTRACT

Due to limited oil reserves, the rising world fuel prices and environmental problems caused by the use of fossil fuels increase the tendency to use alternative fuels such as biodiesel and bioethanol. In this study, the evaluation of energy and exergy flow from seed planting to final production of biodiesel from rapeseed oil was carried out. Biodiesel production from rapeseed was made in three main phases: farm, oil extraction, and industrial biodiesel production. Initially, the input and output variables for rapeseed production were collected through questionnaires from 30 rapeseed farms in Khuzestan province, Iran. Thus, the amount of energy input and output to the field for rapeseed was estimated to be 12826.98 and 22195 MJ/ha, respectively. The highest energy consumption is related to chemical fertilizers with 65 % share of other inputs. Input and output exergy rates were obtained as 3933.494 and 22603.39 MJ/ha, respectively, and the highest exergy consumption related to diesel fuel with 58 % share of other inputs. At the biodiesel production stage, the input energy and output energy were 156.95 MJ and 41.88 MJ, respectively, and the highest amount of electricity consumed was 91.02 MJ. The total amount of exergy in the production of biodiesel and the output exergy was 48.412 MJ and 64.568 MJ, respectively. In this study, the effects of alcohol-to-oil molar ratio, ultrasound power (W), catalyst concentration (w/w %), and the reaction time (min) on methyl ester yield using response surface methodology based on Box Behnken experimental design in the Design Expert software were investigated. Finally, gas emissions were studied at the planting and biodiesel production stages, and the resultsshowed that the highest greenhouse gas emissions at the planting stage were related to chemical fertilizers and alcohol production.

1. INTRODUCTION

World energy demand is steadily increasing due to economic growth and population. This growth is potentially problematic due to reduced non-renewable reserves, large-scale environmental degradation in the form of global warming, and atmospheric pollution caused by the combustion products of these fuels. To overcome the challenges of fossil fuels, renewable and alternative energy sources are now being searched for more than ever before. Biodiesel, derived from vegetable oils and animal fats, has been introduced as an environmentally friendly fuel as an alternative to diesel fuel [1, 2]. Until now, various sources have been introduced as biodiesel process feeds, which vary according to the materials and resources available in each region. One of these sources is oilseeds that is the second-largest food storage in the world. Rapeseed is one of the oilseeds whose cultivation has been considered as the main source of oil due to its adaptation to climate, resistance to drought stress, and alternation with cereals. FAO statistics show that rapeseed is the third-largest source of vegetable oil production in the world [3, 4]. This oilseed grows in most parts of Iran, and its oil content is about 40 to 45 % of the total grain weight [5]. Besides, rapeseed is currently the largest source of biodiesel production in the world. Biodiesel has been widely studied because of its attractive properties such as non-toxic, sulfur-free, oxygen content, biodegradable, and so on [6]. The triglyceride transesterification reaction is produced in the presence of a homogeneous/heterogeneous catalyst to intensify methanolysis [2, 7-9]. In order to produce biodiesel, ultrasound was used in this study. Ultrasonic irradiation has been shown to be one of the most promising techniques for converting different feedstocks to biodiesel by intensifying mass transfer of liquid–liquid heterogeneous medium [10]. The high energy contained in the ultrasonic irradiations generates cavities in the immiscible liquids, leading to the formation of micro fine bubbles. This in turn disrupts the phase boundary owing to the asymmetric collapse of generated microbubbles. Accordingly, a severe emulsification of the system close to the phase boundary is achieved due to the development of micro jets by violently impinged liquids [10].

A key indicator in producing a new energy source is its energy efficiency, which is the correlation between energy and exergy in the products received [11-13]. Energy use in agriculture is divided into direct and indirect energy consumptions [14]. Direct energy consumption in agriculture is achieved through the use of fuel and electricity [15], and indirect energy consumption in agriculture is provided by fertilizers and chemical materials [16]. The exergy method is a relatively new and alternative based on the energy concept, which is defined as a universal measure of the potential of work or the quality of various forms of energy in relation to a given environment. The exergy equilibrium applied to a process or an entire plant tells us how much of the potential

*Corresponding Author's Email: b.hosseinzadehsamani@sku.ac.ir (B. Hosseinzadeh Samani)

work potential usable as the input to the system in question is consumed (irreversibly destroyed). The disappearance of exergy, or irreversibility, provides a fully functional measure of process inefficiency. Many studies have been done on the exergy investigation of biodiesel production including the study of Hou and Zheng (2009) who proposed a novel design using solar-powered steam and electricity to produce biodiesel [17]. In another study, Jaimes et al. (2010) conducted an exergy analysis of biodiesel production from palm oil [18]. A study of the production of biodiesel from Microalga and Jatropha was also conducted by Ofori-Boateng et al. (2012) [19]. In another study, the amount of ExROI (exergy return on investment) and the renewable factor for biodiesel from cooking oil was calculated, indicating better stability of this source than other vegetable oils [20].

One of the factors affecting human health and the environment is greenhouse gas emissions during the agricultural life cycle. Understanding and evaluating the product life cycle is one way of measuring greenhouse gas emissions. Greenhouse gas emissions and their effects on global warming are one of the major challenges for developed and developing countries. Under the Kyoto Protocol, countries are required to calculate and report their greenhouse gas emissions [21]. According to the National Geographic Magazine, more than a million species of plants and animals will be at risk by 2050 due to rising greenhouse gases and global warming. In addition to energy and exergy analysis as a way of energy management, determining the amount of carbon dioxide emitted per energy consumed can be used as an analytical tool to calculate pollutant levels along with energy and exergy analyses. Moreover, because agriculture has a large share of greenhouse gas emissions, environmental management is an important part of production systems to identify points of production that have the greatest environmental and greenhouse gas impact on the environment. Biofuels have become one of the main strategies in developed countries in recent years, and this is due to climate change as one of the major contributors to climate change, i.e., CO_2 emissions. CO_2 prevents heat from escaping into the atmosphere by creating a layer around the Earth, thereby causing global warming. In fact, CO_2 emissions are the main cause of global warming.

It should be noted that no studies have reported about investigating biodiesel production from rapeseed examine exergy side in Iran. In general, the purpose of the present study is to analyze the thermodynamic and environmental analysis of the process of rapeseed production in the field and the process of biodiesel production from its seed oil.

2. MATERIALS AND METHODS

2.1. Energy and exergy cycle analysis method

Biodiesel production from rapeseed was made in three main phases: farm, oil extraction, and industrial biodiesel production. Initially, the input and output variables for rapeseed production were collected through questionnaires from 30 rapeseed farms of Khuzestan province in Iran. Inputs used in the production of rapeseed include labor, diesel fuel, chemical fertilizers, chemical pesticides, and seeds; on the other hand, the output is the amount of rapeseed production. The second stage of rapeseed oil extraction and the final stage (biodiesel production) were conducted at the Bioenergy and Renewable Energy Research Center of Tarbiat Modares University.

2.2. Main principles of exergy and energy analysis

Four equilibrium Equations (1 to 4) for work and heat processes (mass, energy, exergy, and entropy) were used to analyze energy and exergy of cultivation and methyl ester production of rapeseed oil [22]:

Mass balance:

$$\sum m_{in}=\sum m_{out} \quad (1)$$

Energy balance:

$$\sum(mb)_{in}-\sum(mb)_{out}=W-Q \quad (2)$$

Exergy balance:

$$\sum(mb)_{in}-\sum(mb)_{out}+\sum\left(1-\frac{T_0}{T_K}\right)Q_K-W=I \quad (3)$$

Entropy balance:

$$S_{generation}=\sum(ms)_{out}-\sum m_{in}\sum-\frac{Q_K}{T_K} \quad (4)$$

where Qk is the amount of heat transferred across the border (kJ), W is the work (kJ), b is the flow availability of a stream (kJ/kmol), H is the enthalpy (kJ/kmol), m is mass (kg), T is temperature (°K), and S is entropy (kJ/kmol K).

Therefore, the first step of this analysis is to convert all inputs and outputs to their energy and exergy equivalents, given their equivalent coefficients according to Table 1.

Table 1. Energy and exergy input coefficients of different inputs and outputs on the farm.

Input/Output	Unit	Energy factor (MJ/unit)	Source	Standard chemical exergy Ex0 (kJ·kg^{-1})	Source
Inputs					
Nitrogen	kg	78.1	[5]	11,450	[23]
Phosphate	kg	17.5	[24]	3137	[23]
Potassium	kg	13.7	[5]	258	[23]
Herbicides	-	288	[24]	25,000	[23]
Electricity	kWh	11.21	[25]	-	[23]
Diesel fuel	L	47.8	[26]	47,840	[23]
Labor force	h	1.96	[27]	0	[23]
Rapeseed seed	kg	25	[28]	27470	[23]
Output					
Rapeseed	kg	25	[28]	25460	[23]

2.3. Rapeseed oil production

At the cultivated stage, raw seeds are found as the main crop and straw as the by-product. Raw seeds should be dried and stored prior to the extraction process, which can be either physical (pressing) or chemical (solvent extraction). In this study, extraction using hexane is considered as a solvent, obtaining crude oil as the main crop and rapeseed meal as a common product, which can be used for animal feed. Then, to achieve a high-quality product, crude oil must be purified and treated using physical and therapeutic methods.

2.4. Transesterification and optimization of rapeseed oil into fatty acid esterification (FAE)

2.4.1. Transesterification

At this stage of the experiment, the oil reacts in the presence of methoxide, resulting in the production of biodiesel and glycerin. The materials used in this study include methanol (Merck Co., Germany, 99.9 %.) and Potassium hydroxide (Merck Co., Germany, 99.8 %.). An ultrasonic processor (Topsonic Model, UP400, Iran) was used to perform the transesterification reaction (Figure 1). Finally, all inputs and outputs convert to their energy and exergy equivalents, given their equivalent coefficients according to Table 2.

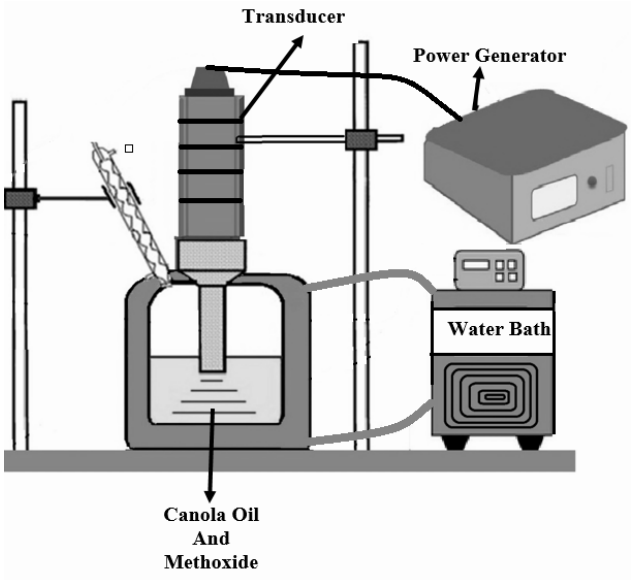

Figure 1. The schematic of setup biodiesel production.

Table 2. Energy and exergy coefficients in biodiesel production.

Input/Output	Unit	Energy factor (MJ/unit)	Source	Standard chemical exergy Ex0 (kJ·kg^{-1})	Source
Inputs					
Electricity	kWh	11.21	[25]	3.6	[23]
Rapeseed oil	kg	37.6	-	39930	[23]
Alcohol	kg	37.6	[29]	22360	[23]
Catalyst	kg	19.87	[30]	1867	[23]
Outputs					
Biodiesel	kg	37.2	[31]	39790	[23]
Glycerin	L	5.06	[30]	18670	[23]

2.4.2. Statistical analysis

The design of the present study is the response-box-Behnken method by the Design Expert software version 7. The response surface methodology is a set of mathematical and statistical techniques that are used to develop, promote, and optimize processes in which the level in question is affected by many variables, and the goal is to optimize the response. To derive optimal value, Regression Equation (5) is used [32, 33].

$$Y_i = \beta_0 + \sum \beta_i X_i + \sum \beta_{ij} X_i X_j + \sum \beta_{ii} X_i^2 + \varepsilon \quad (5)$$

where βo, βi, βij, and βii are constant coefficients, xi and xj are independent variables in the process, and ε is random error. The levels of independent variables were selected according to Table 3.

Table 3. Independent variables on the experiment.

Independent variable	Coded level		
	-1	0	1
Molar ratio (Alcohol to Oil)	4:1	6:1	8:1
Power of ultrasonic (W)	160	280	400
Catalyst (w/w %)	0.75	1	1.25
Reaction time (min)	3	6	9

2.5. Environmental impacts

Environmental impacts of chemical fertilizers, diesel fuel, etc. were considered at the farm stage, and emissions from diesel fuel, electricity, natural gas, methanol, and catalysts were estimated in biodiesel production. Based on the number of inputs consumed and the CO_2 emission factor, the amount of greenhouse gas emissions was calculated according to Table 4.

Table 4. Greenhouse gas emission factor from inputs.

Inputs	Unit	Coefficient GHG (kg	Source
Machine	MJ	0.071	[25]
Diesel fuel	L	2.76	[25]
Chemical fertilizer	-	-	[34]
Nitrogen	kg	1.3	[34]
Phosphorus	kg	0.255	[34]
Potassium	kg	0.2	[34]
Electricity	kW h	0.78	[35]
Methanol	kg	0.79	[29]
Potassium hydroxide	kg	1.20	[29]

3. RESULTS AND DISCUSSION

3.1. Energy and exergy analysis at rapeseed cultivation

All farming activities were considered during the farming season to produce rapeseed. Table 5 shows the content of the inputs and output. To calculate the amount of energy and exergy, the amount of consumption or production of each data is multiplied by the energy and exergy coefficients (Table 1).

Table 5. Amount of energy consumption and exergy of inputs and output in agricultural production of rapeseed per hectare.

Input/Output	Consumption	The amount of energy consumption (MJ ha^{-1})	The amount of energy consumption (MJ ha^{-1})
Inputs			
Nitrogen	83.01	6483.081	950.4645
Phosphate	73.35	1283.625	230.099
Potassium	47.9	656.23	12.3582
Herbicides	6.36	1831.68	159
Electricity	-	-	-
Diesel fuel	48.1	2299.18	2301.104
Labor force	9.15	17.934	-
Rapeseed seed	10.21	255.25	280.4687
Output			
Rapeseed	887.8	22195	22603.39

Compared to the studies of rapeseed conducted by Mousavi-Avval et al. (2011), rapeseed has lower inputs consumption than other crops such as wheat in terms of inputs, manpower, fertilizer, fuel, machinery, etc. The reason for lower input consumption is the rainfed agriculture of rapeseed in the study region. Among the mentioned inputs, nitrogen was the most consumed due to vegetative need and, also, due to farmers' ignorance and excessive use of fertilizer (Table 5); therefore, the total input and the output energy were obtained as 2826. 98 and 22,195 MJ/ha, respectively. The amount of this energy varies from region to region because of the lower yield of the product in different regions, followed by less input energy being consumed. Energy consumption in chemical fertilizers with 65 % share is higher than other inputs. Among the chemical fertilizers, nitrogen was the most consumed with 50 % and flowing by diesel fuel with 17 % and herbicides with 14 %. Therefore, in order to reduce energy consumption, nitrogen fertilizer should be saved (Figure 2).

The total amounts of exergy input and output are 3933.494 and 22603.39 MJ, respectively. The highest amount of exergy consumption is related to diesel fuel with a 58 % share of all other inputs. Among chemical fertilizers, nitrogen with 24 % and rapeseed with 7 % had the highest exergy consumption among the inputs. Therefore, the largest share of exergy consumption is related to diesel fuel (Figure 3).

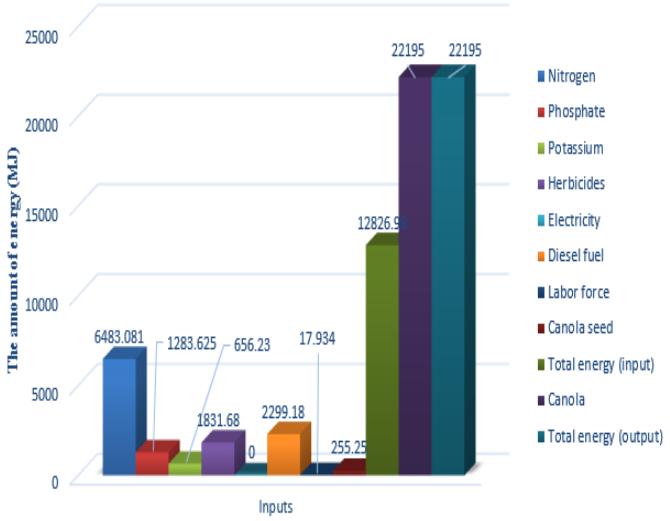

Figure 2. Input and output energy consumption of rapeseed production in the farms.

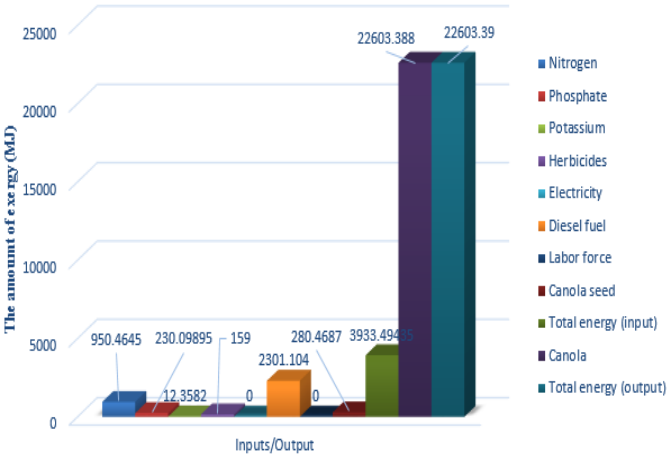

Figure 3. Input and output exergy consumption of rapeseed production in the farms.

3.2. Investigation of biodiesel production performance

To determine the energy and exergy quantities in biodiesel production, it is necessary to calculate the amounts of the biodiesel and glycerol components, and the results are presented in (Table 1). The biodiesel production experiment was conducted to evaluate the yield of biodiesel production in 28 tests, and the results are reported in Table 6.

Table 6. Full mass balance (kg) for the ultrasound-assisted biodiesel production from the rapeseed at different methanol/oil ratios, ultrasonic irradiation times.

Molar ratio	Time (min)	Catalyst (%)	Ultrasonic power (W)	Oil (kg)	KOH (kg)	Alcohol (kg)	Biodiesel (kg)	Glycerin (kg)	Yield (%)
4	6.00	1	400.00	0.05	0.0005	0.00687	0.032954	0.008231	76
8	9.00	1	280.00	0.05	0.0005	0.01358	0.044488	0.011112	93
4	6.00	1.25	280.00	0.05	0.000625	0.00687	0.030786	0.007689	71
8	6.00	1	400.00	0.05	0.0005	0.01358	0.042574	0.010634	89
8	6.00	1	160.00	0.05	0.0005	0.01358	0.040182	0.010037	84
6	6.00	1	280.00	0.05	0.0005	0.01018	0.039645	0.009902	87
6	6.00	1.25	400.00	0.05	0.000625	0.01018	0.038733	0.009674	85
4	3.00	1	280.00	0.05	0.0005	0.00687	0.030353	0.007581	70
6	6.00	1	280.00	0.05	0.0005	0.01018	0.0401	0.010016	88
4	6.00	1	160.00	0.05	0.0005	0.00687	0.032087	0.008014	74
4	9.00	1	280.00	0.05	0.0005	0.00687	0.034255	0.008555	79
6	3.00	1	400.00	0.05	0.0005	0.01018	0.037366	0.009333	82
6	6.00	0.75	160.00	0.05	0.000375	0.01018	0.037366	0.009333	82
8	3.00	1	280.00	0.05	0.0005	0.01358	0.037312	0.00932	78
6	9.00	1	160.00	0.05	0.0005	0.01018	0.041012	0.010243	90
6	6.00	0.75	400.00	0.05	0.000375	0.01018	0.038733	0.009674	85
6	6.00	1	280.00	0.05	0.0005	0.01018	0.0401	0.010016	88
6	3.00	1.25	280.00	0.05	0.000625	0.01018	0.033721	0.008422	74
6	9.00	1.25	280.00	0.05	0.000625	0.01018	0.039189	0.009788	86
6	9.00	1	400.00	0.05	0.0005	0.01018	0.042379	0.010585	93
6	6.00	1.25	160.00	0.05	0.000625	0.01018	0.035999	0.008991	79
6	6.00	1	280.00	0.05	0.0005	0.01018	0.039645	0.009902	87
8	6.00	1.25	280.00	0.05	0.000625	0.01358	0.038747	0.009678	81
8	6.00	0.75	280.00	0.05	0.000375	0.01358	0.040182	0.010037	84
6	3.00	0.75	280.00	0.05	0.000375	0.01018	0.035088	0.008764	77
6	9.00	0.75	280.00	0.05	0.000375	0.01018	0.0401	0.010016	88
6	3.00	1	160.00	0.05	0.0005	0.01018	0.035543	0.008878	78
4	6.00	0.75	280.00	0.05	0.000375	0.00687	0.030786	0.007689	71
6	6.00	1	280.00	0.05	0.0005	0.01018	0.039645	0.009902	87

3.3. Energy and exergy analysis at the biodiesel production stage

The F-value of Model is 547.41, indicating that the model is significant. In this case, A, B, C, D, AB, AC, BC, CD, B2, C2, D2 are significant model terms. Values greater than 0.1000 indicate that the model terms are not significant.

Data analysis showed that the independent variables of molar ratio, ultrasonic power, catalyst concentration, and reaction time had a significant effect on the amount of methyl ester produced. The coefficient and standard error for the model are determined as 0.9982 and 8.433E-003, respectively.

$$\text{Energy} = -1.20194 - 2.49993E{-}004*A + 2.40301*B + 0.35710*C + 0.032232*D + 4.23787E{-}004*A*B + 5.90778E{-}005*A*C - 1.17719E{-}005*A*D - 0.026693*B*C + 5.65049E{-}003*B*D + 5.07305E{-}003*C*D - 3.30514E{-}007*A^2 - 1.22921*B^2 - 0.024698*C^2 - 2.65978E{-}003*D^2 \quad (6)$$

where A is the ultrasonic power (W), B is the catalyst concentration (w/w %), C is the molar ratio (Methanol alcohol to rapeseed oil), and D is time reaction (min). According to the coefficient of equation actual factor (6), the effective factors on energy consumption are molar ratio, time reaction, ultrasonic power, and catalyst concentration, respectively.

Table 7. Analysis of variance of the reactor performance.

Source	Sum of squares	Df	Mean square	Significant factor
Model	0.54	14	0.039	< 0.0001
A-Ultrasonic power	0.013	1	0.013	< 0.0001
B-Catalyst Concenteration	2.977E-003	1	2.977E-003	< 0.0001
C-Molar ratio	0.32	1	0.32	< 0.0001
D-Time	0.12	1	0.12	< 0.0001
AB	6.465E-004	1	6.465E-004	0.0093
AC	8.041E-004	1	8.041E-004	0.0046
AD	7.184E-005	1	7.184E-005	0.3319
BC	7.125E-004	1	7.125E-004	0.0069
BD	7.184E-005	1	7.184E-005	0.3319
CD	3.706E-003	1	3.706E-003	< 0.0001
A2	1.469E-004	1	1.469E-004	0.1726
B2	0.038	1	0.038	< 0.0001
C2	0.063	1	0.063	< 0.0001
D2	3.717E-003	1	3.717E-003	< 0.0001
Residual	9.955E-004	14	7.111E-005	
Lack of fit	6.507E-004	10	6.507E-005	0.6741
Pure error	3.448E-004	4	8.621E-005	
Cor total	0.55	28		

Figures 4.a and 4.b illustrate the comparison of the actual data and the predicted data; given the shape and close compatibility of these numbers, there is a strong correlation between the results obtained by the experimental method and the values predicted by the statistical test.

Values of "Prob > F" less than 0.0500 indicate that the model terms are significant. In this case, A, B, C, D, AB, AC, BC, CD, B2, C2, D2 are significant model terms. Values greater than 0.1000 indicate that the model terms are not significant. The "Lack of Fit F-value" of 0.75 indicates that the Lack of Fit is not significant with respect to the pure error. The coefficient and standard error for the model are determined to be 0.9980 and 9.02, respectively.

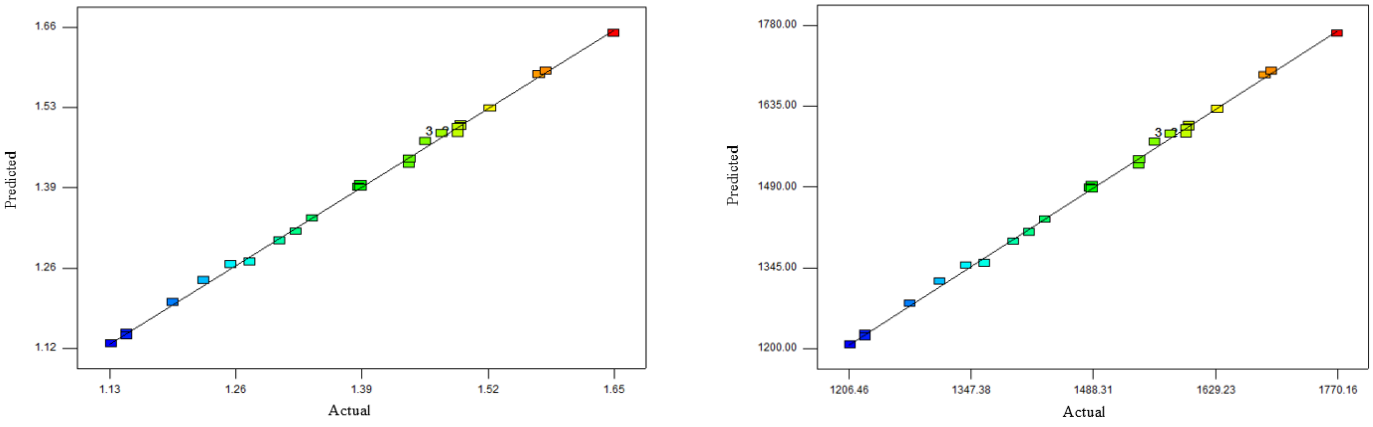

(a) **(b)**

Figure 4. (a) Actual data versus predicted data (enery), (b) Actual data versus predicted data (exery).

Exergy = -1285.62839- .26740*A+2570.31457*B+381.96073*C+34.47620*D+0.45329*A*B+0.063191*A*C-0.012591*A*D-28.55097*B*C+6.04390*B*D+5.42625*C*D-3.53525E-004*A^2-1314.78958*B^2-26.41758*C^2-2.84497*D^2 (7)

According to the coefficient of equation (7) as the actual factor, the effective factors in total exergy include molar ratio, time reaction, ultrasonic power, and catalyst concentration, respectively.

Table 8. The results of the reactor performance model by the response surface method.

Source	Sum of squares	Df	Mean square	Significant factor
Model	6.235E+005	14	44534.91	< 0.0001
A-Ultrasonic power	14684.86	1	14684.86	< 0.0001
B-Catalyst concenteration	3405.57	1	3405.57	< 0.0001
C-Molar ratio	3.604E+005	1	3.604E+005	< 0.0001
D-Time	1.354E+005	1	1.354E+005	< 0.0001
AB	739.71	1	739.71	0.0093
AC	920.01	1	920.01	0.0046
AD	82.19	1	82.19	0.3319
BC	815.16	1	815.16	0.0069
BD	82.19	1	82.19	0.3319
CD	4239.97	1	4239.97	< 0.0001
A2	168.10	1	168.10	0.1726
B2	43800.80	1	43800.80	< 0.0001
C2	72429.52	1	72429.52	< 0.0001
D2	4252.54	1	4252.54	< 0.0001
Residual	1138.98	14	81.36	
Lack of fit	744.47	10	74.45	0.6741
Pure error	394.51	4	98.63	
Cor total	6.246E+005	28		

According to Figure (5a), with an increase in ultrasonic power from 160 W to 280 W, the biodiesel production energy increased to 0.05 MJ; in addition, by increasing the power to 400 W, the energy increased to 0.065 MJ. The highest energy consumption corresponds to the molar ratio of 1:4, ultrasonic power of 400 W, and reaction time of 6 min.

In fact, with an increase in ultrasonic power, the amount of electricity consumed increased; therefore, as the amount of consumed energy increased, the ultrasonic wave intensified the ration of chemical reactions by rising the mass transfer, generating intermediate phases between reaction phases, and increasing the intensity of reaction factors such as temperature and pressure [10].

Figure (6a) shows that with an increase in the ultrasonic power from 160 W to 280 W and, then, with an increase in 400 W, the biodiesel production exergy increased to 50.95 and 69.96 MJ, respectively. The highest exergy occurred at a molar ratio of 4:1, ultrasonic power of 400 W, and reaction time of 6 min. According to Fig. (5b, 6b), increasing the molar ratio from 4:1 to 6:1 increased the energy and exergy of biodiesel production to 0.27 and 289.85 MJ, respectively. In the next step, increasing the molar ratio to 8:1 increased energy and exergy to 0.32 and 346.6 MJ, respectively. The theory of this result is the balance of the transesterification reaction so that an increase in the amount of alcohol caused an increase in the methyl ester (biodiesel) production [36]. It is worth mentioning that an increase in alcohol is limited and dissolves glycerin and reduces the purity of biodiesel [37].

As shown in Figures (5c, 6c), increasing the catalyst concentration from 0.75 to 1 % increased the energy and exergy production of biodiesel to 0.071 and 76.21 MJ, respectively. In addition, when the catalyst concentration increased to 1.25 %, energy and exergy reduced to 0.3 and 33.69 MJ, respectively.

Reduced biodiesel production by increasing the KOH concentration is attributed to the soap formation [38].

By increasing the reaction time from 3 to 6 minutes, the energy and exergy production of biodiesel increased to 0.13 and 142.72 MJ, respectively, and by increasing the reaction time to 9 min, the energy and exergy values increased to 0.19 and 212.47 MJ, respectively (Fig. (5c)).

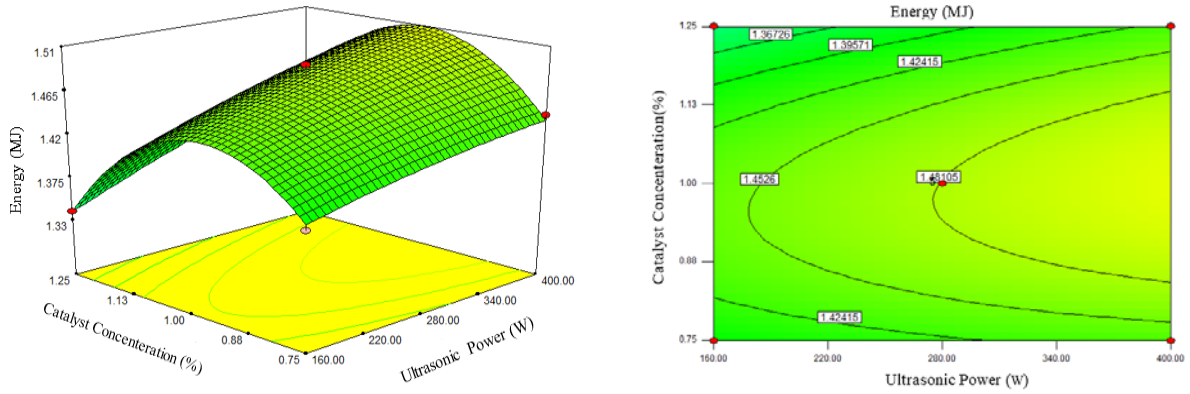

(a)

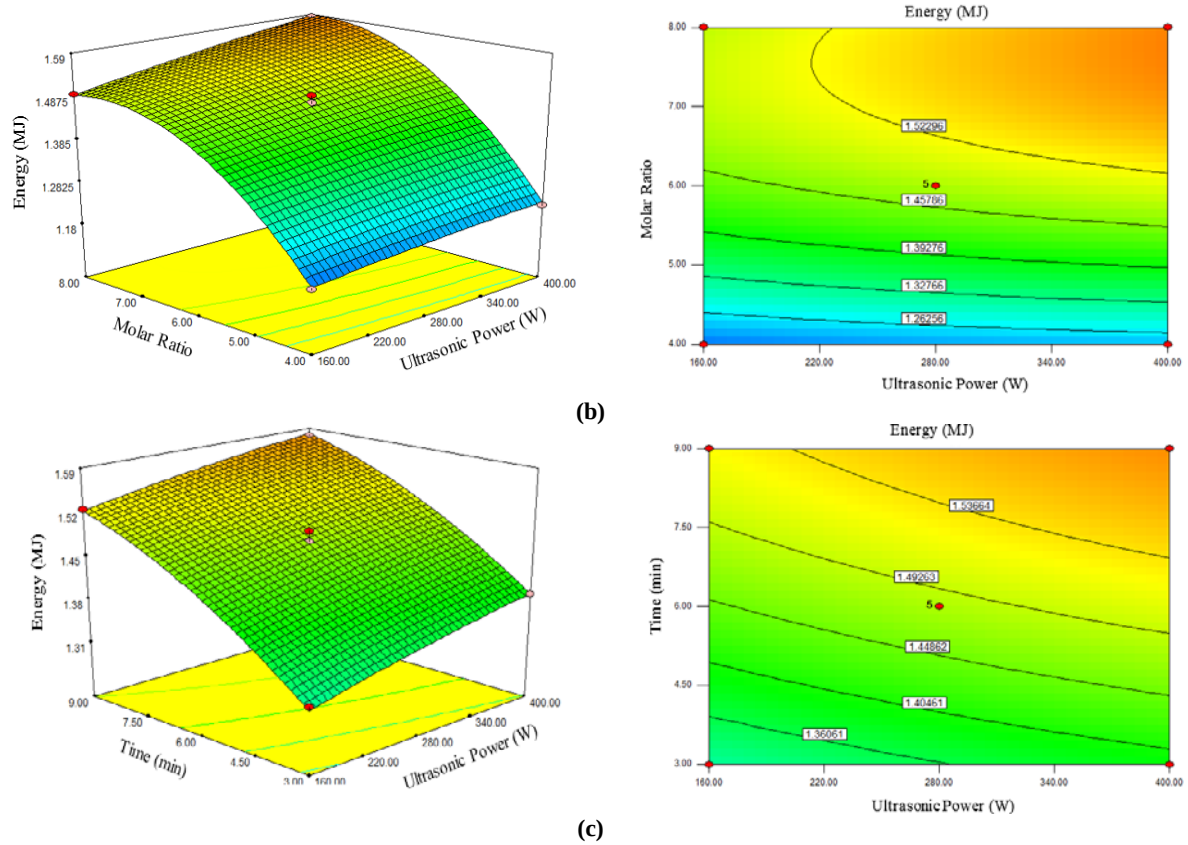

Figure 5. The interaction effects of (a) ultrasonic power (W)-catalyst concentration (w/w %), (b) ultrasonic power (W) molar ratio, (c) ultrasonic power (W)-time (min) on methyl ester conversion energy.

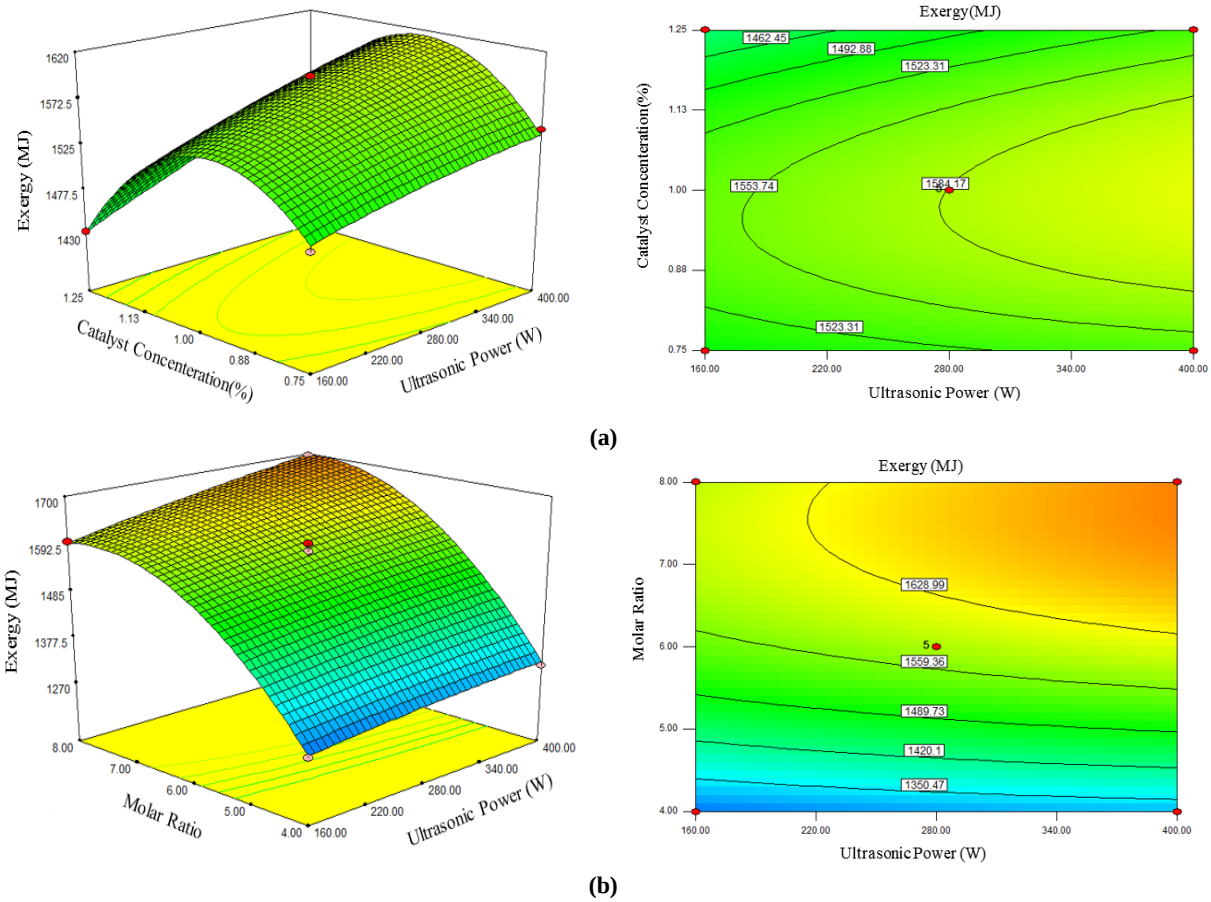

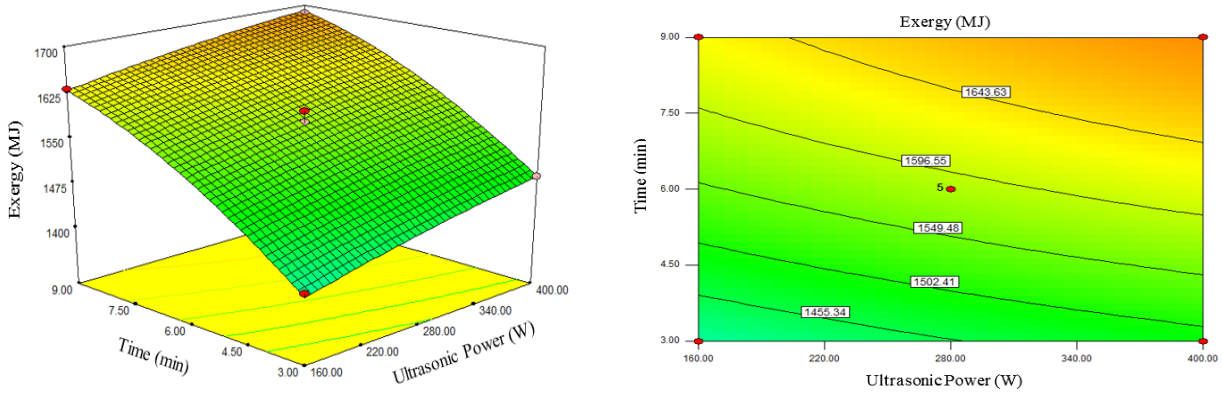

(c)

Figure 6. The interaction effects of (a) ultrasonic power (W)-catalyst concentration (w/w %), (b) ultrasonic power (W)- molar ratio, (c) ultrasonic power (W)-time (min) on methyl ester conversion exergy.

3.4. Greenhouse gas emissions analysis

The most effective factor in the potential of global warming at the agricultural stage is the high use of chemical pesticides with 41.1 % share and fertilizers, especially nitrate fertilizer with 33.5 % share. The results of the study showed that nitrogen dioxide and carbon dioxide emissions from chemical fertilizers and diesel fuel had the highest impact on the potential of global warming, respectively [39]. Studies have shown that agriculture plays an important role in the release of greenhouse gases into the atmosphere [34]. The main sources of emissions to the atmosphere include fossil fuels used in various agricultural operations, carbon losses from the soil due to tillage, burning of plant residues and forest trees, livestock, use of manures, and production and use of chemical fertilizers, especially nitrogen fertilizers [28]. According to Table (9), at the rapeseed seed stage, fertilizer consumption with 132.6 kg and 42.82 % shares had the highest impact on greenhouse gas production.Therefore, nitrogen fertilizer consumption (34.88 %) had the highest share of greenhouse gas emissions (Figure 7.a).

At the biodiesel production stage of rapeseed oil, methanol had the greatest impact on greenhouse gas emissions with a 99.81 % share (Figure 7.b). Biodiesel is an environmentally attractive fuel, because the results of its use have shown a significant reduction in greenhouse gas emissions compared to gasoline and diesel fuel. It also has lower methane emissions in its production cycle.

Table 9. Greenhouse gas emissions (kg CO_2 eq ha^{-1}) from rapeseed agriculture and biodiesel production.

Inputs	The amount of material	Percentage
Machine	2.7	0.87
Diesel fuel	41.6	13.43
Chemical	132.6	42.82
Nitrogen	108	34.88
Phosphorus	15	4.84
Potassium	9.7	3.13
Total	309.6	-
Electricity	0.08	0.15
Methanol	50	99.81
Potassium	0.012	0.02
Total	50.092	-

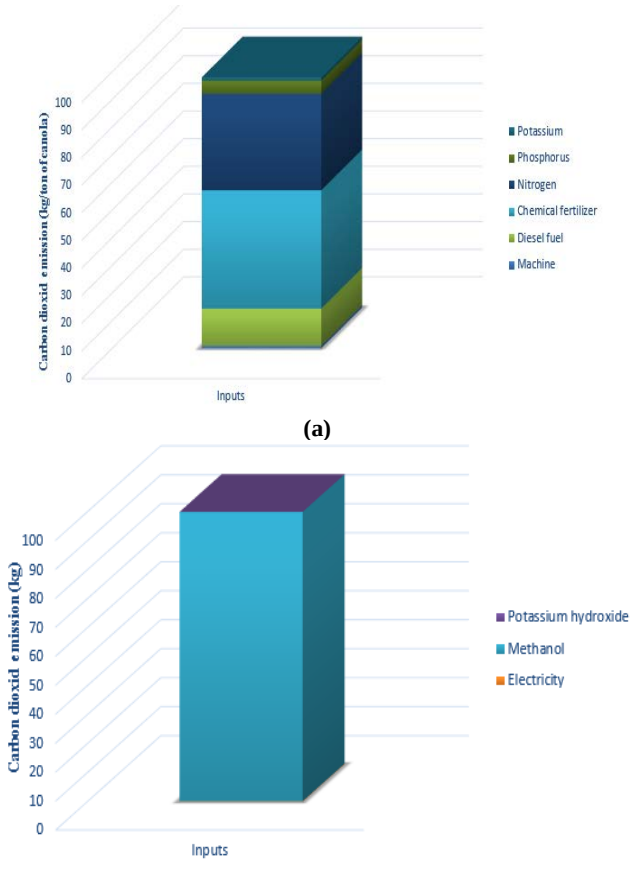

(a)

(b)

Figure 7. (a) Carbon dioxide emissions of rapeseed production, (b) Carbon dioxide emissions in rapeseed biodiesel production.

Grossman diagram (Figure 8) summarizes the results of exergy values of canola seed sowing stage, oiling stage, and biodiesel production from rapeseed oil. In order to calculate 1 tonne of rapeseed produced, the amount of oil obtained from rapeseed at the oil extraction stage was 295.9 kg; therefore, the exergy value of oil was 11815.287 MJ, and the exergy meal was 12026.53 MJ.

The rapeseed oil was the input of the biodiesel production stage; therefore, exergy was calculated in the optimum condition by Design-Expert software (molar ratio of 7, ultrasonic power of 160 watts, and oil catalyst concentration of 1 wt %). At each stage, the value and position of exergy loss are reported; therefore, the highest amount of exergy loss at the biodiesel production phase was 2845.71 MJ.

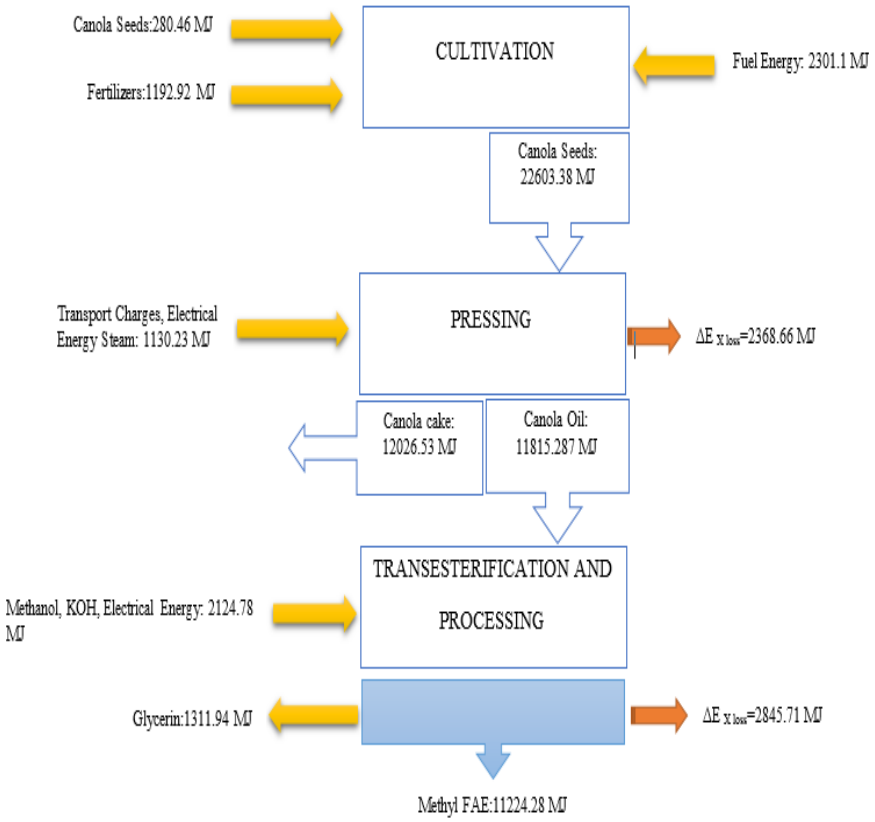

Figure 8. Grassmann diagram for methyl FAE production from rapeseed.

4. CONCLUSIONS

Energy and exergy of rapeseed crop cultivation and biodiesel production was evaluated using an ultrasonic reactor under laboratory conditions with variables of ultrasonic power, methanol to oil molar ratio, catalyst concentration, and reaction time. The results of the exergy index can be used to decide on the efficiency and sustainability of the biodiesel production system. In this study, the input and output energy of the field for cultivating rapeseed were 12826.98 and 22195 MJ/ha, respectively. The highest energy consumption was related to nitrogen fertilizer; therefore, energy consumption should be saved in order to reduce energy consumption. Input and output exergy rates were calculated and estimated to be 3933.494 and 22603.39 MJ/ha, respectively, and the highest share of exergy consumption was related to diesel fuel. In biodiesel production, the total energy input and output were 156.95 MJ and 41.88 MJ, and the highest exergy was associated with alcohol consumption.

5. ACKNOWLEDGEMENT

Research Council of Shahrekord University is thankfully acknowledged for their financial support for conducting this study (grant No:97GRN1M1796).

REFERENCES

1. Ebel, R.E., Croissant, M.P., Masih, J.R., Calder, K.E. and Raju, G.G., "International energy outlook: US department of energy", ***Washington Quarterly***, Vol. 19, No. 4, (1996), 70-99. (https://doi.org/10.1080/01636609609550217).
2. Pearson, R.J. and Turner, J.W.G., "The role of alternative and renewable liquid fuels in environmentally sustainable transport", In Alternative fuels and advanced vehicle technologies for improved environmental performance: Towards zero carbon transportation, Folkson, R. edition, Woodhead Publishing Ltd., Cambridge, U.K., (2014), 19-51. (https://doi.org/10.1533/9780857097422.1.19).
3. Tickell, J. and Tickell, K., "From the fryer to the fuel tank: The complete guide to using vegetable oil as an alternative fuel", ***Biodiesel America***, (2003).
4. Nemecek, T., Kägi, T. and Blaser, S., "Life cycle inventories of agricultural production systems", Final report, ecoinvent data v2.0, No 15, (2007).
5. Rajaeifar, M.A., Ghobadian, B., Heidari, M.D. and Fayyazi, E., "Energy consumption and greenhouse gas emissions of biodiesel production from rapeseed in Iran", ***Journal of Renewable and Sustainable Energy***, Vol. 5, No. 6, (2013), 063134. (https://doi.org/10.1063/1.4854596).
6. Murugesan, A., Umarani, C., Subramanian, R. and Nedunchezhian, N., "Bio-diesel as an alternative fuel for diesel engines— A review", ***Renewable and Sustainable Energy Reviews***, Vol. 13, No. 3, (2009), 653-662. (https://doi.org/10.1016/j.rser.2007.10.007).
7. Hosseinpour, S., Aghbashlo, M., Tabatabaei, M. and Khalife, E., "Exact estimation of biodiesel cetane number (CN) from its fatty acid methyl esters (FAMEs) profile using partial least square (PLS) adapted by artificial neural network (ANN)", ***Energy Conversion and Management***, Vol. 124, (2016), 389-398. (https://doi.org/10.1016/j.enconman.2016.07.027).
8. Miraboutalebi, S.M., Kazemi, P. and Bahrami, P., "Fatty acid methyl ester (FAME) composition used for estimation of biodiesel cetane number employing random forest and artificial neural networks: A new approach", ***Fuel***, Vol. 166, (2016), 143-151. (https://doi.org/10.1016/j.fuel.2015.10.118).
9. Sales, E.A., Ghirardi, M.L. and Jorquera, O., "Subcritical ethylic biodiesel production from wet animal fat and vegetable oils: A net energy ratio analysis", ***Energy Conversion and Management***, Vol. 141, (2017), 216-223. (https://doi.org/10.1016/j.enconman.2016.08.015).
10. Ji, J., Wang, J., Li, Y., Yu, Y. and Xu, Z., "Preparation of biodiesel with the help of ultrasonic and hydrodynamic cavitation", ***Ultrasonics***, Vol. 44, (2006), e411-e414. (https://doi.org/10.1016/j.ultras.2006.05.020).
11. Proskuryakova, L. and Kovalev, A., "Measuring energy efficiency: Is energy intensity a good evidence base?", ***Applied Energy***, Vol. 138, (2015), 450-459. (https://doi.org/10.1016/j.apenergy.2014.10.060).
12. Tsatsaronis, G. and Morosuk, T., "A general exergy-based method for combining a cost analysis with an environmental impact analysis, Part I: Theoretical development", ***Proceedings of ASME 2008 International***

Mechanical Engineering Congress and Exposition, American Society of Mechanical Engineers Digital Collection, (2008). (https://doi.org/10.1115/IMECE2008-67218).

13. Valero, A., Serra, L. and Uche, J., "Fundamentals of exergy cost accounting and thermoeconomics, Part I: Theory", ***Journal of Energy Resources Technology***, Vol. 128, No. 1, (2006), 1-8. (https://doi.org/10.1115/1.2134732).
14. Ozkan, B., Akcaoz, H. and Fert, C., "Energy input–output analysis in Turkish agriculture", ***Renewable Energy***, Vol. 29, No. 1, (2004), 39-51. (https://doi.org/10.1016/S0960-1481(03)00135-6).
15. Food and Agriculture Organization of the United Nations (FAO), Fishery Statistical Collections, Global Capture Production, Recuperado em. 9, (2018a).
16. Schnepf, R.D., "Energy use in agriculture: Background and issues", Congressional Information Service, Library of Congress, (2004).
17. Hou, Z. and Zheng, D., "Solar utility and renewability evaluation for biodiesel production process", ***Applied Thermal Engineering***, Vol. 29, No. 14-15, (2009), 3169-3174. (https://doi.org/10.1016/j.applthermaleng.2009.04.020).
18. Jaimes, W., Acevedo, P. and Kafarov, V., "Exergy analysis of palm oil biodiesel production", ***Chemical Engineering Journal***, Vol. 21, (2010), 1345-1350. (https://doi.org/10.3303/CET1021225).
19. Ofori-Boateng, C., Keat, T.L. and JitKang, L., "Feasibility study of microalgal and jatropha biodiesel production plants: Exergy analysis approach", ***Applied Thermal Engineering***, Vol. 36, (2012), 141-151. (https://doi.org/10.1016/j.applthermaleng.2011.12.010).
20. Font de Mora, E., Torres, C. and Valero, A., "Thermoeconomic analysis of biodiesel production from used cooking oils", ***Sustainability***, Vol. 7, No. 5, (2015), 6321-6335. (https://doi.org/10.3390/su7056321).
21. Eggleston, S., Buendia, L., Miwa, K., Ngara, T. and Tanabe, K., "2006 IPCC guidelines for national greenhouse gas inventories", Vol. 5, (2006), Institute for Global Environmental Strategies, Hayama, Japan.
22. Yildizhan, H., "Energy, exergy utilization and CO_2 emission of strawberry production in greenhouse and open field", ***Energy***, Vol. 143, (2018), 417-423. (https://doi.org/10.1016/j.energy.2017.10.139).
23. Antonova, Z.A., Krouk, V.S., Pilyuk, Y.E., Maksimuk, Y.V., Karpushenkava, L.S. and Krivova, M.G., "Exergy analysis of canola-based biodiesel production in Belarus", ***Fuel Processing Technology***, Vol. 138, (2015), 397-403. (https://doi.org/10.1016/j.fuproc.2015.05.005).
24. Ortiz-Cañavate, J. and Hernanz, J., Energy analysis and saving, CIGR handbook of agricultural engineering, Vol. 5, (1999), 13-42. (doi:10.13031/2013.36412).
25. Pishgar-Komleh, S.H., Omid, M. and Heidari, M.D., "On the study of energy use and GHG (greenhouse gas) emissions in greenhouse cucumber production in Yazd province", ***Energy***, Vol. 59, (2013), 63-71. (https://doi.org/10.1016/j.energy.2013.07.037).
26. Kitani, O. and Jungbluth, T., Energy and biomass engineering, CIGR handbook of agricultural engineering, Vol. 5, (1999), 330. (doi:10.13031/2013.36411).
27. Singh, G., Singh, S. and Singh, J., "Optimization of energy inputs for wheat crop in Punjab", ***Energy Conversion and Management***, Vol. 45, No. 3, (2004), 453-465. (https://doi.org/10.1016/S0196-8904(03)00155-9).
28. Mousavi-Avval, S.H., Rafiee, S., Jafari, A. and Mohammadi, A., "Improving energy use efficiency of canola production using data envelopment analysis (DEA) approach", ***Energy***, Vol. 36, No. 5, (2011), 2765-2772. (https://doi.org/10.1016/j.energy.2011.02.016).
29. De Souza, S.P., Pacca, S., Turrade Ávila, M. and Borges, J.L.B., "Greenhouse gas emissions and energy balance of palm oil biofuel", ***Renewable Energy***, Vol. 35, No. 11, (2010), 2552-2561. (https://doi.org/10.1016/j.renene.2010.03.028).
30. Mohammadshirazi, A., Akram, A., Rafiee, S., Mousavi-Avval, S.H. and Bagheri Kalhor, E., "An analysis of energy use and relation between energy inputs and yield in tangerine production", ***Renewable and Sustainable Energy Reviews***, Vol. 16, No. 7, (2012), 4515-4521. (https://doi.org/10.1016/j.rser.2012.04.047).
31. Krohn, B.J. and Fripp, M., "A life cycle assessment of biodiesel derived from the “niche filling” energy crop camelina in the USA", ***Applied Energy***, Vol. 92, (2012), 92-98. (https://doi.org/10.1016/j.apenergy.2011.10.025).
32. Hosseinzadeh Samani, B., Khoshtaghaza, M.H., Minaee, S. and Abbasi, S., "Modeling the simultaneous effects of microwave and ultrasound treatments on sour cherry juice using response surface methodology", ***Journal of Agricultural Science and Technology***, Vol. 17, No. 4, (2015), 837-846.
33. Shirneshan, A., Almassi, M., Ghobadian, B., Borghei, A.M. and Najafi, G.H., "Response surface methodology (RSM) based optimization of biodiesel-diesel blends and investigation of their effects on diesel engine operating conditions and emission characteristics", ***Environmental Engineering & Management Journal (EEMJ)***, Vol. 15, No. 12, (2016), 2771-2780.
34. Lal, R., "Carbon emission from farm operations", ***Environment International***, Vol. 30, No. 7, (2004), 981-990. (https://doi.org/10.1016/j.envint.2004.03.005).
35. Casey, J. and Holden, N., "Analysis of greenhouse gas emissions from the average Irish milk production system", ***Agricultural Systems***, Vol. 86, No. 1, (2005), 97-114. (https://doi.org/10.1016/j.agsy.2004.09.006).
36. Bagherpour, H., Ghobadian, B., Tavakoli Hashjin, T., Mohammadi, A., Feyz Elahnezhad, M. and Zenouzi, A., "Optimizing effective parameters in biodiesel fuel production using trans-estrification method", ***Iranian Journal of Biosystems Engineering (Iranian Journal of Agricultural Sciences)***, Vol. 41, No. 1, (2010), 37-43.
37. Hingu, S.M., Gogate, P.R. and Rathod, V.K., "Synthesis of biodiesel from waste cooking oil using sonochemical reactors", ***Ultrasonics Sonochemistry***, Vol. 17, No. 5, (2010), 827-832. (https://doi.org/10.1016/j.ultsonch.2010.02.010).
38. Kashyap, S.S., Gogate, P.R. and Joshi, S.M., "Ultrasound assisted synthesis of biodiesel from karanja oil by interesterification: Intensification studies and optimization using RSM", ***Ultrasonics Sonochemistry***, Vol. 50, (2019), 36-45. (https://doi.org/10.1016/j.ultsonch.2018.08.019).
39. Nemecek, T., Dubois, D., Huguenin-Elie, O. and Gaillard, G., "Life cycle assessment of Swiss farming systems: I. Integrated and organic farming", ***Agricultural Systems***, Vol. 104, No. 3, (2011), 217-232. (https://doi.org/10.1016/j.agsy.2010.10.002).

ABSTRACTS

Multi-Objective Optimization of the Humidification-Dehumidification Desalination System for Productivity and Size

Amir Reza Khedmati, Mohammad Behshad Shafii*

Department of Mechanical Engineering, Sharif University of Technology, Tehran, Iran.

PAPER INFO

Paper history:
Received 31 October 2019
Accepted in revised form 29 February 2020

Keywords:
Humidification-Dehumidification
Desalination
Gained Output Ratio
Multi-Objective
Optimization

ABSTRACT

The humidification-dehumidification system is one of the desalination technologies that can utilize non-fossil thermal sources and requires insignificant input energy. This system is usually suitable for rural areas and places far from the main sources of energy. The purpose of this study is to obtain the most suitable working conditions and dimensions of this system. In this research, thermodynamic modeling was first performed for a simple type of the system (water-heated); then, the effect of parameters on the system performance was investigated. Modeling was conducted through a numerical simulation; furthermore, the assumption of the saturation of exhaust air from the humidifier was also considered in the mentioned code. Afterward, a comparison was made between two different forms of the system, and the proper form was chosen for the rest of the research. Moreover, through heat transfer equations, the dimensions of the two main parts of the system, i.e., humidifier and dehumidifier, were calculated. Besides, multi-objective optimization was carried out for two objective functions, i.e., gained output ratio (GOR) and the system volume, to reduce the space occupied by the system and reach the desired efficiency simultaneously. The optimization was performed using a simulation program, and results were obtained for different weights in order to optimize each objective function. For instance, 379 liters of freshwater can be produced in a day with a total volume of 48 liters for the humidifier and the dehumidifier in the optimized system.

چکیده

سامانه رطوبت‌زنی-رطوبت‌گیری از جمله فنّاوری‌های نمک‌زدایی از آب است که می‌تواند با بهره‌گیری از انرژی ورودی کم، شیرین‌سازی آب شور را انجام دهد؛ به همین دلیل این سامانه قابلیت استفاده در مناطق دورافتاده و کم‌بهره از منابع سرشار انرژی را دارد. هدف از این پژوهش یافتن شرایط کاری و ابعاد بهینه برای این سامانه است. در این تحقیق، ابتدا مدل‌سازی ترمودینامیکی نوع ساده‌ای از این سامانه انجام گردیده و سپس مطالعه‌ای پارامتری برای بررسی متغیرهای مؤثر بر عملکرد سیستم صورت گرفته است. لازم به ذکر است که مدل‌سازی ترمودینامیکی در قالب یک برنامه رایانه‌ای انجام گرفته و فرض اشباع بودن هوای خروجی از رطوبت‌زن در آن لحاظ شده است. پس از آن، میزان نسبت کسب شده خروجی بین دو نوع خاص از این سامانه با یکدیگر مقایسه شده و بر آن اساس، دلایل انتخاب یکی از آن دو سامانه بیان گردیده است. در ادامه، به منظور بدست‌آوردن ابعاد سامانه، معادلات انتقال حرارت به فرآیند مدل‌سازی اضافه گردیده و مطالعه پارامتری دیگری نیز برای تعیین ابعاد سامانه انجام گرفته است. در پایان، با درنظرگرفتن "نسبت کسب شده خروجی" و "ابعاد کلی سامانه" به‌عنوان دو تابع هدف، با استفاده از تکنیک وزن‌دهی، بهینه‌سازی صورت پذیرفت. به عنوان مثالی از نتایج، می‌توان به تولید بیشینه ۳۷۹ لیتر در روز برای سامانه بهینه در حالت حجم کلی ۴۸ لیتر برای بخش رطوبت‌زن و رطوبت‌گیر اشاره نمود.

Maximizing Income of a Cascade Hydropower with Optimization Modeling

Hasan Huseyin Coban

Department of Electrical Engineering, Faculty of Engineering, Ardahan University, 75000, Ardahan, Turkey.

P A P E R I N F O

Paper history:
Received 09 September 2019
Accepted in revised form 23 March 2020

Keywords:
Optimization Based Electricity Market
Cascaded Reservoir Operating Rule
Hydroelectric Producer
Short-Term Hydro Scheduling
Nonlinear Optimization

A B S T R A C T

This paper focuses on the short-term cascade hydro scheduling problem, especially in a competitive environment, namely in market conditions. A nonlinear stochastic optimization method is proposed to take into consideration the hydroelectric energy production as a function of hourly electricity market prices and water release rates. In order to solve a case study based on one of the Turkish cascaded hydropower facilities, the proposed method has been successfully applied to a wide variety of problems at a negligible computation time while providing a higher profit. The paper shows the benefits that could be achieved by applying a model based on the Quasi-Newton Method, which finds zeroes or local maxima and minima of solving a certain type of optimization functions because it can better handle the uncertainty, constraints, and complexity of the problem. Ten-year hourly water inflow data and electricity market prices were used as inputs, and the results of the cascade and single optimization were compared. A comparison study with the operation of each hydropower plant (HPP) separately showed that 18 % higher income was obtained with a cascade variant.

چکیده

این مقاله به موضوع برنامه‌ریزی کوتاه مدت برای بهره برداری از نیروی آب در یک آبشار پلکانی، بویژه در یک محیط رقابتی موسوم به شرایط بازار معطوف است. یک روش بهینه‌سازی تصادفی غیرخطی پیشنهاد شده است که تولید انرژی برقآبی را به عنوان تابعی از نرخ بهای ساعتی بازار برق و نرخ شار رهاسازی آب در نظر گرفته است. به منظور حل این مسأله، یک مطالعه موردی در خصوص یکی ازتأسیسات آبشاری برقآبی ترکیه صورت گرفت و روش پیشنهادی درباره بازه گسترده ای از مسائل با صرف زمان محاسباتی قابل چشم‌پوشی و با موفقیت به کارگرفته شد، که در عین حال به تأمین سود بیشتر انجامید. مقاله حاضر مزایایی را نشان می دهد که میتوان بااستفاده از یک مدل مبتنی بر روش شبه نیوتن به دست آورد، که ارقام صفر یا کمینه و بیشینه های محلی را در توابع بهینه‌سازی خاص می‌یابد، زیرا این مدل می‌تواند موارد عدم قطعیت، محدودیتها و پیچیدگیهای مسأله را بهتر برطرف کند. در این مقاله ازداده های ساعتی شار (دبی) آب و نرخ بهای بازار برق به عنوان ورودی استفاده شد و نتایج از این آبشار پلکانی برای بهینه‌سازی واحد مقایسه شدند. یک مطالعه مقایسه ای با عملکرد هرنیروگاه آبی به طور جداگانه نشان داد که درآمد بدست آمده از نیروگاه آبشار پلکانی ۱۸ ٪ بالاتر رفته است.

Economic Evaluation of Cooling Storage Warehouses in Hot and Dry Regions for Fruits Using Different Renewable Energies

Ali Mostafaeipour*, Afsaneh Nasiri

Department of Industrial Engineering, Yazd University, Yazd, Iran.

P A P E R I N F O

Paper history:
Received 17 October 2019
Accepted in revised form 28 March 2020

Keywords:
Renewable Energy
Energy Efficiency
Fruit Storage Warehouses
Solar Air Conditioner
Economic Evaluation

A B S T R A C T

In hot and dry regions, air conditioning is used for many different applications like residential, industry, and agriculture and dairy products. This research studies the applicability of wind and solar energies for cooling fruit storage warehouse in the hot and dry region of Yazd in Iran. The studied case is a fruit warehouse with an area of 4240 m^2 resulting in a storage capacity of about 1000 tons. For this purpose, the heat gain of the warehouse is determined, and the obtained cooling load is then used to examine the solar and wind energy to power a conventional warehouse system. Different scenarios are examined for this research such as solar air conditioner, solar absorption chiller, wind catcher, and a combination of solar air conditioners and solar absorption chiller for cooling the fruit warehouse. Comparison and economic evaluation of different scenarios show that the solar air conditioning ranks first for this purpose. Results are then validated using value engineering methodology. Solar air conditioning with the highest net present value (NPV) of 4,865,040,418 Rials and the best internal rate of return (IRR) value of 182.98 % was determined to be the best approach among the studied methods. The results of this research can be applied to other regions with similar climatic conditions too.

چکیده

در مناطق گرم و خشک، تهویه هوا برای بسیاری از کاربردهای مختلف مانند مسکونی، صنعت و کشاورزی و لبنیات استفاده می‌شود. این تحقیق به کاربرد انرژی باد و خورشیدی در خنک کردن انبار میوه در منطقه گرم و خشک یزد در ایران می‌پردازد. در این تحقیق، انبار میوه با مساحت ۴۲۴۰ مترمربع که ظرفیت ذخیره آن در حدود ۱۰۰۰ تن است، مورد بررسی قرار می‌گیرد. برای این منظور، افزایش گرمای انبار تعیین می‌شود و سپس از بار خنک کننده بدست آمده، برای بررسی انرژی خورشیدی و باد مورد نیاز جهت تأمین انرژی سیستم یک انبار معمولی استفاده می‌شود. سناریوهای مختلفی برای این تحقیق از قبیل: تهویه هوا خورشیدی، چیلر جذب خورشیدی، گیرنده باد و ترکیبی از سیستم های تهویه مطبوع خورشیدی و چیلر جذب خورشیدی برای خنک کردن انبار میوه مورد بررسی قرار می‌گیرد. مقایسه و ارزیابی اقتصادی سناریوهای مختلف نشان می‌دهد که تهویه مطبوع خورشیدی برای این منظور در رتبه نخست قرار دارد. سپس نتایج با استفاده از روش مهندسی ارزش تأیید می‌شود. تهویه مطبوع خورشیدی با بالاترین مقدار خالص ارزش فعلی (NPV) ۴،۸۶۵،۰۴۰،۴۱۸ ریال و بهترین نرخ بازده داخلی (IRR) ۱۸۲/۹۸ ٪ به عنوان بهترین روش در بین روشهای مورد بررسی تعیین شد. نتایج این تحقیق در سایر مناطق با شرایط آب و هوایی مشابه نیز می‌تواند اعمال شود.

Optimization the Performance and Emission Parameters of a CI Engine Fueled with Aviation Fuel-Biodiesel-Diesel Blends

Alireza Shirneshan[a,b*], Mohammad Mostofi[a]

[a] *Department of Mechanical Engineering, Najafabad Branch, Islamic Azad University, Najafabad, Iran.*
[b] *Aerospace and Energy Conversion Research Center, Najafabad Branch, Islamic Azad University, Najafabad, Iran.*

PAPER INFO

Paper history:
Received 28 December 2019
Accepted in revised form 28 March 2020

Keywords:
Optimization
Aviation Fuel
Emission
Performance
Diesel Engine

ABSTRACT

The determination of the optimum engine working conditions plays an important role in increasing engine performance and reducing exhaust emissions. The main objective of this study is to optimize the performance and emission characteristics of a CI engine fueled with aviation fuel-biodiesel-diesel blends at various engine speeds and loads using Mixture-RSM. According to the experimental tests carried on a 4-cylinder engine, the mathematical models were developed. Then, the optimization processes were defined as the six scenarios containing the consideration of performance or emission parameters or both of them. Scenario 1 shows that the higher percentage of diesel and jet fuel can improve the performance parameters of the engine; however, Scenario 2 shows that only higher percentage of diesel can improve the engine emission due to negative effect of biodiesel on the NOx emissions and negative impact of aviation fuel on the CO and HC emissions that limit the amount of biodiesel and aviation fuel in the fuel mixture. The results also show that Scenario 3 does not vary compared to Scenario 2. The optimized point for both of engine performance and emission parameters presented in Scenario 6 was calculated as D48.9B32.7J18.4 at 2526 RPM and full engine load to obtain 88.4 (kW), 337 (N.m), 255 (gr/Kw.hr), 0.0268 (%), 469 (ppm), 7.7 (%) brake power, torque, BSFC, CO, NOx, and HC emission, respectively.

چکیده

تعیین شرایط کاری بهینه موتور نقشی اساسی در افزایش عملکرد و کاهش آلایندگی موتور دارد. هدف اصلی در این تحقیق، بهینه‌سازی مشخصه‌های عملکردی و آلایندگی یک موتور دیزل تحت سرعت‌های دورانی و بارهای اعمالی مختلف به وسیله روش Mixture-RSM بود. بر اساس تست‌های تجربی انجام شده بر روی موتور چهار سیلندر، مدل‌های ریاضی استخراج شد. سپس مراحل بهینه‌سازی به صورت شش طرح شامل درنظر گرفتن جداگانه مشخصه‌های عملکردی یا آلایندگی موتور و یا هر دو باهم تعریف شد. طرح بهینه‌سازی ۱ نشان داد که افزایش درصد سوخت دیزل و سوخت هوایی می‌تواند سبب بهبود شرایط عملکردی موتور شود؛ ولی طرح بهینه‌سازی ۲ نشان داد که فقط افزایش سوخت دیزل در مخلوط سوخت می‌تواند سبب کاهش مشخصه‌های آلایندگی به طور کلی موتور شود که علت آن را باید در اثرات منفی سوخت بیودیزل در افزایش NOx و سوخت هوایی در افزایش آلاینده‌های HC و CO دانست. همچنین نتایج نشان داد که طرح بهینه‌سازی ۳ تغییری نسبت به طرح ۲ ندارد. با توجه به نتایج، نقطه بهینه برای مشخصه‌های عملکردی و آلایندگی موتور (ارایه شده در طرح ۶) به صورت مخلوط D48.9B32.7J18.4 در سرعت دورانی ۲۵۲۶ دور بر دقیقه و بار کامل به مقادیر ۸۸/۴ کیلووات، ۳۳۷ نیوتن‌متر، ۲۵۵ گرم بر کیلووات ساعت، ۷/۷ درصد، ۴۶۹ پی پی ام و ۰/۰۲۶۸ درصد به ترتیب برای توان ترمزی، گشتاور، مصرف سوخت ویژه ترمزی و آلاینده‌های CO، NOx و HC بدست آورده شد.

Electrochemical Modeling and Techno-Economic Analysis of Solid Oxide Fuel Cell for Residential Applications

Sadegh Safari[a], Hassan Ali Ozgoli[b*]

[a] *School of the Environment and Energy, Islamic Azad University, Science and Research Branch, Daneshgah Blvd., Simon Bolivar Blvd., P. O. Box: 1477893855, Tehran, Iran.*
[b] *Department of Mechanical Engineering, Iranian Research Organization for Science and Technology (IROST), Sh. Ehsani Rad St., Enqelab St., Parsa Sq., Ahmadabad Mostoufi Rd., Azadegan Highway, P. O. Box: 3313193685, Tehran, Iran.*

PAPER INFO

Paper history:
Received 20 January 2020
Accepted in revised form 28 March 2020

Keywords:
Solid Oxide Fuel Cell
Electrochemical Model
Sensitivity Analysis
Economic Evaluation

ABSTRACT

In this paper, an electrochemical model was developed to investigate the performance analysis of a Solid Oxide Fuel Cell (SOFC). The curves of voltage, power, efficiency, and the generated heat of cell have been analyzed to accomplish a set of optimal operating conditions. Further, a sensitivity analysis of major parameters that have a remarkable impact on the economy of the SOFC and its residential applications has been conducted. The results illustrate that the current density and cell performance temperature have vital effects on the system efficiency, output power and heat generation of cell of the SOFC. The best system efficiency is approached up to 53.34 % while implementing combined heat and power generation might be further improved up to 86 %. The economic evaluation results indicate that parameters such as overall efficiency, natural gas price and additional produced electricity that has prone to be sold to the national power grid, have a significant impact on the SOFC economy. The results indicate the strong reduction in the purchasing cost of the SOFC, i.e. not more than $2500, and improving the electrical efficiency of SOFC, i.e. not less than 42 %, can be the breakeven points of investment on such systems in residential applications. Also, it is found that the target of this SOFC cogeneration system for residential applications in Iran is relying on considerable technological enhancement of the SOFC, as well as life cycle improvement; improvement in governmental policies; and profound development in infrastructures to mitigate legal constraints.

چکیده

در این مقاله، به توسعه یک مدل الکتروشیمیایی به منظور بررسی خصوصیات عملکردی یک پیل‌سوختی اکسید جامد استوانه‌ای پرداخته شده است و منحنی‌های ولتاژ، توان، راندمان و حرارت تولیدی سلول با هدف پیدا کردن نقاط بهینه عملکردی سلول مورد تحلیل قرار گرفته است. در ادامه، تحلیل حساسیت بر روی پارامترهای اساسی که بیشترین تأثیر را بر اقتصادی شدن پیل سوختی اکسید جامد در کاربردهای خانگی دارند، مورد بررسی قرار گرفته شده است. نتایج این تحقیق نشان می‌دهد دانسیته جریان و همچنین دمای عملکردی سلول، اثر چشمگیری بر راندمان، توان تولیدی و حرارت تولیدی در پیل‌سوختی اکسید جامد دارند. بیشترین مقدار برای راندمان سیستم برابر ۵۳/۳۴ ٪ بدست آمده است که با تولید همزمان به ۸۶ ٪ می‌رسد. نتایج حاصل از ارزیابی اقتصادی نشان می‌دهد پارامترهای راندمان، قیمت تمام شده خرید پیل‌سوختی، قیمت گاز طبیعی و همچنین قیمت فروش مازاد تولید الکتریسیته به دولت، تأثیر قابل توجهی بر اقتصاد پیل‌سوختی دارد. علاوه بر آن، ارزیابی نتایج مذکور نشان می‌دهد، کاهش قیمت خرید پیل‌سوختی به کمتر از ۲۵۰۰ دلار و افزایش راندمان به بالای ۴۲ ٪ و یا کاهش قیمت به کمتر از ۳۶۰۰ دلار و افزایش راندمان به بالاتر از ۴۶ ٪ می‌تواند نقطه سر به سر سرمایه‌گذاری بر روی سیستم پیل‌سوختی اکسید جامد در کاربردهای خانگی باشد.

Energy, Exergy, and Environmental Analysis and Optimization of Biodiesel Production from Rapeseed Using Ultrasonic Waves

Bahram Hosseinzadeh Samani[a*], Marzieyeh Ansari Samani[a], Rahim Ebrahimi[a], Zahra Esmaeili[a], Ali Ansari Ardali[b]

[a] *Department of Mechanical Engineering of Biosystem, Shahrekord University, Shahrekord, Iran.*
[b] *Department of Applied Mathematics, Faculty of Methematical Sciences, Shahrekord University, Shahrekord, Iran.*

P A P E R I N F O

Paper history:
Received 28 January 2020
Accepted in revised form 31 March 2020

Keywords:
Exergy
Energy Consumption
Rapeseed
Biodiesel
Renewable Energy

A B S T R A C T

Due to limited oil reserves, the rising world fuel prices and environmental problems caused by the use of fossil fuels increase the tendency to use alternative fuels such as biodiesel and bioethanol. In this study, the evaluation of energy and exergy flow from seed planting to final production of biodiesel from rapeseed oil was carried out. Biodiesel production from rapeseed was made in three main phases: farm, oil extraction, and industrial biodiesel production. Initially, the input and output variables for rapeseed production were collected through questionnaires from 30 rapeseed farms in Khuzestan province, Iran. Thus, the amount of energy input and output to the field for rapeseed was estimated to be 12826.98 and 22195 MJ/ha, respectively. The highest energy consumption is related to chemical fertilizers with 65 % share of other inputs. Input and output exergy rates were obtained as 3933.494 and 22603.39 MJ/ha, respectively, and the highest exergy consumption related to diesel fuel with 58 % share of other inputs. At the biodiesel production stage, the input energy and output energy were 156.95 MJ and 41.88 MJ, respectively, and the highest amount of electricity consumed was 91.02 MJ. The total amount of exergy in the production of biodiesel and the output exergy was 48.412 MJ and 64.568 MJ, respectively. In this study, the effects of alcohol-to-oil molar ratio, ultrasound power (W), catalyst concentration (w/w %), and the reaction time (min) on methyl ester yield using response surface methodology based on Box Behnken experimental design in the Design Expert software were investigated. Finally, gas emissions were studied at the planting and biodiesel production stages, and the resultsshowed that the highest greenhouse gas emissions at the planting stage were related to chemical fertilizers and alcohol production.

چکیده

با توجه به ذخایر محدود نفت، افزایش قیمت جهانی سوخت و مشکلات زیست‌محیطی ناشی از استفاده از سوخت‌های فسیلی، تمایل به استفاده از سوخت‌های جایگزین مانند بیودیزل و بیواتانول را افزایش می‌دهد. در این مطالعه، ارزیابی جریان انرژی و اگزرژی از کاشت بذر تا تولید نهایی بیودیزل از روغن کلزا مورد بررسی قرار گرفت. تولید بیودیزل از کلزا در سه مرحله اصلی، مزرعه، استخراج روغن و تولید بیودیزل صنعتی انجام شد. در ابتدا، متغیرهای ورودی و خروجی تولید کلزا از طریق پرسشنامه ۳۰ مزرعه کلزا از استان خوزستان در ایران جمع‌آوری شد. بنابراین میزان ورودی و خروجی انرژی از مزرعه برای کلزا به ترتیب ۱۲۸۲۶/۹۸ و ۲۲۱۹۵ مگاژول در هکتار تخمین زده شده است. بیشترین میزان مصرف انرژی مربوط به کودهای شیمیایی با ۶۵ ٪ سهم سایر ورودی‌ها است. اگزرژی ورودی و خروجی به ترتیب ۳۹۳۳/۴۹۴ و ۲۲۶۰۳/۳۹ مگاژول در هکتار به دست آمد و بیشترین میزان مصرف اگزرژی مربوط به سوخت دیزل با سهم ۵۸ ٪ سایر ورودی‌ها است. در مرحله تولید بیودیزل، انرژی ورودی و انرژی خروجی به ترتیب ۱۵۶/۹۵ و ۴۱/۸۸ مگاژول بود و بیشترین میزان مصرف برق ۹۱/۰۲ مگاژول بود. مقدار کل اگزرژی در تولید بیودیزل و اگزرژی خروجی به ترتیب ۴۸/۴۱۲ و ۶۴/۵۶۸ مگاژول بود. در این مطالعه، اثرات نسبت مولی الکل به روغن، توان فراصوت (W)، غلظت کاتالیزور (درصد وزنی / وزنی) و زمان واکنش (دقیقه) بر عملکرد متیل استر با استفاده از روش سطح پاسخ بر اساس طرح آزمایشی Box Behnken در نرم افزار Design Expert مورد بررسی قرار گرفت. سرانجام، انتشار گازهای گلخانه‌ای در مراحل کاشت و تولید بیودیزل مورد بررسی قرار گرفت و نتایج نشان داد که بیشترین میزان انتشار گازهای گلخانه‌ای در مرحله کاشت، مربوط به کودهای شیمیایی و تولید الکل است.

CONTENTS

Journal Homepage: www.jree.ir